Late Miocene-Pliocene glacial cyclicity in a deep-sea sediment drift on the Antarctic Peninsula continental margin: Sedimentary and diagenetic processes

Dissertation
zur Erlangung des
Doktorgrades in den Naturwissenschaften
am Fachbereich Geowissenschaften
der Universität Bremen

vorgelegt von
M. A. Daniel A. Hepp

Bremen, Mai 2007

Tag des Kolloquiums:
22. Juli 2007

Gutachter:
Prof. Dr. T. Mörz
Prof. Dr. R. Stein

Prüfer:
Prof. Dr. R. Henrich
Prof. Dr. H.-J. Kuss

Table of Content

Abstract (Zusammenfassung)

The presented sedimentological, geochemical and paleoceanographical work is intended to improve the understanding of the regional influence of West Antarctic Ice Sheet dynamics and changes in oceanographic conditions on (1) sedimentary processes and (2) the preservation of proxies in the sedimentary record. A crucial feature for interpreting ice sheet dynamics is the understanding of the glacial driven sedimentary transport system across the shelf to the slope and subsequently to the deep-sea sediment bodies. Giant deep-sea sediment drifts are widespread features along the Pacific Continental Margin of the West Antarctic Peninsula, representing the most proximal continuous sedimentary recorders for West Antarctic ice events and glacial-interglacial cyclicity. Sediment physical and geochemical records, and X-ray images derived from ODP Site 1095 (Drift 7, ODP Leg 178) were used to identify pattern in glacial-interglacial cyclicity and associated sedimentary and diagenetic processes during late Miocene and Pliocene. Two boundary types dividing half-cycles have been recognized: (1) interglacial-to-glacial transitions are characterized by a sharp boundary and abrupt change in lithology, (2) glacial-to-interglacial transitions are diffuse and can be described as a gradual change from a full glacial to a full interglacial stage. The transitions are characterized by a gradual decline of sediment physical and geochemical values with a marked reduction in sedimentation rates. A prominent feature of the glacial-to-interglacial transition is the loss of the magnetic susceptibility signal. This loss is related to a massive ice sheet collapse at the end of deglaciation phases. Ice sheet collapse and meltwater formation increase the stratification of the water column and weaken the bottom water formation and convection, but foster short lived diatom blooms resulting in high fluxes of organic matter to the seafloor. The high organic fluxes result in temporary suboxic to anoxic near surface sediment conditions causing pronounced diagenetic alteration and demagnetization of magnetic iron. At long time-scales the intensity and loss of magnetic susceptibility in sixty-four zones of sediment cores from ODP Site 1095 reflect global long-term trends as well as the local variability of primary export production. In this context, warm Pliocene climate conditions for West Antarctic Peninsula region are characterized by short retention times of the grounded ice sheet at the shelf edge with sporadic fluctuations as well as periodic collapses of the ice-sheet front. To quantify the slope failure frequencies, we used the long term sedimentation rate dependency of the marine carbon burial efficiency in the drift sediment to calculate a ratio of glacial-to-interglacial sedimentation rates. Using the decompacted average length of glacial-interglacial cycles it was possible to solve a set of linear equations to derive average half periods of 61.59 and 59.77 kyr respectively for the Pliocene time interval between 5.8 and 3.2 Ma. The evidence for the dominance of short eccentricity periodicities at ~120 kyr corresponds to results of wavelet and power spectra analyses on proxi data, as reported in the literature. The resulting frequency distribution of slope failures reflects short and rapid but cyclic ice advances every ~375 yrs. Short retention times between slope loading and slope failure are supported by biogenic silica dissolution analyses. The results demonstrate the close link between ice sheet evolution and changes in oceanographic condition on the one hand and sedimentary processes and their preservation in the sedimentary record on the other hand. The investigations on ODP Site 1095 cores show the excellence applicability of West Antarctic drift sediments in regional paleoceanographic studies.

Im Mittelpunkt dieser sedimentologischen, geochemischen und paläozeanographischen Arbeit steht der Einfluss der westantarktischen Eisschildentwicklung sowie regionaler Veränderungen in den ozeanographischen Randbedingungen auf bestimmte sedimentäre Prozesse und deren Signalerhaltung im Sediment. Ein genaues Verständnis des sedimentären Transportsystems, ausgehend vom Schelf, über den Hang, bis hin zur Ablagerung auf Tiefseedriften, ist für die Interpretation der Eisschilddynamik von entscheidender Bedeutung. Beispielhaft wurde hierfür ein Sedimentdriftkörper vom Kontinentalfuß der westantarktischen Halbinsel untersucht. Die Sedimentkerne der Bohrlokation ODP 1095 (Drift 7, Leg 178) stellen ein nahezu kontinuierliches Archiv für das orbital gesteuerte Eisgeschehen auf dem Schelf dar. Anhand von sedimentphysikalischen und geochemischen Datensätzen sowie Röntgenaufnahmen von Kernen der Bohrlokation ODP 1095 wurden, für das Spätmiozän und Pliozän, glaziale und interglaziale Muster herausgearbeitet und die damit verbundenen sedimentären und diagenetischen Prozesse untersucht. Dabei konnten zwei charakteristische Übergänge beobachtet werden, wobei sich die Wechsel vom Interglazial zum Glazial durch eine scharfe Grenze und einen plötzlichen Wechsel in der Lithologie auszeichnen. Die Wechsel vom Glazial zum Interglazial sind dagegen fließend und durch graduelle Veränderungen ihrer sedimentphysikalischen und geochemischen Eigenschaften gekennzeichnet. Ein auffälliges Merkmal ist der zyklische Verlust des magnetischen Suszeptibilitätsignals, der regelmäßig am Wechsel vom Glazial zum Interglazial auftritt. Der Suszibilitätsverlust steht dabei in deutlicher Beziehung zu einem massiven Zusammenbruch des regionalen Eisschildes, jeweils am Ende der Abschmelzphase. Ein solcher Eischildzusammenbruch ist mit einem intensiven Schmelzwasserausstoß verbunden, der wiederum eine Stratifizierung der Wassersäule sowie eine Abschwächung der Bodenwasserbildung und -konvektion zur Folge hat. Gleichzeitig wird die Ausbildung einer intensiven Diatomeenblüte begünstigt, die kurzfristig für einen hohen organischen Eintrag in den Meeresboden sorgt. Dies führt wiederum vorübergehend zu suboxischen bis anoxischen Bedingungen im Sediment und damit zu einer diagenetischen Umwandlung der im Sediment enthaltenen Minerale und einem deutlichen Verlust ihrer gesteinsmagnetischen Eigenschaften. Entsprechende diagenetische Prozesse wurden an insgesamt vierundsechzig Zonen der Kerne der Bohrlokation ODP 1095 beobachtet. Auf langen Zeitskalen betrachtet zeichnet das aus diesen diagenetischen Zonen gewonnene Intensitätssignal einen Trend nach, der mit lokalen Veränderungen in der Primärproduktion und dem globalen Klimatrend vergleichbar ist. In der vorliegenden Arbeit wurde die Häufigkeit des Hangversagens infolge der glazialen Sedimentbeladung quantitativ bestimmt. Der Berechnung des Verhältnisses der glazialen zur interglazialen Sedimentationsrate wurde das Abhängigkeitsverhältnis von Sedimentaionsrate und Einbettungsgeschwindigkeit des marinen Kohlenstoffs in das Driftsediment zu Grunde gelegt. Anhand einer Abschätzung der dekompaktierten mittleren Längen der glazialen und interglazialen Intervalle und eines linearen Gleichungssystems konnte, für den Zeitraum zwischen 5,8 und 3,2 Millionen Jahre vor unserer Zeit, die mittlere Intervalldauer auf 6 159 bzw. 5 977 Jahre bestimmt werden. Die aus den Messdaten berechnete Periodizität weist demnach eine Zyklendauer von ~120 000 Jahren auf. Das Ergebnis bestätigt die aus Wavelet- und Spektralanalysen bekannten kurzen Exzentrizitätszyklendauern für diesen Zeitraum. Die Häufigkeitsverteilung der Turbiditereignisse infolge von Hangversagen deutet auf kurze und schnelle zyklischen Eisvorstöße etwa alle 375 Jahre hin. Untersuchungen zur Lösungsrate des biogenen Opals weisen zudem auf eine kurze Verweildauer zwischen der sedimentären Hangbeladung und dem Hangversagen hin. Die untersuchten Datensätzen liefern verschiedene Hinweise auf allgemein warme Klimabedingungen im Pliozän, mit offenen Seeeisbedingungen während der Glaziale, schnellen und kurzen Vorstößen des gegründeten Eisschildes zur Schelfkante sowie zyklischen Eisschildzusammenbrüchen am Ende der

Abschmelzphasen. Die Ergebnisse dieser Arbeit machen den engen Zusammenhang von einerseits Eisschildentwicklung und ozeanographischen Bedingungen und andererseits sedimentären Prozessen und diagenetischen Veränderungen ihres Signals im Sediment deutlich. Die kleinskaligen Untersuchungen an den Kernen der Bohrlokation ODP 1095 haben gezeigt, dass sich die verwendeten Driftsedimente hervorragend zur Rekonstruktion der regionalen Klimageschichte des pazifischen Kontinentalrandes der westantarktischen Halbinsel eignen.

1 Introduction

1.1 The role of southern high latitude processes in the global climate regime

1.1.1 West and East Antarctic Ice Sheet dynamic

The Antarctic ice-sheet dynamic is a major factor controlling the global climate regime in past, present and future (Exon et al., 2000; Stocker, 2003; Stoll 2006; Bowen 2007). The recent Antarctic ice sheet contains 90% of world's ice volume and hold 70% of Earth's fresh water. Variations in ice volume influence the albedo, the ocean thermohaline circulation (THC) and control the eustatic sea level. A complete deglaciation of the polar caps would affect a hypothetical sea level rise of about 70 m. The complete collapse of the recent West Antarctic Ice Sheet would raise global sea level by around 5 m (Vaughan and Spouge, 2002). From human perspective a sound quantitative understanding of the past ice sheet volume over time is therefore the key to future model scenarios subject to today's more rapidly changing conditions.

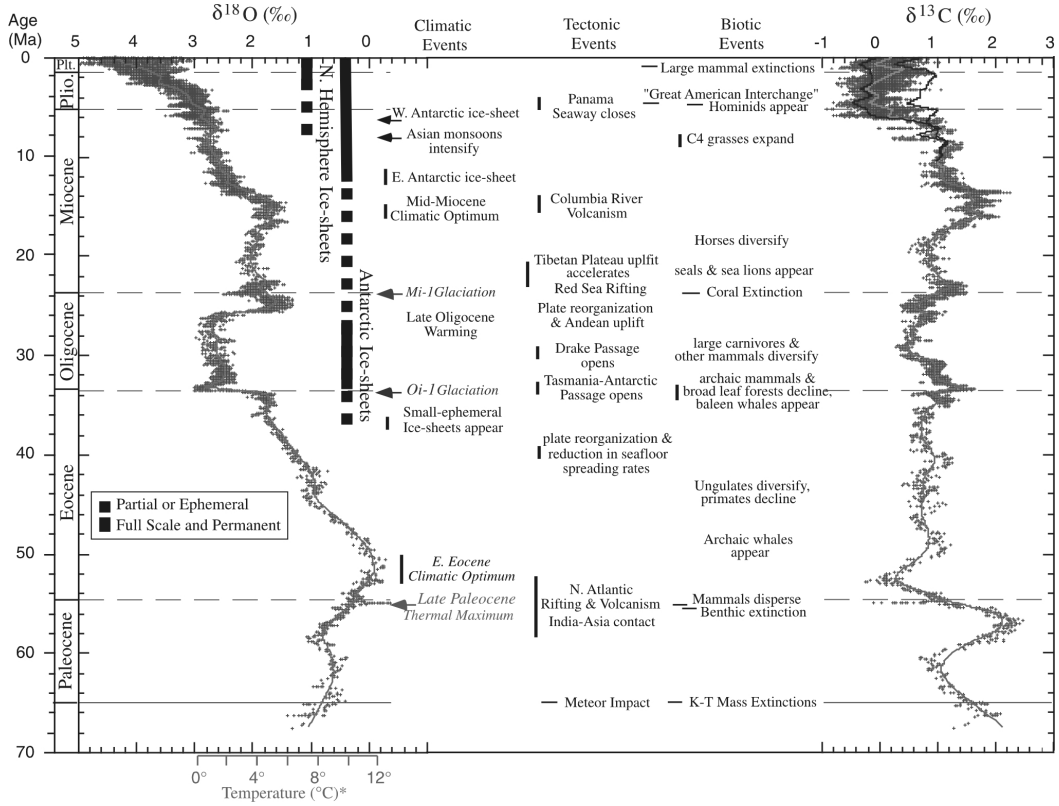

Fig. 1. Compilation of global deep-sea oxygen and carbon isotope records by Zachos et al. (2001). Since the beginning of the Oligocene epoch more than 70 percent of the variability in the $\delta^{18}O$ record reflects changes in Antarctica and Northern Hemisphere ice volume.

It has been nearly 34 Ma since Earth was last free of large continental ice sheets (Bowen 2007). Since the beginning of the Oligocene epoch, 33.7 Ma ago, the Antarctic ice volume was subject to several major variations (Fig. 1). A dramatic ice-sheet expansion over Antarctica, occurs about 13.9 Ma (Mid-Miocene global cooling) and marks the Earth's final transition into an 'icehouse' climate (Zachos et al., 2001). This event is linked to orbital forcing and atmospheric carbon dioxide (Fig. 1).

Within the general cooling trend, from mid-Miocene to present, Grützner et al. (2005) identified a number of global warming and cooling episodes during the late Miocene and the early Pliocene. An early Pliocene warming episode is generally accepted for Antarctica (Andersson et al., 2002; Grützner et al., 2005). A Comparison with the global ice-volume curve by Lear et al. (2002) confirms that the late Miocene and the early Pliocene have been times of dramatically reduced ice volume. The middle Pleistocene climate transition about 0.85 Ma has been attributed to global cooling. This event is accompanied by the glacial cycles change from 41,000 to 100,000 years likely triggered by a gradual decrease in atmospheric carbon dioxide concentrations (De Garidel-Thoron et al., 2005).

1.1.2 Thermohaline circulation and the Southern Ocean

Heat and salt driven density contrasts in the world oceans drive a global belt of moving water masses. This thermohaline circulation (Fig. 2) is the most prominent interspheric link of high and low latitudes, transporting heat, salt and moisture. Basic THC is a largely self-organizing feature that requires a deep enough body of water, and stimulation and exchange with the atmosphere. However, there are more prerequisites to form ice caps in polar regions: Plate tectonic is required to shift large major landmasses to high latitudes, and global green house gases have to drop below certain thresholds (DeConto and Pollard, 2003).

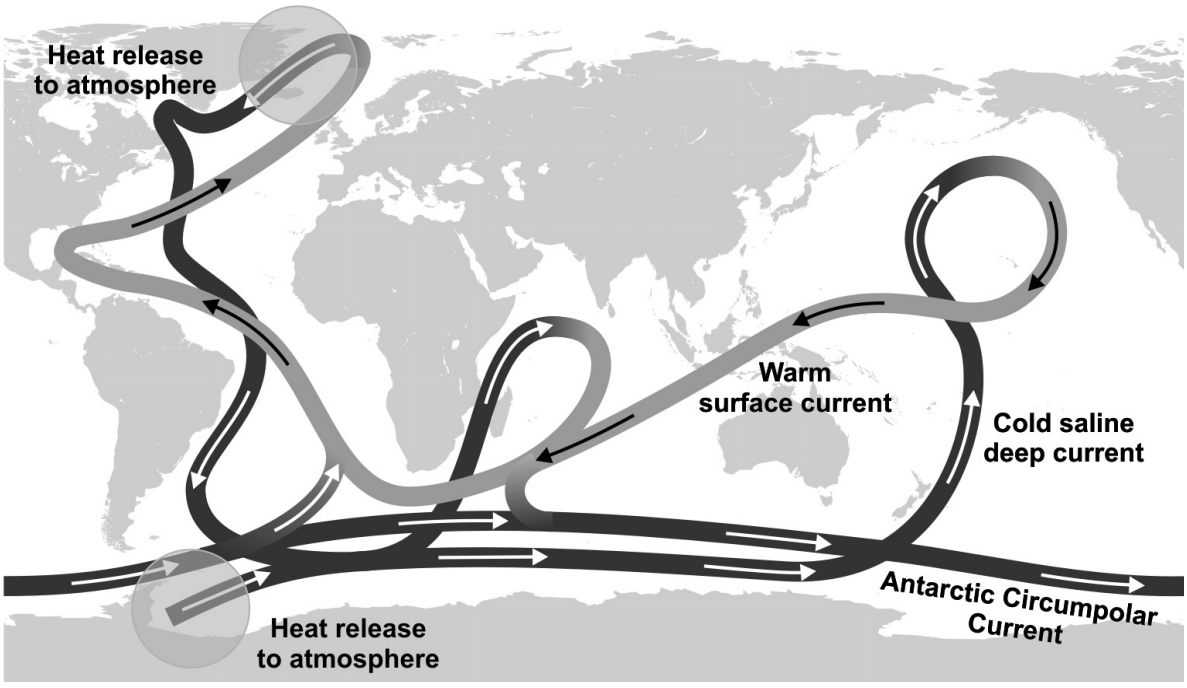

Fig. 2. Idealized sketch of the global ocean circulation 'conveyor belt' (Modified from Broecker, 1991 and Knorr, 2005).

In the case of Antarctica, a tectonic opening of gateways in the Southern Ocean supported this process 34 Ma ago by enabling the formation of the Antarctic Circumpolar Current (ACC) and the subsequent thermal isolation of the Antarctic continent (Kennett, 1977). However, it took another 31 Ma to form ice caps in the Arctic. This required the interplay of THC with a glaciated Antarctica surrounded by open waters in conjunction with the formation of the Panama Isthmus starting 5 Ma ago (Haug and Tiedemann, 1998). This combination led to an intense moisture transport to Eurasia that resulted in strong fresh water fluxes to the Arctic Ocean, likely weakening the northern branch of the oceans conveyer, and in turn drastically cooled the northern hemisphere starting northern hemisphere glaciation about 3 Ma ago.

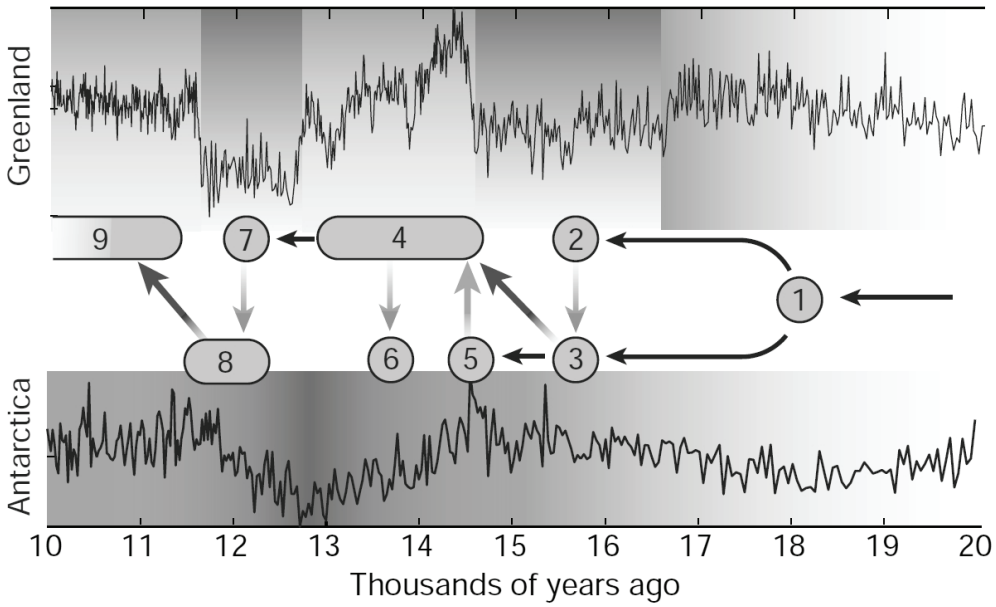

Fig. 3. South dials north, published by Stocker (2003). The diagram shows coolings and warmings between 20,000 and 10,000 years ago from temperature records from ice cores from Greenland and Antarctica. The Arrows shows the inferred course of events (numbers) in the north and south: (1) end of ice age 18,000 years ago, (2) shut down of thermohaline circulation in the Northern Atlantic by melting ice sheets, (3) 'seesaw' mechanism connects the polar regions north and south. Warming in the south turns the thermohaline circulation on, (4) surface advection of saline waters and (5) meltwater discharge in the south reduce the density of Antarctic deep water, (6) meltwater discharge in north and cooling in Antarctica reduces the Atlantic thermohaline circulation and (7) triggers an abrupt cooling in the north, this stimulates southern warming by 'seesaw' and (9) leads to a final warming in the north.

Cyclic growth and retreat of the ice sheets is orbital triggered and the THC forms the teleconnection between the high latitudes. Studies of the modern interglacial and the last glacial climate suggest that the glacial THC was weaker (approx. 30-40%) than the modern THC. During the last decade numerous studies suggest that warming and freshening of northern high latitude surface waters may weaken the THC (Ganopolski and Rahmstorf, 2001; Knorr and Lohmann, 2003; McManus et al., 2004). Critical times in the acceleration and the slowdown of the THC are the terminations, when global climate switches between ice house and greenhouse conditions. During the deglaciation, Heinrich modes with massive meltwater fluxes cause additional cooling in the North Atlantic (Severinghaus and Brook, 1999), whereas contemporary warming in some locations in the southern hemisphere is observed (Hemming et al., 2000; Mix et al., 2001). This indicates that the reduction of North Atlantic Deep Water (NADW) formation decreases the heat transport from the

Antarctic Oceans to the North Atlantic leading to an antiphase 'bipolar seesaw' effect (Stocker, 1998; Fig. 3).

During Heinrich events the reduction of the THC may have come close to a shut down with negligible overturn (McManus et al., 2004). Up to now, the majority of studies with well resolved stratigraphy dealing with meltwater events, and their likely trigger mechanisms are focused on the northern hemisphere. Based on this northern view the classical picture emerged, highlighting processes around the Greenland and Labrador ice masses and the effects of northern melting and fresh water input on the formation of NADW, seen as the major driver of the THC. Recently, the Southern Oceans became more in focus since precise dating reveals that the south is leading the north in terms of warming during deglaciations ('South dials north': Stocker, 2003; Fig. 3). Like in the north cold but light meltwater may play an important role in Southern Oceans, Weaver et al. (2003) demonstrated that Meltwater pulse 1A acts as a trigger to restart a strengthening of the NADW formation. So far, it looks like that meltwater fluxes in the north shot down or damps the THC whereas meltwater in the Circum Antarctic Ocean reduces the Antarctic Bottom Water (AABW) formation making the NADW denser than the Antarctic Intermediate Water (AAIW). This leads to an intensification of the THC (Stocker, 2000), heat mining the south and warming in the north.

With their ocean-atmospheric models Knorr and Lohmann (2003) support a leading role of the Southern Ocean in influencing the overturning strength of the NADFW resulting in a deglaciation in the north. Sea-ice extends (Width of the open Drake Passage) and elevated Circum Antarctic temperatures are additional parameters that emerge to be important. Attaching, importance in those parameters is not a contradiction to the idea of meltwater and AABW influence. Bottom water formation, sea- and shelf ice extend are inseparably connected and getting reduced during deglaciations and related meltwater events.

1.1.3 Why is the late Miocene/early Pliocene warming episode from special interest?

According to the current discussion between scientists and policy makers of the industrialized countries about the effect of climate changes on human and Earth's future it is essential to know more about the interaction of climate warming and Antarctic ice sheet behavior. The late Miocene/early Pliocene warming is the largest warming episode since the beginning of the mid-Miocene global cooling. The continental ice sheet extend during late Miocene/early Pliocene warming can be attributed to a 2.0°C increase in deep-sea temperature (see Zachos et al., 2001). Because deep ocean waters are derived primarily from cooling and sinking of water in Polar Regions, the deep-sea temperature data can be used as a time-averaged record of high-latitude sea-surface temperatures and a proxy for global climate (Zachos et al., 2001).

Many recent discussions question the assumed stability of the Antarctic ice. Evidence for a young West Antarctic Ice Sheet collapse, is e.g. presented by Scherer (1993; Scherer et al. 1998; Fricker et al. 2002). Based on isotopic ^{10}Be contents from microfossils (diatoms), recovered underneath ice streams, he postulated a major deglaciation event during the late Pleistocene (likely during marine isotope stage 11, 400,000 years ago). A Recent work of Lear et al. (2000) support the idea of a strongly reduced ice sheet during the early Pliocene (Fig. 3).

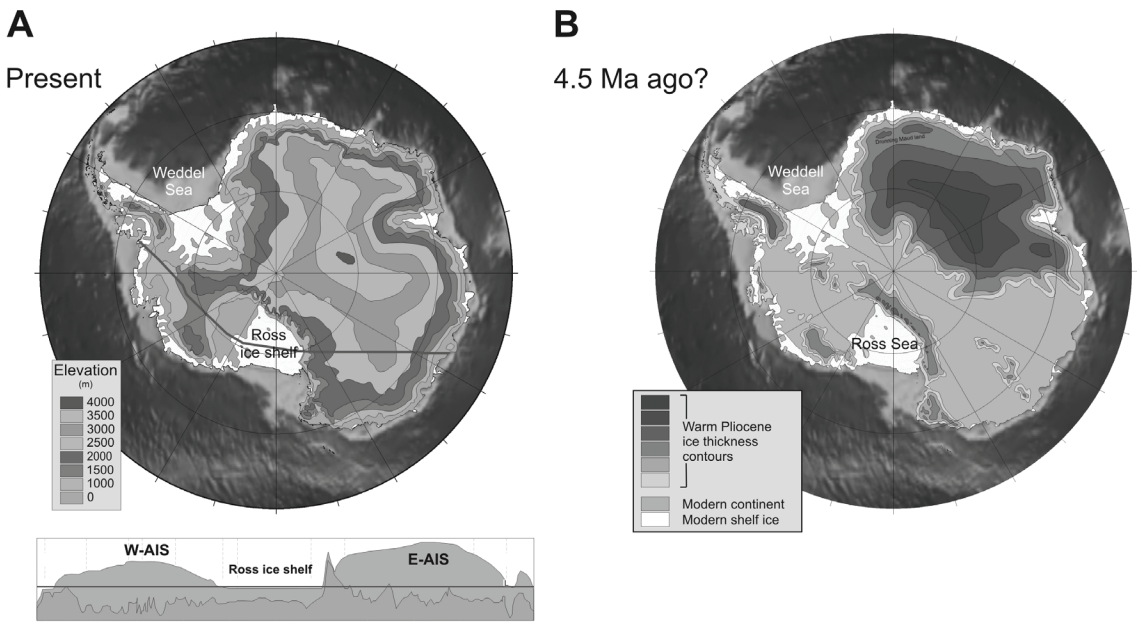

Fig. 4. Example of Antarctic ice sheet variability. (A) Elevation of present ice sheets show on East Antarctica the continental ice sheet and on West Antarctica the marine-based ice sheet that is largely grounded below sea-level. The history and stability of these ice sheets differ: The West Antarctic Ice Sheet is less stable and developed later (Late Miocene) than the East Antarctic Ice Sheet, which is believed to have developed to its present form by the middle Miocene (~14 Ma) (modified from Kennett and Hodell, 1995). (B) Ice sheets during the warm Pliocene, according to the model of Denton et al. (1991) following the EPD hypothesis of Webb et al. (1984). Ice volume was reduced to a third of its modern value and shallow marine basins border the continent. Contours are relative thickness (Modified from Denton et al., 1991).

The effect of late Miocene/early Pliocene warming on the extent and behavior of the East and West Antarctic Ice Sheets is a source of debate (Fig. 4). The conflict between the stability hypothesis Warm Stable Ice-Sheet (WSI; e.g. hypothesis from: Kennett and Hodell, 1993; Barker, 1995; Barrett, 1999) and the Early Pliocene Deglaciation (EPD) scenario (Webb et al., 1984; Webb and Harwood, 1991) is now almost 20 years old.

The dispute started when Webb et al. (1984) described fossil-bearing deposits of the Sirius Group in the Transantarctic Mountains. Marine diatoms of the assemblage dated as Pliocene in age have been interpreted by Webb et al. (1984) as being deposited in an ice-free flooded East Antarctic interior, subsequently to be glacially eroded and transported to their present location by a younger Antarctic ice sheet in cooler, late Pleistocene times. On the base of their fossil assemblages Webb and Harwood (1993) proposed mean annual temperatures of up to 5°C. Models based on this scenario concluded that East and West Antarctica must have been deglaciated to a third of the present ice volume (Webb et al, 1984; Denton et al., 1991).

Representatives of the WSI hypothesis (Kennett and Hodell, 1993; Barker, 1995, Barrett, 1999) attacked the EPD hypothesis. They doubt the diatom-based ages assigned to the microfossil assemblage of the Sirius Group because biogenic particles and diatom material sampled from Sirius Group tills and surrounding outcrop faces containing similar diatom assemblages from the inland ice sheet at the South Pole and two other locations (Kellogg and Kellogg, 1996). Hence, several atmospheric transport mechanisms have been proposed, including the Eltanin asteroid impact around 2.2 Ma (Gersonde, 1997). Other fossils of the assemblage (e.g. *Nothofagus*) remain to be older than Pliocene and Barker (1995) assigned a hypothetical mid-Miocene age. This would resolve the problem since the oxygen isotopic record shows that the middle Miocene was a prolonged warm period.

Kennett and Hodell (1995) and Barker (1995) discussed the effect of the observed reduced $\delta^{18}O$ values of benthic foraminifera in early Pliocene times (Shackleton et al., 1995; Tiedemann et al., 1994). They conclude that the proposed 60% reduction in Antarctic ice volume is only achievable if the decrease in $\delta^{18}O$ is totally the result of ice volume changes. This seems unrealistic since a major deglaciation would also be accompanied by a substantial increase in surface water temperature. They summarize that the observed changes in isotopic data in the early Pliocene of the Sub Antarctic are insufficient to accommodate both substantial Southern Ocean warming and major deglaciation.

However, parameters like isotopes and sea level data so far have not solved the conflict since they are in disagreement (Miller et al., 1987; Haq et al., 1987; Zachos et al., 2001). Ice sheet models (Anderson et al., 2002; Bentley, 1999; Huybrechts, 2004; Peltier, 1994; Zwartz et al., 1997) are no real solutions since different authors based their model scenarios on contradicting input-parameters. Since the Antarctic ice sheet behavior over time is not understood as an entirety, questions regarding the relative stability of the East versus the West Antarctic Ice Sheet are even more complex.

1.2 The Pacific continental margin of the West Antarctic Peninsula

1.2.1 Geological and oceanographic background

The geological, bathymetric and tectonic setting of the Pacific margin off the Antarctic Peninsula have been well described in several bathymetric, seismic and sediment-based studies (Tucholke et al., 1976; Larter and Barker, 1989; Anderson et al., 1991; Tomlinson et al., 1992; Rebesco et al., 1996; 1998; 2002; Camerlenghi et al., 1997a; Pudsey and Camerlenghi et al., 1998; Canals et al., 2000; Pudsey, 2000; Barker and Camerlenghi, 2002; Lucchi et al., 2002b; Rebesco et al., 2006, Uenzelmann-Neben, 2006).

A series of twelve large sediment drifts along the Antarctic Peninsula continental rise between 63°S and 69°S is directly associated with the glacial morphology of the outer continental shelf (Faugères et al., 1999; Pudsey and Camerlenghi, 1998; Rebesco et al., 2002; Fig. 5). They are part of a complex glacial sedimentary feeder system. Large turbidity current channels separate the drifts (Pudsey and Camerlenghi, 1998). These channel system is connected to troughs between prograding depositional lobes on the outer shelf (Barker and Camerlenghi, 1999). The largest drifts (Drift 6 and 7) attain elevations of 700 m of above the surrounding sea floor and reach more than 130 km outward from the food of the steep continental slope. The width of a drift typically exceeds 50 km. The shape of the drift bodies generally is asymmetric with steeper and rougher slopes in southeast, toward the shelf, and in southwest (Rebesco et al., 1997). The gently dipping side in northeast and northwest merges gradually with the lower continental rise and the abyssal plain. The steeper side is always separated from the steep continental slope (Average angle 16°; Rebesco et al., 1996) by a sea-floor trough or channel. The average water depth of the drift crests lies between 2500 and 2800 meter below sea level (mbsl). The southwest-northeast asymmetry is attributed to bottom currents with a net westward component. This is most likely the Antarctic bottom water which originates in the Weddell Sea and flows north through deep gaps in the South Scotia Ridge and then westwards along the Antarctic Peninsula Margin (Nowlin and Zenk, 1988; Pudsey and Camerlenghi, 1998).

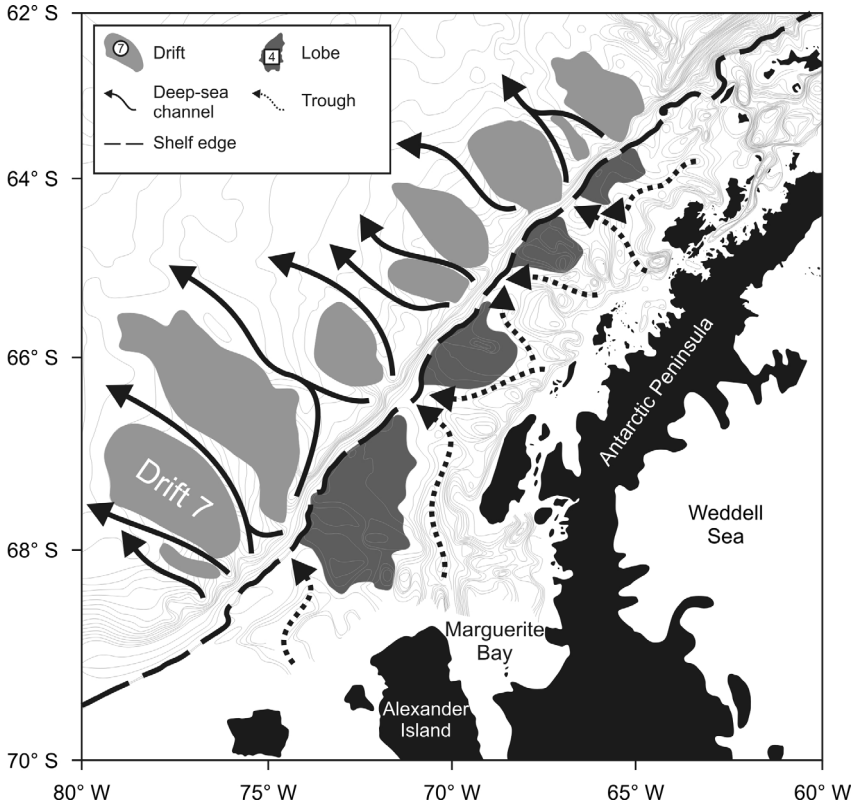

Fig. 5. Bathymetric map of Antarctic Peninsula Pacific margin showing Drift 7. The arrows and gray shadings illustrate the sedimentary feeder system that transports terrigenous material from the shelf on the drifts.

The origin of these sediment bodies is discussed controversially. McGinnis and Hayes (1995) proposed that turbidity down-slope currents forcing the development of the mounds, whereas Rebesco et al. (1996, 1997, 2002) favored a strong influence of contour-current activity and interpreted the mounds as drift bodies. Recent measurements, 8 m above the seabed, on both sides of Drift 7 revealed southwest directed bottom currents with average speeds around 6 cm/sec and maxima sometimes exceeding 14 cm/sec (Camerlenghi et al., 1997). These modern currents are considered to be too weak to cause significant erosion of continental rise sediment, though they may hold fine silt and clay in suspension (Pudsey and Camerlenghi, 1998).

Traces of gravity-driven downslope turbidity currents (Known as fine laminated silt layers) are the most conspicuous feature in glacial sediment depositions on the West Antarctic Peninsula continental rise. The grounded ice sheet transports eroded terrigenous material over the shelf edge to the oversteepened slope. Frequent slope failures trigger turbidity currents, which run along the axis of the channels between the large elongated drift bodies to the abyssal plain. The passage of large turbidity currents through channels (Diviacco et al., 2006) results in spillover ‘turbidity’ currents and silt lamina deposits on the drifts.

The sediment drifts were developed by a complex interplay of down-slope and along-slope processes. The origin of these so called 'drift bodies' is still discussed controversy according to the question for the main influence by these processes (McGinnis and Hayes, 1995; Rebesco et al., 1996; Rebesco et al., 2002; Uenzelmann-Neben, 2006).

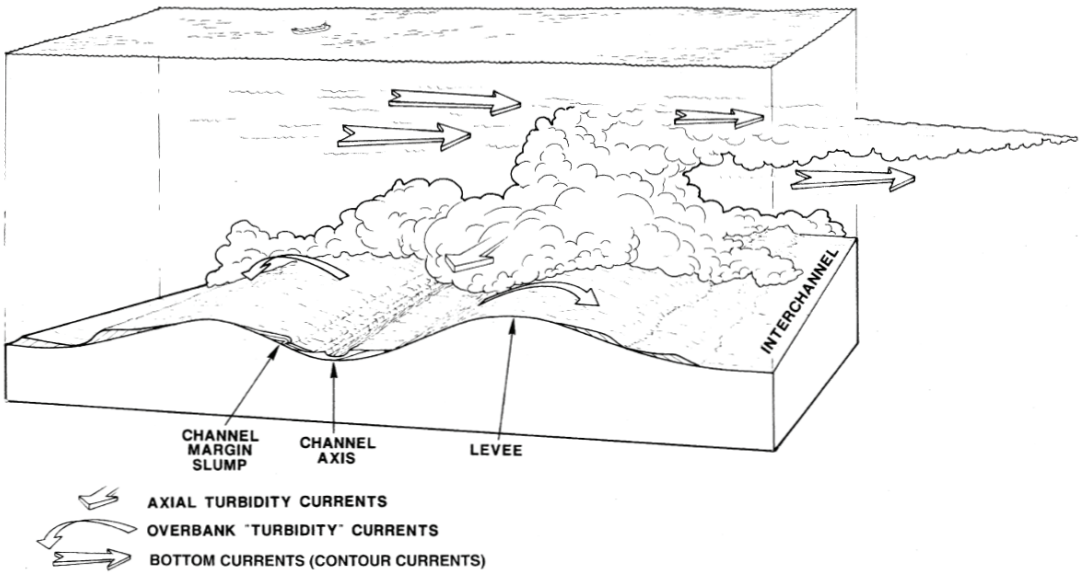

Fig. 6. Schematic diagram showing gravity-driven downslope turbidity currents running along a channel axis between two drift bodies to the abyssal plain. Simultaneously spillover or overbank currents transport 'turbidity' sediments laterally on the drifts. Parallel-to-slope bottom currents (contour currents) shape the drifts (from Shanmugam, 2000).

In a recent study Uenzelmann-Neben (2006) proposed in a depositional model compiled from maps of reflectors depth and seismic unit thickness, that the along-slope transport was the major component of the drift evolution between 25 and 15 Ma. According to the Antarctic Peninsula ice sheet growth the drift evolution processes changed to a dominance of strong turbidity down-slope transports between 15 and 9.5 Ma. A decrease in sediment input since 9.5 Ma indicates a retreat of the ice but not an increased along-slope transport. Uenzelmann-Neben observed a re-onset of the bottom current starting at 5.3 Ma.

The presented studies show that the discussion of along-slope versus down-slope sediment transport requires further studies from a sedimentological view point.

1.2.2 Why is Drift 7 (ODP Site 1095) the place to go for?

Drilling on the continental rise (ODP Leg 178) was conducted following the ANTOSTRAT approach that considers the rise sediments along the Antarctic Peninsula to be a distal but continuous recorder of ice sheet history and fine-grained equivalent of the slope foresets that are the direct product of ice advance and retreat on the shelf (Mörz, 2002). All other possible environments are either too distal (deep sea) or not continuous enough (shelf). Therefore the quasi continuous drift record from the rise is the most suitable data set for an attempt to reconstruct the glacial history of the West Antarctic Peninsula ice shield. The distal and indirect record of the drifts is unique in its high resolution but still influenced by many differing factors (Counter currents, hemipelagic sedimentation, and shelf development). Interpretations toward an ice-sheet history must be supplemented by a principal understanding of the shelf modes. Mörz (2002) showed that each advance of grounded ice to the shelf break leaves a distinct 'grain size' fingerprint in the drift record.

Drift 7 is one of the largest sediment drifts located to the southwest of the Antarctic Peninsula (Fig. 7). Its asymmetrical shape, with a short steep side facing southeast and a long gently-sloping side

facing northwest, is similar in shape to other sediment drifts in this area. The drift build-up is the result of glacially driven turbidity currents and interglacial pelagic settling. The shapes were formed by weak non-erosive bottom currents flowing along the bathymetric contour (Camerlenghi et al., 1997a; Pudsey and Camerlenghi, 1998). From seismic profiles Rebesco et al. (1997) proposed three major stages of Drift 7 evolution, which are marked by distinct reflectors. The first 'pre-drift stage' (~35 to 15 Ma) is mainly characterized by turbidity sequences. The end of this stage is possibly linked to the opening of the Drake Passage and the onset of the Antarctic Polar Current (ACC; Rebesco et al., 1997). During the second 'drift-growth stage' (~15 Ma to 5 Ma) the drift development is characterized by increased down-slope and along-slope processes. Cyclic grounded ice-sheet advances onto the shelf and increase the sediment supply to the drift. The third 'drift-maintenance stage' (Since ~5 Ma) shows preservation and enhancement of the elevation of the drifts under decreasing sediment supply.

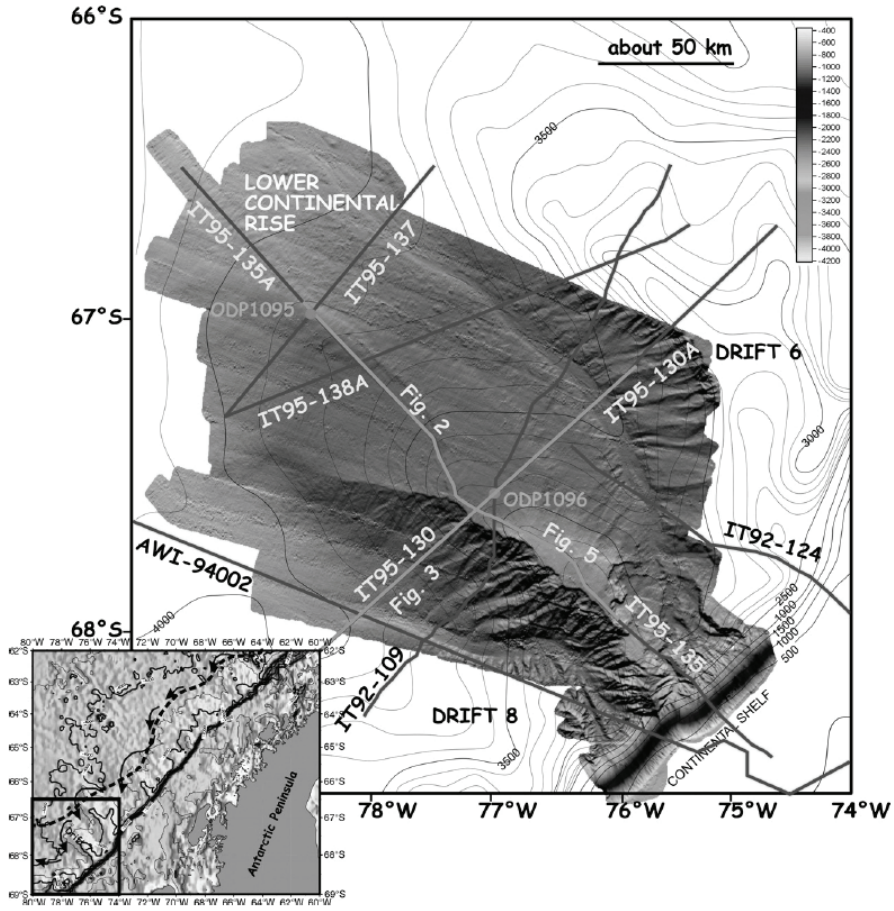

Fig. 7. Swath bathymetric map of Drift7 (Published by Uenzelmann-Neben, 2006).

Sediment Drift 7 and the proximal area were drilled by advanced piston corers (APC) and extended core barrels (XCB) at two sites (Site 1095 and 1096) during ODP Leg 178 in 1998 (Shipboard Scientific Party, 1999a), and by short piston corers at 19 sites (SED-1 to SED-19) during SEDANO (SEdiment Drifts of the ANtarctic Offshore) Project-I and -II (Lucchi et al., 2002a; 2002b; Pudsey and Camerlenghi, 1998; core SED-15 is located on Drift 7, Fig. 7). Both projects provided sediment cores with prominent glacial cyclicity. The SEDANO cores are up to 7 m long and cover the isotopic stages 1-11, whereas the ODP cores, with recoveries of up to 600 m length, provide a 10-Ma

sedimentary record. The SEDANO-I survey (1995) examined contour current patterns in the area of Drift 7, which contributes to the drift surface (Camerlenghi et al., 1997b; Pudsey and Camerlenghi, 1998). The short piston cores collected during the SEDANO-II project (1997-1998) document the major large-scale processes which govern the bottom current regime (Lucchi et al., 2002b; Giorgetti et al., 2003; Villa et al., 2003). Site 1095 lies in 3840 mbsl on the lower NE flank of Drift 7 and is the more distal of the two Sites (1095 and 1096) drilled (Fig. 7). Our investigations focus on Site 1095 cores collected from multiple Holes A and B. 1095A was cored from 0 to 87.79 (mbsf) with 99.1% recovery, core 1095B was recovered from 83 to 561.78 mbsf with 79.2% recovery. Together, both cores comprise a continuous record from the late Miocene to the Holocene (~10 Ma) and covers two-thirds of the drift-growth-stage and the complete drift-maintenance stage.

1.2.3 The link between ice sheet dynamics, sedimentary processes and drift build up

The Antarctic ice-sheet dynamic causes cyclic sedimentation at proximal sites. Hence, the sedimentary record is a key factor for the reconstruction of the ice sheet evolution. Drift sediments are excellent archives for shelf ice dynamic signals. The cyclic sedimentation is linked to Milankovitch cycles, which are superimposed on the general climate trend (Shackleton and Hall, 1997). Proximal Antarctic high-resolution records that document ice sheet variation of the last 10 Ma are rare. ODP drill Sites 1095 provide continuous records over this time span. Grützner et al. (2003) calculated iron mass-accumulation rates, as a proxy for sediment accumulation rates, and demonstrated synchronous changes in accumulation rate with comparable magnitudes based on orbital tuned time scales. A synchronous behavior of East (ODP Site 188) and West Antarctic Ice Sheets is an important finding encouraging studies that compare cyclic sedimentary pattern from both Antarctic spheres.

This study contributes to the understanding of the interaction between ice sheet evolution, and sedimentary processes in the Pliocene and the influence on the sedimentary record of ODP Site 1095. Following questions motivated the present work:

1. What parameters in the sedimentary record reflect the ice sheet evolution?
2. Does sediment physical and geochemical proxy data follow glacial-interglacial pattern and can these pattern be used to fix glacial-interglacial transitions?
3. What is the origin and influence of early diagenetic processes on the preservation of the sedimentary record and how is early diagenesis linked to the glacial-interglacial cyclicity?
4. What are the paleoceanographic consequences of the diagenetical findings in drift sediments?
5. How can we reconstruct the frequency of turbidity depositions on Drift 7 to get informations about slope loading by ice sheet activity and what other indicators can be used to support the derived model for paleo ice sheet dynamics?
6. Is the postulated switch of an early Pliocene warm, highly dynamic Antarctic ice sheet regime to Pleistocene cold-based, stable conditions at about 3 Ma expressed in the tubidite frequency record?

The findings will be discussed in the context of West Antarctic Ice Sheet evolution and oceanography.

1.3 Publications

This study was conducted at University of Bremen as part of the project „Quantitative reconstruction of the Neogene East and West Antarctic Ice Sheet history from drift sediments (ODP Leg 178 and Leg 188): A Synthesis" in the context of the DFG Schwerpunktprogramms IODP/ODP. This work is submitted as a dissertation and has been supervised by Prof. Dr. Tobias Mörz.

The presented work is structured in three separate manuscripts, which are either published or submitted for publication. The manuscripts in Chapter 2 have been written as stand-alone scientific papers. Chapter 3 contains a selection of four abstracts, which were presented at national and international conferences.

The first Manuscript deals with characteristics in glacial-interglacial cyclicity, their transitions, and associated sedimentary processes during early Pliocene. The found boundaries form the framework for the calculation of relative sedimentation and accumulation rates, which were used for the reconstruction of the early Pliocene paleoproductivity and terrigenous flux to the drift. The findings are summarized in a five-phase drift sedimentation model for the early Pliocene.

A closer look on the glacial-interglacial transitions is subject of the second Manuscript. The study is based on the long and short time scale analysis of sedimentary and geochemical signals of magnetic susceptibility minima zones. The work outlines the diagenetic effects of regional changes in the cryosphere and oceanographic realm on the deep-sea sedimentary record during a period of global enhanced primary productivity in late Miocene/early Pliocene.

The main focus of the third manuscript lies on the quantification of slope failure frequencies recorded in Pliocene core intervals. In addition, biogenic silica dissolution analyses give an idea of the retention times between slope loading and slope failure.

The presented work is an edited version of the originally submitted thesis. Following the suggestions of the reviewers the second and third manuscripts were slightly revised and the introduction part was carefully adjusted.

1.4 References

Anderson, R.F., Chase, Z., Fleisher, M.Q., and Sachs, J., 2002. The Southern Ocean's biological pump during the Last Glacial Maximum. Deep-Sea Res. II, 49 (9-10):1909-1938.

Andersson, C., Warnke, D.A., Channell, J.E.T., Stoner, J.S., and Jansen, E., 2002. The mid-Pliocene (4.3–2.6 Ma) benthic stable isotope record of the Southern Ocean: ODP Sites 1092 and 704, Meteor Rise. Palaeogeogr., Palaeoclimatol., Palaeoecol., 182 (3-4):165-181.

Barker, P.F., 1995. The proximal marine sediment record of Antarctic climate since the late Miocene. In Cooper, A.K., Barker, P.F., and Brancolini, G. (Eds.), Geology and seismic stratigraphy of the Antarctic margin. Antarctic Research Series, 68: Washington, DC (American Geophysical Union), 25-57.

Barrett, P.J., 1999. Antarctic climate history over the last 100 million years. Terra Antarc. Rpts., 3:53-72.

Bentley, M.J., 1999. Volume of Antarctic ice at the last glacial maximum, and its impact on global sea level change. Quaternary Sci. Rev., 18 (14):1569-1595.

Bowen, G.J., 2007. Palaeoclimate: When the world turned cold. Nature, 445:607-608.

Broecker, W.S., 1991. The great ocean conveyor. Oceanography, 4:79-89.

Camerlenghi, A., Crise, A., Pudsey, C.J., Accerboni, E., Laterza, R., and Rebesco, M.A., 1997a, Ten-month observation of the bottom current regime across a sediment drift of the Pacific margin of the Antarctic Peninsula: Antarctic Science, v. 9, p. 426-433.

Camerlenghi, A., Rebesco, M.A., and Pudsey, C.J., 1997b, High resolution terrigenous sedimentary record of a sediment drift on the continental rise of the Antarctic Peninsula pacific margin (inital results of the 'SEDANO' Program), in Ricci, C.A., ed., The Antarctic region: Geological evolution and processes: Siena, Terra Antarctica Publication, p. 705-710.

DeConto, R.M., and Pollard, D., 2003. Rapid Cenozoic glaciation of Antarctica induced by declining atmospheric CO_2. Nature, 421:245-249.

De Garidel-Thoron, T., Rosenthal, Y., Bassinot, F.C., and Beaufort, L., 2005. Stable sea surface temperatures in the western Pacific warm pool over the past 1.75million years. Nature, 433:294-298.

Denton, G.H., Prentice, M.L., and Burckle, L.H., 1991. Cenozoic history of the Antarctic ice sheet. In Tingey, R.J. (Ed.), The Geology of Antarctica. Oxford Monographs on Geology and Geophysics, 17: Oxford (Oxford University Press), 365-433.

Exon, N., Kennett, J.P., Malone, M., and Shipboard Scientific Party, 2000. The opening of the Tasmanian gateway drove global Cenozoic paleoclimatic and paleoceanographic changes: Results of Leg 189. JOIDES J, 26 (2):11-18.

Fricker, H.A., Young, N.W., Allison, I., and Coleman, R., 2002, Iceberg calving from the Amery Ice Shelf, East Antarctica: Annals of Glaciology, v. 34, p. 241-246.

Ganopolski, A., and Rahmstorf, S., 2001. Rapid changes of glacial climate simulated in a coupled climate model. Nature, 409:153-158.

Gersonde, R.E., Kyte, F.T., Bleil, U., Diekmann, B., Flores, J.A., Gohl, K., Grahl, G., Hagen, R., Kuhn, G., Sierro, F.J., Völker, D., Abelmann, A., and Bostwick, J.A., 1997. Geological record and reconstruction of the Late Pliocene impact of the Eltanin asteroid in the Southern Ocean. Nature, 390:357-363.

Giorgetti, A., Crise, A., Laterza, R., Perini, L., Rebesco, M.A., and Camerlenghi, A., 2003, Water masses and bottom boundary layer dynamics above a sediment drift of the Antarctic Peninsula Pacific margin: Antarctic Science, v. 15, p. 537-546.

Grützner, J., Rebesco, M.A., Cooper, A.K., Forsberg, C.F., Kryc, K.A., and Wefer, G., 2003, Evidence for orbitally controlled size variations of the East Antarctic ice sheet during the late Miocene: Geology, v. 31, p. 777-780.

Grützner, J., Hillenbrand, C.-D., and Rebesco, M.A., 2005. Terrigenous flux and biogenic silica deposition at the Antarctic continental rise during the late Miocene to early Pliocene: Implications for ice sheet stability and sea ice coverage. Global Planet. Change, 45:131-149.

Haq, B.U., Hardenbol, H., and Vail, P.R., 1987. The chronology of fluctuating sea-level since the Triassic. Science, 235:1156-1167.

Haug, G.H., and Tiedemann, R., 1998. Effect of the formation of the Isthmus of Panama on Atlantic Ocean thermohaline circulation. Nature, 393 (6686):673-676.

Hemming, S.R., Bond, G., Broecker, W.S., Sharp, W.D., and Klas-Mendelson, M., 2000. Evidence from Ar-40/Ar-39 ages of individual hornblende grains for varying Laurentide sources of icebergs discharges 22,000 to 10,500 yr BP. Quaternary Res., 54:372-383.

Holbourn, A., Kuhnt, W., Schulz, M., and Erlenkeuser, H., 2005. Impacts of orbital forcing and atmospheric carbon dioxide on Miocene ice-sheet expansion. Nature, 438:483-487.

Huybrechts, P. (Ed.) 2004. Antarctica: Modelling. Mass balance of the cryosphere: Observations and modelling of contemporary and future changes: New York (Cambridge University Press).

Kellogg, D.E., and Kellogg, T.B., 1996. Diatoms in South Pole ice: Implications for Eolian contamination of Sirius Group deposits. Geology, 24:115 -118.

Kennett, J.P., 1977. Cenozoic evolution of Antarctic glaciation, the circum Antarctic ocean, and their impact on global paleoceanography. J. Gephys. Res., 82 (27):3843-3860.

Kennett, J.P., and Hodell, D.A., 1993. Evidence for relative climatic stability of Antarctica during the Early Pliocene: A marine perspective. Geogr. Ann., Ser. A, 75:205-220.

Knorr, G., and Lohmann, G., 2003. Southern Ocean origin for the resumption of Atlantic thermohaline circulation during deglaciation. Nature, 424 (6948):532-536.

Knorr, G., 2005. Collapse and resumption of the thermohaline circulation during deglaciation: Insights by models of different complexity [doctoral thesis]. Universität, Hamburg.

Lear, C.H., Rosenthal, Y., and Slowey, N., 2002. Benthic foraminiferal Mg/Ca-paleothermometry: A revised core-top calibration. Geochim. Cosmochim. Acta, 66 (19):3375-3387.

Lucchi, R.G., Rebesco, M.A., Busetti, M., Caburlotto, A., Colizza, E., and Fontolan, G., 2002a, Sedimentary processes and glacial cycles on the sediment drifts of the Antarctic Peninsula Pacific margin: Preliminary results of SEDANO-II project: New Zealand Journal of Geology and Geophysics, v. 35, p. 275-280.

Lucchi, R.G., Rebesco, M.A., Camerlenghi, A., Busetti, M., Tomadin, L., Villa, G., Persico, D., Morigi, C., Bonci, M.C., and Giorgetti, G., 2002b, Mid-late Pleistocene glacimarine sedimentary processes of a high-latitude, deep-sea sediment drift (Antarctic Peninsula Pacific margin): Marine Geology, v. 189, p. 343-370.

McManus, J.F., Francois, R., Gherardi, J.-M., Keigwin, L.D., and Brown-Leger, S., 2004. Collapse and rapid resumption of Atlantic meridional circulation linked to deglacial climate changes. 428 (6985):834-837.

Miller, K.G., Fairbanks, R.G., and Mountain, G.S., 1987. Tertiary oxygen isotope synthesis, sea level history, and continental margin erosion. Paleoceanogr., 2 (1):1-19.

Mix, A.C., Bard, E., and Schneider, R.R., 2001. Environmental processes of the ice age: land, oceans, glaciers (EPILOG). Quaternary Sci. Rev., 20:627-657.

Mörz, T., 2002. From the inner shelf to the deep sea: Depositional environments on the West Antarctic Peninsula margin: A sedimentological and seismostratigraphic study (ODP Leg 178). Ber. Polar- u. Meeresforsch., 427: Bremerhaven (Alfred-Wegener-Institut für Polar- und Meeresforschung).

Peltier, W.R., 1994. Ice age palaeotopography. Science, 265:194-201.

Pudsey, C.J., and Camerlenghi, A., 1998, Glacial-interglacial deposition on a sediment drift on the Pacific margin of the Antarctic Peninsula: Antarctic Science, v. 10, p. 286-308.

Rebesco, M.A., Larter, R.D., Barker, P.F., Camerlenghi, A., and Vanneste, L.E., 1997, The history of sedimentation on the continental rise west of the Antarctic Peninsula, in Barker, P.F., and Cooper, A.K., eds., Geology and seismic stratigraphy of the Antarctic margin, Part 2, Volume 71: Washington, DC, American Geophysical Union, p. 29-49.

Shackleton, N.J., Hall, M.A., and Pate, D., 1995. Pliocene stable isotope stratigraphy of site 846. In Pisias, N.G., Mayer, L.A., Janecek, T.R., Palmer-Julson, A., and van Andel, T.H. (Eds.), Proc. Ocean Drill. Program Sci. Results, 138: College Station, TX (Ocean Drilling Program), 337-353.

Scherer, R.P., 1993, There is direct evidence for collapse of the West Antarctic ice sheet: Journal of Glaciology, v. 39, p. 716-722.

Scherer, R.P., Aldahan, A., Tulaczyk, S., Possnert, G., Engelhardt, H.F., and Kamb, B., 1998. Pleistocene collapse of the West Antarctic ice sheet: Science, v. 281, p. 82-85.

Severinghaus, J.P., and Brook, E.J., 1999. Abrupt climate change at the end of the last glacial period inferred from trapped air in polar ice. Science, 286:930-934.

Shanmugam, G., 2000. 50 years of the turbidite paradigm (1950s-1990s): Deep-water processes and facies models - A critical perspective. Marine and Petroleum Geology, 17 (2):285-342.

Stoll, H.M., 2006. Climate change: The Arctic tells its story. Nature, 441 (7093):579-581.

Stocker, T.F., 1998. The seesaw effect. Science, 282:61-62.

Stocker, T.F., 2003. South dials north. Nature, 424:496-499.

Stocker, T.F., 2000. Past and future reorganizations in the climate system. Quaternary Sci. Rev., 19:301-319.

Tiedemann, R., Sarnthein, M., and Shackleton, N.J., 1994. Astronomic timescale for the Pliocene Atlantic d18O and dust flux records of Ocean Drilling Program Site 659. Paleoceanogr., 9 (4):619-638.

Uenzelmann-Neben, G., 2006, Depositional patterns at Drift 7, Antarctic Peninsula: Along-slope versus down-slope sediment transport as indicators for oceanic currents and climatic conditions: Marine Geology, v. 233, p. 49-62.

Vaughan, D.G., and Spouge, J.R., 2002. Risk estimation of collapse of the West Antarctic ice sheet. Climatic Change, 52 (1-2):65-91.

Villa, G., Persico, D., Bonci, M.C., Lucchi, R.G., Morigi, C., and Rebesco, M.A., 2003, Biostratigraphic characterization and Quaternary microfossil palaeoecology in sediment drifts west of the Antarctic Peninsula – implications for cyclic glacial-interglacial deposition: Palaeogeography, Palaeoclimatology, Palaeoecology, v. 198, p. 237-263.

Webb, P.-N., Harwood, D.M., McKelvey, B.C., Mercer, J.H., and Stott, L.D., 1984. Cenozoic marine sedimentation and ice volume variation on the East Antarctic craton. Geology, 12 (5):287-291.

Webb, P.-N., and Harwood, D.M., 1991. Late Cenozoic glacial history of the Ross Embayment, Antarctica. Quaternary Sci. Rev., 10 (2-3):215-223.

Weaver, A.J., Saenko, O.A., Clark, P.U., and Mitrovica, J.X., 2003. Meltwater Pulse 1A from Antarctica as a Trigger of the Bolling-Allerod Warm Interval. Science, 299:1709-1713.

Zachos, J.C., Pagani, M., Sloan, L., Thomas, E., and Billups, K., 2001. Trends, rhythms, and aberrations in global climate 65 ma to present. Science, 292:686-693.

Zwartz, D., Lambeck, K., Bird, M., and Stone, J.O., 1997. Constraints on the former Antarctic ice sheet from sea-level observations and geodynamic modelling. In Ricci, C.A. (Ed.), The Antarctic region: Geological evolution and processes. International Symposium on Antarctic Earth Sciences, 7: Siena (Terra Antarctica), 821-828.

2 Manuscripts

Published in Palaeogeography, Palaeoclimatology, Palaeoecology 231, 2006, p. 181-198

2.1 Manuscript 1: Pliocene glacial cyclicity in a deep-sea sediment drift on the Pacific Margin of the Antarctic Peninsula (ODP Leg 178, Site 1095)

Daniel A. Hepp[a,b], Tobias Mörz[b], Jens Grützner[a]

[a] Department of Geosciences, Bremen University, P.O. Box 330440, 28334 Bremen, Germany
[b] Research Center Ocean Margins, Bremen University, P.O. Box 330440, 28334 Bremen, Germany
Corresponding author. phone: +49 421-218-65844 / fax: +49 421-218-65810 / e-mail: dhepp@uni-bremen.de

2.1.1 Abstract

Giant deep-sea sediment drifts are widespread features along the continental rise of the West Antarctic Peninsula, representing the most proximal continuous sedimentary recorders for West Antarctic ice events and glacial-interglacial cyclicity. Sediment physical, geochemical records and X-ray images derived from ODP Leg 178 Site 1095 (Sediment Drift 7) show characteristics in glacial-interglacial cyclicity and associated sedimentary processes during early Pliocene. Two boundary types dividing half-cycles have been recognized: (1) interglacial-to-glacial transitions that are distinct and characterized by a sharp boundary and abrupt change in lithology, (2) glacial-to-interglacial transitions that are diffuse and characterized by a gradual decline of sediment physical and geochemical values with a marked reduction in sedimentation rates. The boundaries defined in conjunction with magneto- and biostratigraphic tie-points form the framework for the calculation of relative sedimentation and accumulation rates used for reconstructing early Pliocene paleoproductivity and terrigenous flux to the drift. Warm early Pliocene climate conditions for West Antarctic Peninsula region are indicated by open ocean conditions in glacials, short residence times of the grounded ice sheet at the shelf edge with sporadic fluctuations as well as periodic collapses of the ice-sheet front. We propose a 5-phase drift sedimentation model for the early Pliocene and postulate a highly dynamic ice sheet, likely reduced in thickness, resulting in oscillations which lie closer to the shelf edge than was the case during the late Quaternary.

Keywords: Antarctic Peninsula, deep-sea sedimentation, drift, early Pliocene, Leg 178, Ocean Drilling Program, paleoclimatology, sedimentary processes, ODP Site 1095

2.1.2 Introduction

The combined East and West Antarctic ice sheets are the largest on earth today. Both have acted as key components in the global climate regime since the late Eocene (Lawver et al., 1992; Fitzgerald, 1999; Exon et al., 2000; O'Brien et al., 2000). They influence the albedo, widely initiate and terminate ocean thermohaline circulation, control eustatic sea levels, and their absolute volume is a major source in the global oxygen isotopic record (Barker and Cooper, 1997; Thiede and Tiedemann, 1998; Barker and Camerlenghi, 1999). The compilation of benthic oxygen isotope data describes a general cooling trend for the global climate during the Neogene (Zachos et al., 2001). Within this general cooling trend, a number of global warming and cooling episodes can be identified (Grützner et al., 2005).

The Pacific margin off the Antarctic Peninsula is very sensitive to climate and ice-sheet volume changes (Goodridge, 2000; Stammerjohn et al., 2003). The geometric framework of a relatively narrow continental shelf area and an oversteepened continental slope (Camerlenghi et al., 1997a) interacts with long-term variations in the polar regime, glacial cyclicity and regional climatic and oceanographic conditions (e.g., bottom currents; Pudsey et al., 1994). Climatic variations on the Antarctic Peninsula continental shelf control regional sedimentary depositional processes and affect the build-up of giant deep-sea sediment drifts. These drifts are widespread features along the continental rise of the Antarctic Peninsula Pacific margin (Fig. 1; Rebesco et al., 1996; Pudsey and Camerlenghi et al., 1998), but comparable sediment mounds have been identified in the Central Bransfield Basin, Antarctic Peninsula (Canals et al., 2002), Wilkes Land, East Antarctica (Escutia et al., 2002; Busetti et al., 2003) and Prydz Bay, East Antarctica (Shipboard Scientific Party, 2001; Cooper and O'Brien, 2004).

Early Pliocene warm climate conditions are generally accepted for Antarctica (Andersson et al., 2002; Grützner et al., 2005). However, there is still controversial discussion on the East and West Antarctic ice-sheet response to these warmer oceanographic conditions. As a contribution to this discussion we report on early Pliocene cyclicity in sediments of Drift 7 and the parameters for the definition of glacial-interglacial boundaries. Sediment physical and geochemical proxy data in combination with X-ray images are used to describe and characterize glacial and interglacial intervals. We present a new model for early Pliocene drift formation and compare the model to those for sedimentation in late Quaternary time, in terms of climate conditions, ice-sheet dynamics and ice-sheet volumes. Our study is based on three sections of the uppermost (~3.6-3.8 Ma), middle (~4.0-4.2 Ma) and lowermost (~5.1-5.2 Ma) early Pliocene (102-112, 121-130, and 169-177 meters below seafloor = mbsf, Fig. 2), Ocean Drilling Program (ODP) Leg 178 Site 1095.

2.1.3 Regional setting

The topographical settings of the Pacific margin off the Antarctic Peninsula have been well described in several bathymetric, seismic and sediment-based studies (Tucholke et al., 1976; Larter and Barker, 1989; Anderson et al., 1991; Tomlinson et al., 1992; Rebesco et al., 1996; 1998; 2002; Camerlenghi et al., 1997a; Pudsey and Camerlenghi et al., 1998; Canals et al., 2000; Pudsey, 2000; Barker and Camerlenghi, 2002; Lucchi et al., 2002b). The sequence stratigraphy of the outer continental shelf evolution (foresets and topsets) has been reconstructed on the basis of the sedimentological interpretation of acoustic profiles and sediment cores (Barker, 1995; Bart and

Anderson, 1995; Eyles et al., 2001). A series of eight sediment drifts on the upper continental rise is directly associated with the glacial morphology of the outer continental shelf (Fig. 1; Faugères et al., 1999; Pudsey and Camerlenghi, 1998; Rebesco et al., 2002). These sediment drifts are part of a complex glacial sedimentary feeder system composed of lobes and troughs on the outer shelf, a steep slope (average 16°; Rebesco et al., 1996), and deep-sea channels separating the drifts on the upper rise. The channel system, separating the drifts from each other and the continental slope, is formed by downslope turbidity currents and alongslope bottom currents (Rebesco et al., 1997; Pudsey and Camerlenghi, 1998). The drifts are primarily composed of fine-grained components from turbidity currents (Rebesco et al., 1996). Fine silt laminae, primarily observed in cores from distal drift sites, are interpreted as turbiditic spillover depositions (Pudsey, 2000; Barker and Camerlenghi, 2002; Lucchi et al., 2002b). Significant turbidity currents were channeled along the bathymetric depressions between the drifts.

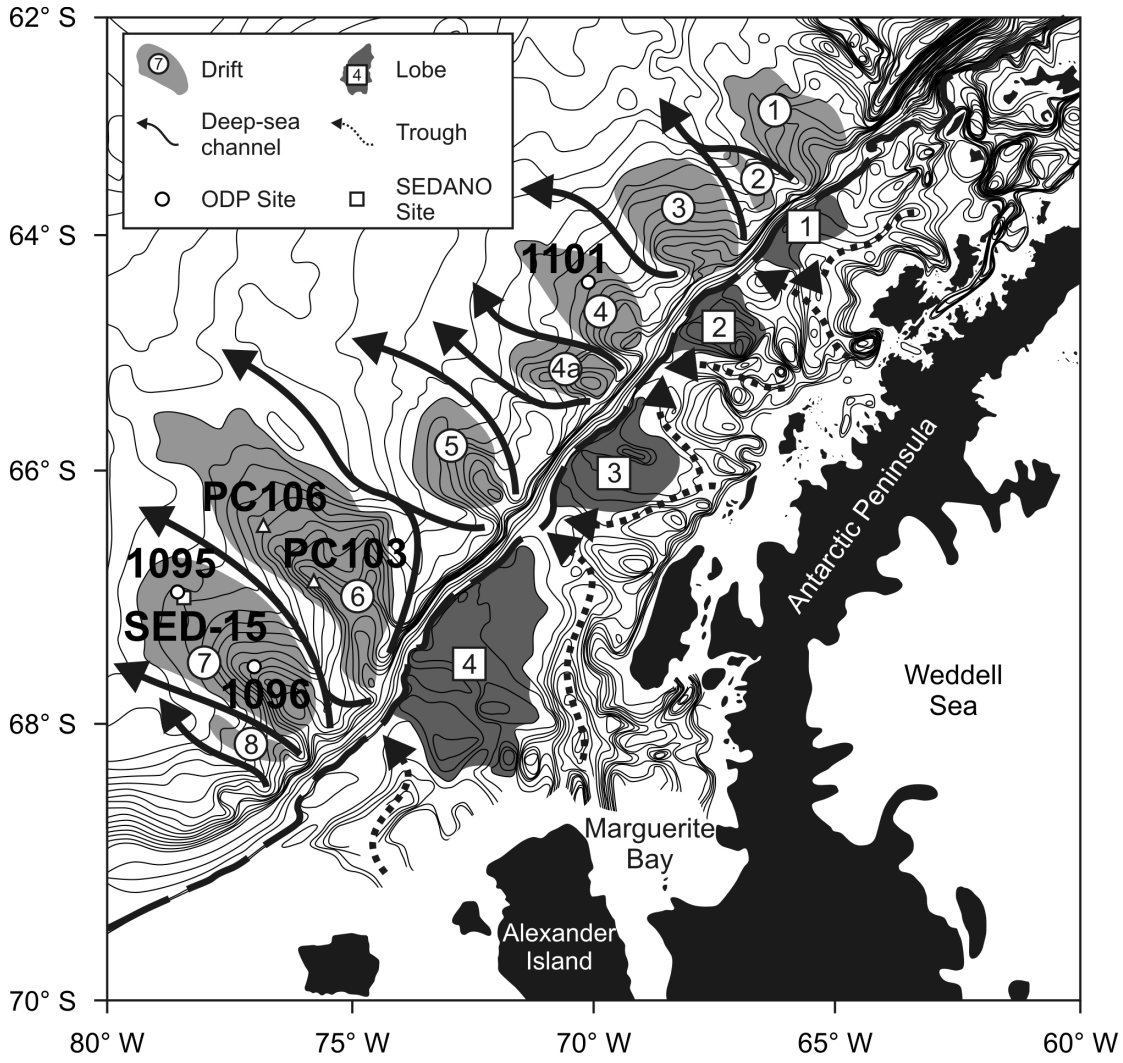

Fig. 1. Bathymetric map of Antarctic Peninsula Pacific margin showing a glacially controlled sediment feeder system of lobes and troughs on the outer shelf linked to deep-sea channels and drifts on the upper rise, and a relatively narrow shelf and a very steep slope (modified after Lucchi et al., 2002 and Rebesco et al., 2002).

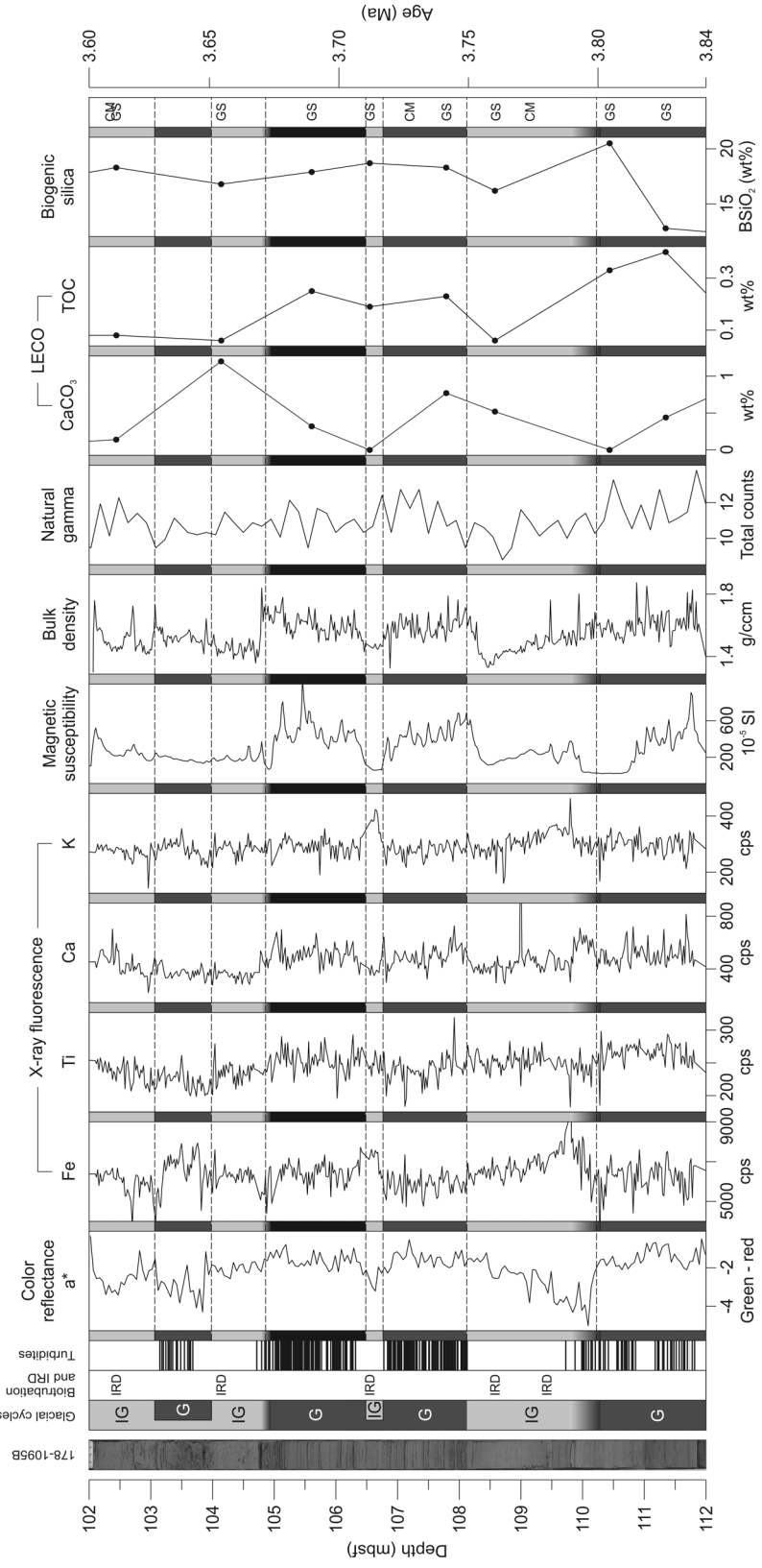

Fig. 2a. Comparison of visual description, color reflectance, XRF, logging and biostratigraphic data (ODP Site 1095B) from the (a) uppermost early Pliocene (102-112 mbsf, ~3.6-3.8 Ma), (b) middle early Pliocene (121-130 mbsf, ~4.0-4.2 Ma), and (c) lowermost early Pliocene (169-177 mbsf, ~5.1-5.2 Ma). The data show characteristic patterns of glacial-to-interglacial (GIGT) and interglacial-to-glacial transitions (IGGT; CM = clay minerals, G = glacial, GS = grain size, IG = interglacial, IRD = ice rafted debris). Boundaries beyond the figures depth range: (a) 113.28 and 102.08, (b) 130.48 and 120.81, and (c) 177.60 and 168.53.

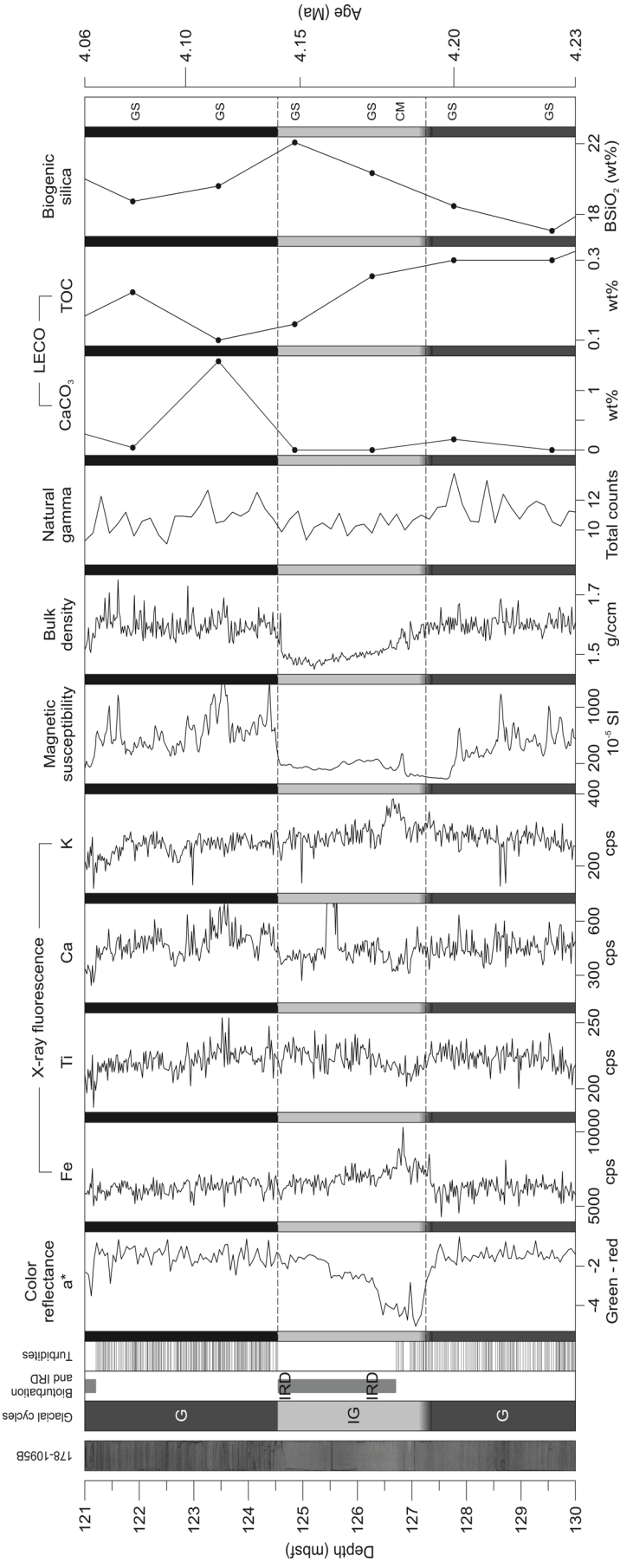

Fig. 2b. See caption above.

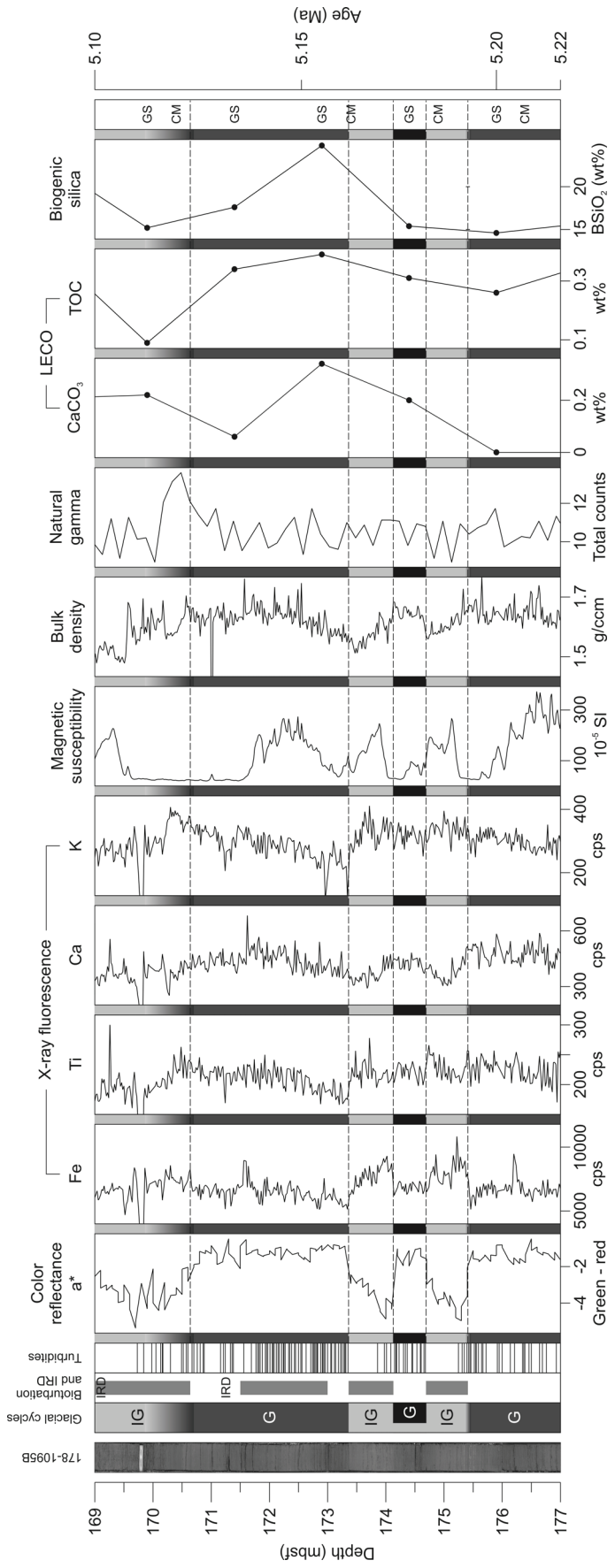

Fig. 2c. See caption above.

Drift 7 is one of the largest sediment drifts located to the southwest of the Antarctic Peninsula (Fig. 1). Its asymmetrical shape, with a short steep side facing southeast and a long gently-sloping side facing northwest, is similar in shape to sediment drifts in this area. Drift build-up occurs by glacially driven turbidity currents and the interglacial pelagic settling. The shapes were formed by weak non-erosive bottom currents flowing along the bathymetric contour (Camerlenghi et al., 1997a; Pudsey and Camerlenghi, 1998).

Sediment Drift 7 and the proximal area were drilled by advanced piston corers (APC) and extended core barrels (XCB) at two sites (Site 1095 and 1096) during ODP Leg 178 (Shipboard Scientific Party, 1999a), and by short piston corers at 19 sites (SED-1 to SED-19) during SEDANO (SEdiment Drifts of the ANtarctic Offshore) Project-I and -II (Lucchi et al., 2002a; 2002b; Pudsey and Camerlenghi, 1998; core SED-15 is located on Drift 7, Fig. 1). Both projects provided sediment cores with prominent glacial cyclicities. The SEDANO cores are up to 7 m long and cover the isotopic stages 1-11, whereas the ODP cores, with recoveries of up to 600 m length, provide a 10-my sedimentary record. The SEDANO-I survey (1995) examined contour current patterns in the area of Drift 7, which contributes to the drift surface (Camerlenghi et al., 1997b; Pudsey and Camerlenghi, 1998). The short piston cores collected during the SEDANO-II project (1997-1998) document the major large-scale processes which govern the bottom current regime (Lucchi et al., 2002b; Giorgetti et al., 2003; Villa et al., 2003). Our investigations focus on Site 1095 cores collected from multiple Holes A and B during ODP Leg 178 in 1998 (Fig. 1). 1095A was cored from 0 to 87.79 (mbsf) with 99.1% recovery, core 1095B was recovered from 83 to 561.78 mbsf with 79.2% recovery. Together, both cores comprise a continuous record from the Holocene to the late Miocene (~10 Ma).

For the Holocene/Pleistocene time section, several authors have developed models of sedimentary processes for the Antarctic Peninsula continental rise (Grobe and Mackensen, 1992; Pudsey and Camerlenghi, 1988; Pudsey, 2000; Leventer et al., 2002; Lucchi et al., 2002b; Villa et al., 2003). These researchers have proposed that glacial periods are characterized by grounded ice sheets extending across the continental shelf edge combined with closed sea-ice cover. Sedimentary supply to the drift during this stage is dominated by turbidity currents triggered by shelf-ice advance, whereas biogenic supply and ice-rafted debris (IRD) is reduced. Interglacials are dominated by high biogenic productivity, iceberg calving and reduced terrigenous supply from the shelf in conjunction with a retreated ice sheet.

2.1.4 Methods

Our study is based on a cm-scale visual reexamination of sedimentary features at ODP Site 1095 in combination with new high-resolution geochemical core logging data, shipboard physical property records, and published biogenic opal measurements (Fig. 2). We re-opened the 600-m-long core for cm-scaled description with primary focus on turbidite and ice-rafted debris (IRD) distribution and their relation to color changes. New digital X-ray images were made from selected core sections (Fig. 3). Characteristic patterns have been used as prominent visual proxies of glacial-interglacial transitions.

X-ray fluorescence (XRF) measurements were carried out at the Bremen IODP Core Repository using an XRF scanner. This non-destructive method yields element intensities on the surface of split sediment cores and provides statistically significant data for the elements Fe, Ti, Ca, K, Mn, and Sr. (Jansen et al., 1998; Westerhold, 2003). High-resolution data sets (2-cm intervals) of Fe,

Ti, Ca, and K have been used in this study. Fe and Ti are interpreted as indicators of terrigenous components, whereas Ca mainly reflects the biogenic $CaCo_3$ content of sediments. The data are given as element intensities in counts per second (cps).

Physical properties were obtained during ODP Leg 178 using the shipboard whole-core multisensor track logger (Shipboard Scientific Party, 1999b). Magnetic susceptibility and bulk density were measured at 2-cm intervals while total natural gamma radiation measurements were taken at 15-cm intervals (data are available from Janus Web Database < http://www-odp.tamu.edu/database/>).

Diffuse spectral reflectance measurements using a Minolta color scanner (5-cm intervals) were taken immediately after core splitting to minimize redox-associated color changes (Wolf-Welling et al., 2002a). The data are given using the CIELAB system, which provides lightness (L*) and chromaticity (a* and b*) parameters. Here, we prefer to use the green-red color ratio indicated by parameter a*, because it seems to be most significant for the cores.

Opal contents were analyzed in 320 samples from Holes 1095A and 1095B (Hillenbrand and Fütterer, 2002). Sample spacing is equivalent to time intervals of 31 ka. Total organic carbon (TOC) measurements were taken on a total of 325 samples (one sample per core section) using a LECO CS-125 analyzer (Wolf-Welling et al., 2002b). Grain-size data sets (~20-ka resolution) from Mörz and Wolf-Welling (2002) and clay mineral data from Hillenbrand and Ehrmann (2002) were used for interpretation.

For preliminary age calibrations for Site 1095, we computed a linear interpolated age model from magnetostratigraphic-biochronologic tie-points given in Acton et al. (2002) and Iwai et al. (2002). Site 1095 was not fully multiple-cored, so that coring gaps hold some uncertainties in core continuity (Barker, 2002).

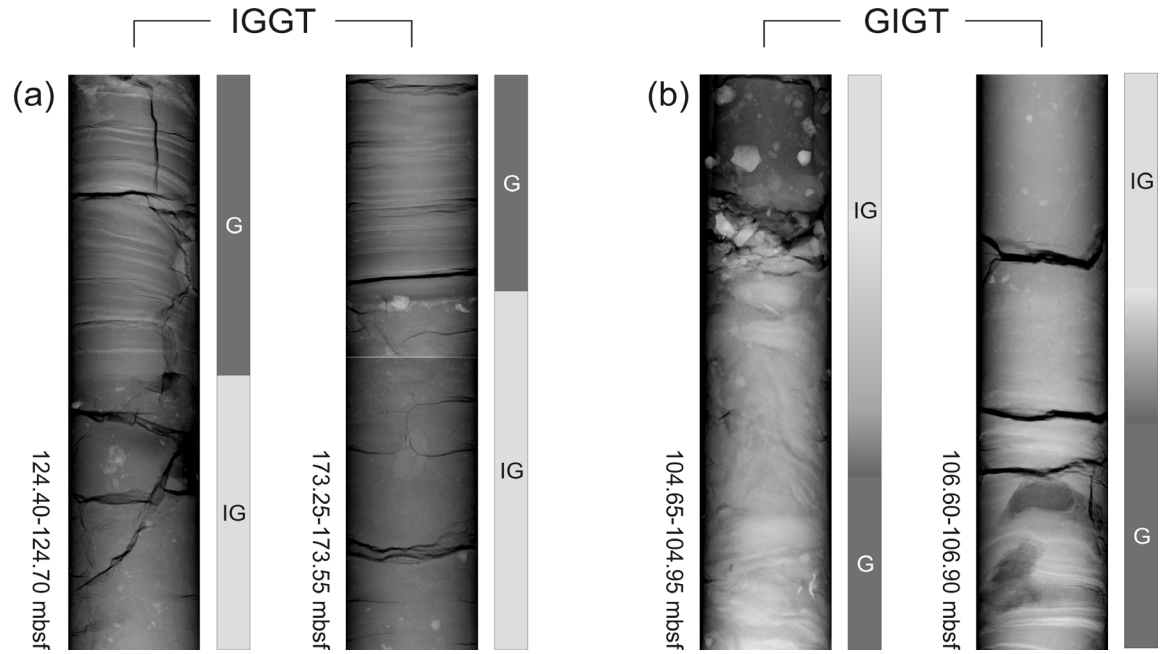

Fig. 3. The X-ray images (ODP Site 1095B) show two characteristic types of glacial-interglacial boundaries: (a) a sharp boundary dividing interglacial IRD supply from glacial turbidite events at interglacial-to-glacial transitions (124.70-124.40 and 173.55-173.25 mbsf) and (b) a gradual decay of turbidite events vs. increase of IRD supply at glacial-to-interglacial transitions (104.95-104.65 and 106.90-106.60 mbsf). The IRD layer in (c) is interpreted as ice sheet collapse zone.

2.1.5 Results

Core description, physical property and chemical data were used to identify characteristics of glacial and interglacial units and associated sedimentary processes (Fig. 2). The following results are given in upcore direction.

In general light greenish-gray units of core sections alternate with dark greenish-gray units. These units are defined by two characteristic color transitions. The dark-to-light transition (DLT) is shaped gradually (e.g. at 177.60, 175.41, 174.13, 170.64, 127.30, 120.81, 110.22, 106.77, 104.86, and 103.03 mbsf; Fig. 2 and 3b) whereas the light-to-dark transition (LDT) is commonly sharp (e.g. at 174.69, 173.36, 168.53, 130.48, 124.54, 113.28, 108.12, 106.49, 103.98, and 102.08 mbsf; Fig. 2 and 3a). The DLT and LDT patterns are systematic throughout the core sections observed. The alternations are best expressed in the color reflectance parameter a* (more negative values are brighter in color), the transitions are not always represented in the a*-values. Exceptions are the short units with abrupt changes in a*-values between 175.41 and 173.36 mbsf (Fig. 2c). All core sections are characterized by a gradual increase in a*-values in the light units, starting with an abrupt negative peak above, at the DLT. This negative peak occurs persistently at zones in which silt laminae occur within the light units (175.41-175.25, 174.13-173.86, 170.64-169.73, 127.30-126.71, 110.22-109.72 mbsf).

			Glaciation (b)		Glacial (c)	Deglaciation (d) and (e)		Interglacial (a)
			Glaciation IG	Glaciation G		Deglaciation G	Deglaciation IG	
Color a*	green-red	mean	**-1.94**	**-1.70**	**-1.54**	**-1.81**	**-3.32**	**-2.51**
		1*σ	0.56	0.58	0.46	0.47	1.00	0.55
Fe	cps	mean	**6401.97**	**6022.48**	**6279.42**	**6342.53**	**7222.00**	**6535.97**
		1*σ	510.34	589.72	574.16	799.93	1017.21	365.36
Ti	cps	mean	**210.01**	**192.57**	**209.88**	**214.97**	**200.66**	**198.20**
		1*σ	17.08	16.85	17.87	19.15	23.23	20.81
Ca	cps	mean	**379.61**	**467.71**	**539.67**	**459.23**	**431.44**	**449.37**
		1*σ	51.27	72.61	87.71	59.40	104.24	162.79
K	cps	mean	**283.57**	**266.84**	**277.19**	**311.22**	**321.21**	**279.29**
		1*σ	31.17	40.50	31.49	32.32	40.51	32.10
MagSus	SI	mean	**263.05**	**378.85**	**588.14**	**97.10**	**105.74**	**163.08**
		1*σ	197.16	263.42	222.18	168.29	92.23	28.22
Bulk Density	g/cm3	mean	**1.50**	**1.56**	**1.61**	**1.60**	**1.55**	**1.40**
		1*σ	0.10	0.08	0.07	0.14	0.08	0.04
Natural Gamma	total counts	mean	**10.36**	**10.53**	**11.12**	**11.23**	**11.01**	**9.96**
		1*σ	0.61	0.80	0.78	0.79	1.10	0.81

Tab. 1. Summary of early Pliocene physical and chemical high resolution parameters of ODP Site 1095B cores used during this study. The core data illustrate (a) three interglacials (169.4-169, 125.7-125.5 and 108.9-108.5 mbsf), (b) three glaciation phases (108.27-108.12-107.87, 124.69-124.54-124.39 and 173.51-173.36-173.21 mbsf), (c) three glacials (123.8-123.4, 111.7-113.3 and 105.8-105.4 mbsf), and (d-e) five deglaciation phases (105.26-104.86-104.46, 110.62-110.22-109.86, 127.7-127.3-126.9. 171.04-170.64-170.24, and 175.81-175.41-175.01 mbsf). The captions (a-e) refer to the climate stages of the model of early Pliocene depositional processes (Fig.4a-e).

The occurrence of silt laminae, ice-rafted debris (IRD) and bioturbation in the core sections we examined follows a clear pattern. The dark units are characterized by highly frequent silt laminae and a lack of IRD (excepted three small dropstones at 171 mbsf; Fig. 2c). Commonly, silt laminae thickness ranges between <1 and 4 mm. Silt laminae frequency decays in the lowermost portion of the light units, whereas the middle and upper portion are free of silt laminae, but commonly contain IRD (e.g. at 169.04 and 109.42 mbsf). The LDT is marked by a sharp boundary separating the IRD occurrence of the light unit from the onset of silt laminae in the overlying dark unit (Fig. 3a). The grain-size spectrum of all silt laminae is strictly within the silt range. The IRD content of the light units varies between 1 and 6% (6% at 102.44 mbsf) and has been extracted from the fraction >63-µm of wet sieved samples. A large dropstone (3 cm in diameter) was observed at 109.42 mbsf (Fig. 2a).

Bioturbation is common in the light units, independently of silt laminae or IRD occurrences (175.41-174.69, 174.13-173.36, 170.64-169.0, and 126.71-124.54 mbsf). Bioturbation in the light units never passes the LDT. We found only one example of a bioturbated dark section between 173.0 and 171.5 mbsf.

In general, geochemical and geophysical data show trends that mimic the alternations of dark and light units and their transitions. Fe and Ti trends are generally synchronous, but the variance of Ti values is less pronounced. Fe values in the dark units are rather monotone (e.g., between 130.0 and 127.43 mbsf: values vary around 6,140 cps), whereas values show clear trends in the light units (e.g., between 126.84 and 124.54 mbsf: values decrease from 10,300 to 6,760 cps). Averages of neighboring dark and light units indicate that Fe content in the light units is slightly higher (Tab. 1). The trend in Fe counts is inversely correlated to the trend in color reflectance. In all core sections a gradual Fe decrease is observed within the light units, starting with an iron peak above the DLT, where silt lamination terminates (175.30, 174.0, 170.30, 126.84, 109.79-110.08, and 106.64 mbsf). In some sections (175.41-174.13, 127.43-126.36, and 110.22-109.38 mbsf) the progression of Fe and Ti is opposite. In general, Ca values follow the Ti trend, whereas K values resemble the Fe trend. In summary, we note that the XRF data have maximum amplitudes at the termination of the silt-laminae zone above the DLT, whereas the LDT is characterized by an abrupt increase and/or decrease in values.

Magnetic susceptibility data show highly variable values in dark units and generally lower values in the light units. The DLT is characterized by zones of depressed magnetic susceptibility values with zero variance, extending from the upper portions of the dark units to the termination of the silt laminae at 175.62-175.26, 174.31-174.0, 171.65-169.51, 127.75-126.85, and 110.97-110.76 mbsf. The LDT is marked by a positive excursion of values (e.g., at 124.54, and 108.42-108.12 mbsf). Within the light units, magnetic susceptibility values gradually decrease toward the LDT. Similar to color reflectance and XRF data, the magnetic susceptibility trend shows a large peak above the DLT in light units (175.12, 173.89, 126.81, 109.81, 104.80, and 104.57 mbsf).

Bulk density values show a consistent alternation of high values in the dark units and lower values in the light units, with a gradual decreases in DLT and an abrupt increases in LDT (e.g., at 124.54 mbsf the bulk density increases from 1.35 to 1.58 g/ccm, and at 108.12 mbsf the bulk density increases from 1.43 to 1.66 g/ccm; Fig. 2a and 2b). Increases and decreases in bulk density are positively correlated to silt laminae frequency in dark units and during the DLT. The general decline in bulk density of those parts of light units without silt laminae correlates with a decrease in IRD concentration and with a likely increase in biogenic silica content (e.g., 126.71-124.54 mbsf; Fig. 2b).

The low-resolution natural gamma dataset suffers additionally from short measurement times, resulting in less distinct trends. The natural gamma value trend is best correlated to K data. A summary of all data described is given in Tab. 1.

Total organic carbon content (TOC) is generally very low at Site 1095 (0.85 weight percent = wt% at maximum). Values range between 0.04 and 0.41 wt% (mean 0.23 wt%) and are higher in the dark units. In contrast to TOC, the biogenic silica concentration is remarkably high in dark and light units, ranging between 12.1 and 24.8 wt%. The mean value of the early Pliocene core section (17.36 wt%) is clearly higher than the average of the total 1095 core (13.9 wt%).

2.1.6 Discussion

Alternating color units are conspicuous characteristics for the core intervals selected and are often described for Antarctic Peninsula drift sediment cores (Pudsey, 2000; Lucchi et al., 2002b). The interpretation of these alternating intervals is generally accepted as glacial cyclicity. Dark units dominated by frequent silt laminae are interpreted as glacials intervals. Lighter units with IRD and bioturbation are interpreted as interglacials (Pudsey, 2000; Barker and Camerlenghi, 2002).

2.1.6.1 Definition of glacial and interglacial boundaries

We used shipboard sediment physical properties, new XRF data and X-ray images to define glacial and interglacial cycles of the early Pliocene for the first time (Fig. 2 and 3). Two characteristic transitions were distinguished and defined by their steep geochemical and physical gradients.

Interglacial-to-glacial transition (IGGT, previously LDT) is distinct and characterized by a sharp decline in sediment lightness, an abrupt increase in Ca, magnetic susceptibility and bulk density and moderate decline in Fe values (Tab. 1). This is expressed lithostratigraphically by an abrupt end of IRD and bioturbation at the IGGT and the onset of frequent silt lamination directly above. This drastic change is clearly displayed in X-ray images (Fig. 3a).

Glacial-to-interglacial transition (GIGT, previously DLT) is diffuse and characterized by a gradual decline in sediment bulk density but prominent changes in color reflectance a*, Fe, Ti and Ca. Consistently, all GIGT's are accompanied by a minima zone in magnetic susceptibility which comprises the upper portion of glacials and lower portions of interglacials. The diffuse character of this transition is lithostratigraphically expressed by a gradual onset of IRD across the GIGT and a synchronous decay in silt laminae frequency (Fig. 3b).

We reviewed our definition of glacial-interglacial intervals with published grain size (Mörz and Wolf-Welling, 2002) and clay mineral data (Hillenbrand and Ehrmann, 2002; 2005) from the same core (Fig. 2). The coarse fraction (>63 μm) served as a proxy for IRD. In accordance with core observations and our definition of transitions, coarse fractions larger than 1 wt% occurred only in interglacials. Clay mineral assemblage deposits at the Antarctic Peninsula continental rise alter between two end-member compositions characterizing glacial and interglacial conditions. Eleven samples from Hillenbrand and Ehrmann (2002) covering the studied core sections confirm to our definition of transitions. The shelf source and ice-derived end member characterized by <20% smectite and >40% chlorite occur only in intervals characterized as glacial whereas the smectite dominated samples occur only in intervals characterized as interglacial.

2.1.6.2 Sedimentation rates, cyclicity and accumulation of biogenic silica

Based on magnetostratigraphic and biostratigraphic age tie-points (Acton et al., 2002; Iwai et al., 2002), the average sedimentation rate (SR_{av}) for the entire early Pliocene is:

$$(1)\quad SR_{AV} = \frac{\Delta Depth}{\Delta Age} = \frac{17786\ cm - 10099\ cm}{5.23\ ka - 3.58\ ka} = 4.66\ cm/ka$$

In addition, we calculated the average interval thickness of six glacials (GIT_{av} = 3.02 m) and five interglacials ($IGIT_{av}$ = 2.36 m) based on our defined glacial and interglacial boundaries. Boundaries of glacial and interglacial intervals that lie above and below the depth range shown in Fig. 2 were identified in the cores using the criteria outlined above (section 3 and 5.1), and were included in this calculation. Despite some variations in interval length, the thickness ratio between neighboring intervals are notably similar. Short-term excursions within major intervals remained unconsidered (174.69-174.13 mbsf and 103.98-103.06 mbsf; Fig. 2a and c). The average glacial-to-interglacial thickness ratio ($Ratio_{GIT/IGIT}$) is:

$$(2)\quad Ratio_{GIT/IGIT} = \frac{GIT_{av}}{IGIT_{av}} = 1.27$$

This average ratio is considered to be representative of the early Pliocene cyclicity at Site 1095, since we examined core sections spanning the whole early Pliocene.

The average cycle duration (CD_{av}) is estimated from the combined average glacial-interglacial thickness and the average sedimentation rate:

$$(3)\quad CD_{av} = \frac{(GIT_{av} + IGIT_{av})\,100}{SR_{av}} \approx 115\ ka$$

Tentatively we deduce a 100-ka eccentricity signal for the early Pliocene. This contradicts purely parameter-based cyclicity calculations by Pudsey (2002) and Lauer-Lerede et al. (2002) which do not see a clear astronomical forcing. If we assume that glacial and interglacial intervals are of nearly identical duration, then we can estimate average sedimentation rates of 5.55 cm/ka for glacials (SR_G) and of 3.92 cm/ka for interglacials (SR_{IG}) during the early Pliocene.

Accumulation rates for biogenic silica reveal important information concerning ocean circulation and paleoproductivity (Anderson et al., 2002; DeMaster, 2002). Today the bulk accumulation of biogenic silica takes place within the “opal belt” south of the Antarctic Polar Front (APF; Anderson et al., 2002; Raguenau et al., 2000). Wind-driven upwelling from the Antarctic circumpolar current (ACC) supplies surface waters with high nutrient concentrations (Anderson et al., 2002). This nutrition delivery and the cold surface waters of the Southern Ocean prevail in a complex system of production and accumulation of biogenic opal. The export of opal to the sea floor is controlled by the efficiency of the Southern Ocean’s biological pump (Anderson et al., 2002). The preservation of biogenic silica in marine sediments depends on dissolution in the water column and surface sediments. Main controlling factors are water temperature, water depth and sedimentation rate (Hillenbrand and Fütterer; 2002). These need to be considered when using the opal record of our drift sediments as a proxy for paleoproductivity.

We calculated accumulation rates of biogenic silica (AR_{Opal}) for glacials and interglacials of the early Pliocene were calculated using opal data from Hillenbrand and Fütterer (2002).

$$(4)\quad AR_{Opal} = SR_{av} \cdot [WD_{BULK} - (1.0363 \cdot POR \cdot 100^{-1})] \cdot SIO2_{BIO} \cdot 100^{-1}$$

Wet bulk density (WD_{BULK}), porosity (POR) and opal content ($SIO2_{BIO}$) were taken from the ODP Janus Web Database, and 1.0363 is a correction value for porewater (Boyce, 1976). We considered the well-established SR_{av} value to be less biased than our estimated individual SR_G and SR_{IG} values. As an example interglacial opal accumulation rates are 0.55 (108.72 mbsf) and 0.67 g/cm^2*ka (124.85 mbsf), whereas in adjacent glacial intervals the rates are 0.93 (107.98 mbsf) and 0.87 g/cm^2*ka (123.92 mbsf), respectively.

However, due to limited opal sample measurement, the calculated opal accumulation for glacials may be overestimated by the presence of up to 30% (by volume) silt laminae with low opal contents and by the observation that higher sedimentation rates during glacials favored opal preservation (Hillenbrand and Fütterer, 2002).

2.1.6.3 Early Pliocene model of sedimentary processes and environmental conditions

Based on our definition of glacial and interglacial boundaries, we propose a 5-phase model to reconstruct early Pliocene drift sedimentation processes (Fig. 4).

2.1.6.3.1 Interglacial conditions

The interglacial stage (Fig. 4a) is dominated by the pelagic settling of biogenic and terrigenous materials, the latter derived from ice rafting and wind transport. The absence of silt laminae and the presence of low bulk densities indicate little debris export to the slope, which in turn suggests that the shelf ice was of minimal extent. High eustatic sea-level at this time facilitate iceberg rafting across the shelf edge, as documented in a continuous IRD record. Low sedimentation rates permit the active bioturbation of surface sediments.

Opal content in the early Pliocene section at Site 1095 is generally higher (average 18 wt%) than for the late Quaternary (average 8 wt%; data from Hillenbrand and Fütterer, 2002). During the early Pliocene, the climate over the Southern Oceans was warmer than today (Barker et al., 1999).

The Northern Component Water (NCW; Hillenbrand and Fütterer, 2002) may have strengthened at this time, and increased heat input and upwelling of Circum Polar Deep Water (CPDW) close to the shelf break. This in turn led to warmer surface water conditions south of the APF, reduced or no sea ice and enhanced opal deposition. The early Pliocene sedimentation regime resembles late Quaternary interglacial scenarios developed by Lucchi et al. (2002b) and Pudsey (2000).

Early Pliocene interglacial Ca values are very low in comparison to Pleistocene interglacial measurements of Pudsey (2000). The low Ca values in surficial drift sediments in early Pliocene may result from enhanced Ca dissolution caused by the rise of carbonate compensation depth (CCD). A rise of the CCD in interglacials and lowering of the CCD in glacials is caused by a strengthening of southward-flowing Northern Component Water (NCW), which is analogous to modern Northern Atlantic Deep Water (NADW; Grobe and Mackensen, 1992; King et al., 1997). Therefore, the Ca signal may only reflect a change in the CCD and cannot be used here as a proxy for paleoproductivity.

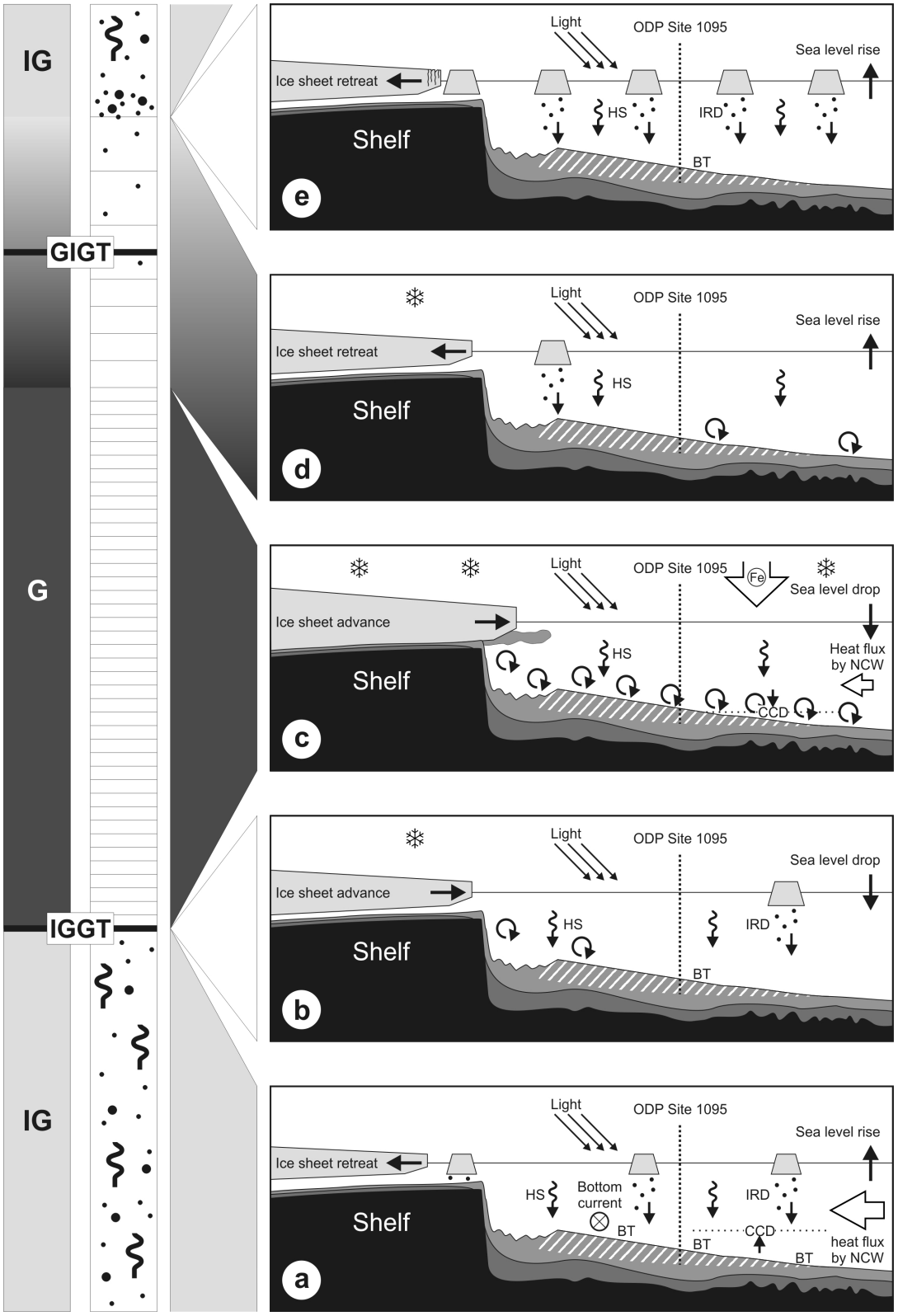

Fig. 4. Model of depositional and erosional processes for the early Pliocene. The synthesis of turbidite frequency, IRD and bioturbation occurrence, opal contents, color reflection, sedimentation and accumulation rates, and interpretation of X-ray images lead us to differentiate five characteristic climatic stages (a = interglacial, b = glaciation phase, c = glacial maximum, d = deglaciation phase, e = ice-sheet collapse) with two distinct transitions, see text for discussion. Shelf ice advance/retreat and sea level variation is primarily reflected in sedimentary features such as turbidite events (rotating arrows), ice-rafted debris (IRD), hemipelagic settling (HS), and bioturbation (BT). Heat flux intensity by Northern Component Water (NCW) and variation of carbonate compensation depth (CCD) are reflected in opal and biogenic carbonate content in drift sediments. The profile of Drift 7 is modified from multichannel seismic profiles and interpretations of Volpi et al. (2003).

The bottom-current transport of smectite along the continental rise, from its source on the continental shelf northwest of the Antarctic Peninsula, becomes important in interglacials (Hillenbrand and Ehrmann 2002; 2005).

2.1.6.3.2 Glaciation phase: interglacial-to-glacial transition (IGGT)

We characterized the sharp IGGT (Fig. 4b) with Ca, magnetic susceptibility and bulk density data and high-quality X-ray images (Fig. 2 and 3). The IGGT is marked by a sharp boundary separating the IRD occurrence in interglacials from the onset of silt laminae in glacials (Fig. 3a). The sharpness of IGGT stands in stark contrast to late Quaternary interglacial-to-glacial transitions, which have been described as more gradual by Lucchi et al. (2002b).

Our examples show a distinct change in smectite-chlorite ratio and an abrupt end in IRD, whereas Lucchi et al. (2002b) described a gradual decrease in smectite and mixing with chlorite towards the transition and an upcore decrease in IRD.

The mechanism that causes this sharp transition is not understood, because building of an ice sheet commonly takes more time than its collapse. High opal contents across this transition indicate a reduced sea ice coverage. Therefore sea ice is would not be available to trap rafting ice bergs. Also a lowering of the sea level during the onset of renewed Antarctic glaciation would resulting in grounding of icebergs at the shelf edge. But, this process is not fast enough to explain the abrupt end in IRD supply at this transition. The abrupt transition could be caused by large changes in sedimentation rates at the end of the interglacial periods, however, there is no clear evidence for such changes in the sedimentary record. Possible consequences of an abrupt IGGT are a very rapidly advancing ice sheet and/or an ice sheet that is not fully retreated to the shore during interglacials.

2.1.6.3.3 Glacial maximum conditions

The sediments of the glacial maximum (4c) are dominated by terrigenous supply with high sedimentation rates, high bulk densities and an absence of bioturbation. The grounded ice sheet has reached its maximum extension and coarser terrigenous material is transported over the shelf edge to the oversteepened slope by continuous ice flow. Frequent slope failures trigger turbidity currents, which run in channels between the drifts to the abyssal plain. Turbidity events result in overspill silt laminae deposits on the distal part of Drift 7 (Lucchi et al., 2002b).

The absence of prominent IRD indicates that rafting icebergs did not reach the drift. This is different to late Quaternary drift cores, where IRD is still present in glacials. Ó Cofaigh et al. (2001) explain the reduction of IRD in glacials with terrigenic dilution as an effect of higher glacial sedimentation rates. This approach is not applicable for our sedimentation rate estimates (Eq. 1) and the near absence of IRD.

The general glacial oceanographic conditions of the early Pliocene differ considerably from Last Glacial Maximum scenarios and models (Grobe and Mackensen, 1992; Pudsey, 2000; Lucchi et al., 2002b), but seem to be similar to modern interglacial (rather than glacial) conditions (Anderson et al., 2002). High biogenic silica contents in early Pliocene glacials (up to 24 wt%) even exceed observations in the late Quaternary, which have up to 6 wt% in glacials and up to 14 wt% in interglacials (Hillenbrand and Ehrmann, 2002). Average accumulation rates of biogenic silica range from 0.079 to 0.075 g/cm^2*ka in late Quaternary glacials (marine oxygen isotope stages 2-4, and 6) and from 0.064 and 0.083 g/cm^2*ka in interglacials (marine oxygen isotope stages 5 and 7).

Accumulation rates have been calculated using average sedimentation rates of 5.0 cm/ka in glacials and 1.8 cm/ka in interglacials (Pudsey, 2000), opal data from Hillenbrand and Fütterer (2002), stage boundaries from Lucchi et al. (2002b) and ages from Martinson et al. (1987). Our estimate of combined glacial-interglacial early Pliocene opal accumulation is however ten times larger than for the Pleistocene. The relative glacial to interglacial opal accumulation ratio (AR_{OpalG} / AR_{OpalIG}) is ~1.5 in early Pliocene and ~1 in late Pleistocene, accentuating the comparable high opal contents of early Pliocene glacial drift sediments.

From the many factors controlling the efficiency of the Southern Ocean's biological pump, Hillenbrand and Fütterer (2002) regard sea-ice coverage as the main factor in limiting primary paleoproductivity at our proximal drift site. Warmer climate conditions without sea-ice coverage enhance light availability, while meltwater plumes and intensified poleward winds provide additional Fe-rich material to the nutrient budget (Anderson et al., 2002). Other factors influencing local primary production and preservation are air temperature, the upwelling rate of CDW or the geographic position of the APF. Higher Ca contents in the glacial early Pliocene drift sediments may be linked to a lowering of the CCD below surface drift sediments, indicating a decrease in NCW heat transfer compared to interglacial conditions. If we assume that no shift in the position of the bottom topography controlled APF (Anderson et al., 2002), then we must expect an intensified biological pump system similar to modern interglacial conditions with increased nutrient supply by glacial winds and subglacial meltwater plumes.

In contrast to the bottom-current transport of smectite along the continental rise during early Pliocene interglacials, glacials are marked by a increased chlorite input from the continental shelf and a strong decline of smectite (Hillenbrand and Ehrmann, 2002; 2005).

Sediment color hues are in general controlled by the concentration of iron rich minerals like oxides, oxyhydroxides, sulfides and iron-rich clay minerals, whereas the lightness of sediment is positively correlated to carbonate and opal contents and inversely correlated with TOC and manganese oxides (e.g., sediment becomes darker with increasing TOC; Potter et al., 1980; Balsam and Deaton, 1991; 1996; Mix et al., 1995; Giosan et al., 2002). We link the dark greenish-gray sediment color of Site 1095 glacials to the dominance of Fe^{2+}- and Mn-rich, shelf derived chlorite, whereas we link the reddish-brown color of interglacial Pleistocene core sections (ODP Site 1095A, 0-49.3 mbsf) to the occurrence of Fe^{3+} (e.g., from smectite). We interpret the light greenish-gray appearance of the early Pliocene interglacial as a result of diagenetic reduction of Fe^{3+} to Fe^{2+}. Lightness and green hue contrasts between the early Pliocene glacials and interglacials is again controlled by the chlorite flux, and is twice as high in glacials. TOC and Ca values are higher in early Pliocene glacials than in interglacials, may play a minor role in sediment lightness because their combined weight % is below 1.5.

2.1.6.3.4 Deglaciation phase: glacial-to-interglacial transition (GIGT)

The deglaciation phase (Fig. 4d) is accompanied by a minima zone in magnetic susceptibility at the GIGT, which comprises the upper portion of glacials and lower portions of interglacials. Lithostratigraphically, we observe a decay in silt laminae frequency synchronous with a gradual onset of IRD.

There are two approaches to explain the magnetic susceptibility minima zones: a change in source provenance or diagenetic alteration of magnetic minerals. A change in provenance could deliver non-magnetic material during the deglaciation phase. However, the occurrences of similar silt

laminae and constant bulk density values across the magnetic susceptibility minima zone suggest that sediment delivery did not change. More likely, the magnetic susceptibility minima zone is linked to diagenetic processes that transform magnetic iron minerals to paramagnetic minerals. Two diagenetic processes have been suggested: (1) anaerobic oxidation of methane at the sulfate methane transition with a release of hydrogen sulfide that in turn reduces ferrimagnetic magnetite to paramagnetic sulfides (e.g., Pyrite; Riedinger et al., in press), this process gets especially prominent in sections with low sedimentation rates and high organic fluxes, and (2) demagnetization by a transformation of magnetite to smectite caused by elevated dissolved silica concentrations in the porewater (Florindo et al., 2003). Both processes may play a role for ODP Site 1095. The GIGT in our early Pliocene drift sediments is especially vulnerable to diagenetic magnetite loss since grain sizes are smaller during the early phase of deglaciation and the decrease in siliclastic input combined with high biogenic opal fluxes lead to a reduction in sedimentation rate and high TOC.

We explain the low sedimentation rates by decrease of sediment supply to the shelf edge by grounded shelf ice which is still intact but starts to lift-off and slowly retreats from the shelf edge. The decay in turbidite occurrence may be explained by two scenarios: (1) a decrease in the frequency of ice advances to the shelf edge, or (2) an abrupt end of slope loading because ice does not deliver sediment to the shelf edge while the slope continuos to fail for a short period of time until it regains stability.

2.1.6.3.5 Ice-sheet collapse

At the end of the deglaciation phase, the shelf-ice sheet collapses rapidly (Fig. 4e). The disintegration of the shelf-ice front into icebergs, synchronous with a eustatic sea-level rise, initiates extensive iceberg rafting. This ice-sheet collapse and strong terrigenous supply to the drift is also expressed in maximum XRF data amplitudes (Fe, K). Terrigenous IRD supply marks the termination of the magnetic susceptibility minima zone by delivering less diagenetic vulnerable coarse material and rapidly increasing the sedimentation rate. No turbidite events occur after ice-sheet collapse.

2.1.6.4 Early Pliocene conditions

Early Pliocene warm climate conditions are generally accepted for Antarctica (Andersson et al., 2002; Grützner et al., 2005). Comparison with the global ice-volume curve by Lear (2002) confirms that the Messinian and the early Pliocene have been times of dramatically reduced ice volume.

There is still much controversial discussion on the East and West Antarctic ice-sheet response to warmer oceanographic conditions. The conflict between the warm stable ice-sheet hypothesis (Kennett and Hodell, 1993; Barker, 1995; Wilson, 1995; Barrett, 1999) and the early Pliocene deglaciation hypothesis (Webb et al., 1984; Webb and Harwood, 1991) is now almost 20 years old. According to the Pliocene warm stable ice-sheet scenario, ice sheets reached the continental shelf during glacial half-cycles, possibly for a greater fraction of time than in the late Quaternary, leading to increased sedimentation rates on the slope and rise. However, to compare sedimentation rates over time, it may be more accurate to use sedimentation rate ratios of the half-cycles ($Ratio_{GIT/IGT}$) to gain a measure for the time fraction of ice-sheet extension to the shelf edge. This in effect considers changes in drift morphology over time (e.g., changes in drift size and distance to the shelf edge as the drift develops). The late Quaternary $ratio_{GIT/IGIT}$ of ~2.78 is significantly higher than our estimate for the

early Pliocene of ~1.27 (see Eq. 2). We therefore conclude that ice sheets reached the continental shelf edge during early Pliocene glacial half-cycles, possibly for a smaller fraction of time than during the Pleistocene.

We postulate a fast moving and highly dynamic early Pliocene ice sheet, likely reduced in thickness but highly sensitive to Milankovich eccentricity forcing at 100-ka frequency. A fast ice sheet response time is inferred from the abruptness of the IGGT. Rapid ice sheet movements are derived from the frequent occurrence of short-term events (e.g., as seen in cores from 174.69-174.13, 106.77-106.49, and 103.98-103.06 mbsf; Fig. 2) where the ice sheet advances to the shelf edge during interglacials and retracts from the shelf edge during glacials. Glacial and interglacial short-term events may reflect an increased ice-sheet sensitivity to regional climate conditions through the early Pliocene. Milankovich eccentricity forcing for the early Pliocene Antarctic Peninsula drift deposits has also proposed by Iorio et al. (2005). This is in contrast to ice-shield autocyclicity for this time interval postulated by Pudsey (2001). Overall, ice sheet oscillations in early Pliocene may have occurred closer to the shelf edge and with shorter ice sheet residence times than during Pleistocene times.

High opal contents in glacial and interglacial intervals indicate a significant reduction in annual sea-ice coverage with a corresponding increase in general open ocean conditions. The temporary opening of polynyas is not sufficient to explain high glacial opal contents in the drift deposits (Lucchi et al., 2002b; Villa et al., 2003).

2.1.7 Conclusions

Sediment physical and geochemical properties in sediments of Drift 7 (West Antarctic Peninsula continental rise) provide a proximal record of early Pliocene West Antarctic ice-sheet dynamics. Boundaries of glacial and interglacial cycles were defined by their physical and chemical gradients and X-ray core images. Two characteristic transitions were distinguished by their steep gradients. The interglacial-to-glacial transition is distinct and characterized by a sharp boundary and abrupt changes in lithology. The factors controlling the rapid interglacial-to-glacial transition are not completely understood, but rapid ice re-advances may point towards an ice sheet which does not fully retreat to the shore during interglacials. The glacial-to-interglacial transition is diffuse, and is characterized by a gradual decline of sediment physical and geochemical values and a corresponding marked reduction in sedimentation rates. Periodic collapses of the ice-sheet front and discharge of ice bergs are indicated by numerous IRD occurrences. High opal contents in glacial and interglacial intervals indicate a significant reduction in annual sea-ice with corresponding increase in open ocean conditions. High paleoproductivity in glacials points toward warm oceanographic conditions with an increased nutrient flux. The presence of IRD throughout the early Pliocene cores implies to us that during interglacials the Antarctic Peninsula was not deglaciated. Common turbidite occurrences are consistent with a grounded ice sheet at the shelf edge during glacials. Low glacial-to-interglacial sedimentation rate ratios indicate that ice sheets reached the continental shelf edge for a smaller fraction of time during the early Pliocene.

Based on our observations we propose a 5-phase drift sedimentation model for the early Pliocene and postulate a fast moving and highly dynamic early Pliocene ice sheet, highly sensitive to Milankovich eccentricity forcing and regional climate conditions.

2.1.8 Acknowledgements

Samples were provided by Ocean Drilling Program (ODP). We thank the Bremen Core Repository (BCR) team for their kind support. X-ray images were carried out at the Rotes Kreuz Krankenhaus Bremen. This research was funded by the Deutsche Forschungsgemeinschaft (DFG project MO1059/1) and by the DFG-Research Center Ocean Margins (RCOM) of Bremen University (No. RCOM0284). We thank Alan Cooper, Michele Rebesco and Ellen Cowan for their helpful reviews which substantially improved the manuscript and Jayne Welling-Wolf and Thomas Wolf-Welling for carefully revising the English.

2.1.9 References

Acton, G.D., Guyodo, Y., Brachfeld, S.A., 2002. Magnetostratigraphy of sediment drifts on the continental rise of West Antarctica (ODP Leg 178, Sites 1095, 1096, and 1101). In: Barker, P.F., Camerlenghi, A., Acton, G.D., Ramsay, A.T.S. (Eds.), Proc. ODP, Sci. Res. 178. Texas A&M University, College Station, TX, pp. 1-61 [CD-ROM].

Anderson, J.B., Bartek, L.R., Thomas, M.A., 1991. Seismic and sedimentological record of glacial events on the Antarctic Peninsula shelf. In: Thomson, M.R.A., Crame, J.A., Thomson, J.W. (Eds.), Geological evolution of Antarctica. World and regional geology 1. Cambridge University Press, New York, pp. 687-691.

Anderson, R.F., Chase, Z., Fleisher, M.Q., Sachs, J., 2002. The Southern Ocean's biological pump during the Last Glacial Maximum. Deep-Sea Res. II 49,1909-1938.

Andersson, C., Warnke, D.A., Channell, J.E.T., Stoner, J.S., Jansen, E., 2002. The mid-Pliocene (4.3–2.6 Ma) benthic stable isotope record of the Southern Ocean: ODP Sites 1092 and 704, Meteor Rise. Palaeogeogr., Palaeoclimatol., Palaeoecol. 182, 165-181.

Balsam, W.L., Deaton, B.C., 1991. Sediment dispersal in the Atlantic Ocean: Evaluation by visible light spectra. Rev. Aquatic Sci. 4, 411-447.

Balsam, W.L., Deaton, B.C., 1996. Determining the composition of late Quaternary marine sediments from the NUV, VIS, and NIR diffuse reflectance spectra. Mar. Geol. 134, 31-55.

Barker, P.F., 1995. The proximal marine sediment record of Antarctic climate since the late Miocene. In: Cooper, A.K., Barker, P.F., Brancolini, G. (Eds.), Geology and seismic stratigraphy of the Antarctic margin. Antarctic Research Series 68. American Geophysical Union, Washington, DC, pp. 25-57.

Barker, P.F., Cooper, A.K., 1997. Preface. In: Barker, P.F., Cooper, A.K. (Eds.), Geology and seismic stratigraphy of the Antarctic Margin, Part 2. Antarctic Research Series 71. American Geophysical Union, Washington, DC, pp. XIII-XIV.

Barker, P.F., Barrett, P.J., Cooper, A.K., Huybrechts, P., 1999. Antarctic glacial history from numerical models and continental margin sediments. Palaeogeogr., Palaeoclimatol., Palaeoecol. 150, 247-267.

Barker, P.F., Camerlenghi, A., Acton, G.D. (Eds.), 1999. Proc. ODP, Init. Rpts. 178. Texas A&M University, College Station, TX, pp. 1-60 [CD-ROM].

Barker, P.F., 2002. Data report: Composite depths and spliced sections for Leg 178 Sites 1095 and 1096, Antarctic Peninsula continental rise. In: Barker, P.F., Camerlenghi, A., Acton, G.D., Ramsay, A.T.S. (Eds.), Proc. ODP, Sci. Res. 178. Texas A&M University, College Station, TX, pp. 1-15 [CD-ROM].

Barker, P.F., Camerlenghi, A., 2002. Glacial history of the Antarctic Peninsula from Pacific margin sediments. In: Barker, P.F., Camerlenghi, A., Acton, G.D., Ramsay, A.T.S. (Eds.), Proc. ODP, Sci. Res. 178. Texas A&M University, College Station, TX, pp. 1-40 [CD-ROM].

Barrett, P.J., 1999. Antarctic climate history over the last 100 million years. Terra Antarc. Rpts. 3, 53-72.

Bart, P.J., Anderson, J.B., 1995. Seismic record of glacial events affecting the Pacific margin of the northwestern Antarctic Peninsula. In: Cooper, A.K., Barker, P.F., Brancolini, G. (Eds.), Geology and seismic stratigraphy of the Antarctic margin. Antarctic Research Series 68. American Geophysical Union, Washington, DC, pp. 75-95.

Boyce, R.E., 1976. Definitions and laboratory techniques of the compressional sound velocity parameters and wet-water content, wet-bulk density, and porosity parameters by gravimetric and gamma-ray attenuation techniques. In: Schlager, S.O., Jackson, E.D. et al., Init. Rpts. DSDP 33. U.S. Govt. Printing Office, Washington, DC, pp. 1115-1128.

Busetti, M., Caburlotto, A., Armand, L.K., Damiani, D., Giorgetti, G., Lucchi, R.G., Quilty, P.G., Villa, G., 2003. Plio-Quaternary sedimentation on the Wilkes Land continental rise: Preliminary results. Deep-Sea Res. II 50, 1529-1562.

Camerlenghi, A., Crise, A., Pudsey, C.J., Accerboni, E., Laterza, R., Rebesco, M.A., 1997a. Ten-month observation of the bottom current regime across a sediment drift of the Pacific margin of the Antarctic Peninsula. Antarc. Sci 9, 426-433.

Camerlenghi, A., Rebesco, M.A., Pudsey, C.J., 1997b. High resolution terrigenous sedimentary record of a sediment drift on the continental rise of the Antarctic Peninsula pacific margin (initial results of the 'SEDANO' Program). In: Ricci, C.A. (Ed.), The Antarctic region: Geological evolution and processes. Terra Antarctica Publication, Siena, pp. 705-710.

Canals, M., Urgeles, R., Calafat, A.M., 2000. Deep sea-floor evidence of past ice streams off the Antarctic Peninsula. Geology 28, 31-34.

Canals, M., Casamor, J.L., Urgeles, R., Calafat, A.M., Domack, E.W., Baraza, J., Farran, M., De Batist, M., 2002. Seafloor evidence of a subglacial sedimentary system off the northern Antarctic Peninsula. Geology 30, 603-606.

Cooper, A.K., O'Brien, P.E., 2004. Leg 188 synthesis: Transitions in the glacial history of the Prydz Bay region, East Antarctica, from ODP drilling. In: Cooper, A.K., O'Brien, P.E., Richter, C. (Eds.), Proc. ODP, Sci. Res. 188. Texas A&M University, College Station, TX, pp. 1-42 [CD-ROM].

DeMaster, D.J., 2002. The accumulation and cycling of biogenic silica in the Southern Ocean: Revisiting the marine silica budget. Deep-Sea Res. II 49, 3155-3167.

Escutia, C., Nelson, C.H., Acton, G.D., Eittreim, S.L., Cooper, A.K., Warnke, D.A., Jaramillo, J.M., 2002. Current controlled deposition on the Wilkes Land continental rise, Antarctica. In: Stow, D.A.V., Pudsey, C.J., Howe, J.A., Faugères, J.-C., Viana, A.R. (Eds.), Deep-water contourite systems: Modern drifts and ancient series, seismic and sedimentary characteristics. Geological Society Memoir 22. Geological Society, London, pp. 373-384.

Exon, N., Kennett, J.P., Malone, M., Shipboard Scientific Party, 2000. The opening of the Tasmanian gateway drove global Cenozoic paleoclimatic and paleoceanographic changes: Results of Leg 189. JOIDES J 26, 11-18.

Eyles, N., Daniels, J., Osterman, L.E., Januszczak, N., 2001. Ocean Drilling Program Leg 178 (Antarctic Peninsula): Sedimentology of glacially influenced continental margin topsets and foresets. Mar. Geol. 178, 135-156.

Faugères, J.-C., Stow, D.A.V., Imbert, P., Viana, A.R., 1999. Seismic features diagnostic of contourite drifts. Mar. Geol. 162, 1-38.

Fitzgerald, P., 1999. Cretaceous - Cenozoic tectonic evolution of the Antarctic Plate. Terra Antarc. Rpts. 3, 109-130.

Florindo, F., Roberts, A.P., Palmer, M.R., 2003. Magnetite dissolution in siliceous sediments. Geochem., Geophys., Geosyst. 4 (7), doi: 10.1029/2003GC000516.

Giorgetti, A., Crise, A., Laterza, R., Perini, L., Rebesco, M.A., Camerlenghi, A., 2003. Water masses and bottom boundary layer dynamics above a sediment drift of the Antarctic Peninsula Pacific margin. Antarc. Sci 15, 537-546.

Giosan, L., Flood, R.D., Aller, R.C., 2002. Paleoceanographic significance of sediment color on western North Atlantic drifts: I. Origin of color. Mar. Geol. 189, 25-41.

Goodridge, C., 2000. Mid-Holocene warmth in the Antarctic Peninsula: Analog to global Warming? Colgate Univ. J. Sci. 32, 67-84.

Grobe, H., Mackensen, A., 1992. Late Quaternary climatic cycles as recorded in sediments from the Antarctic continental margin. In: Kennett, J.P., Warnke, D.A. (Eds.), The Antarctic paleoenvironment: A perspective on global change, Part 1. Antarctic Research Series 56. American Geophysical Union, Washington, DC, pp. 349-376.

Grützner, J., Hillenbrand, C.-D., Rebesco, M.A., 2005. Terrigenous flux and biogenic silica deposition at the Antarctic continental rise during the late Miocene to early Pliocene: Implications for ice sheet stability and sea ice coverage. Global Planet. Change 45, 131-149.

Hillenbrand, C.-D., Ehrmann, W.U., 2002. Distribution of clay minerals in drift sediments on the continental rise west of the Antarctic Peninsula, ODP Leg 178, Sites 1095 and 1096. In: Barker, P.F., Camerlenghi, A., Acton, G.D., Ramsay, A.T.S. (Eds.), Proc. ODP, Sci. Res. 178. Texas A&M University, College Station, TX, pp. 1-29 [CD-ROM].

Hillenbrand, C.-D., Ehrmann, W., 2005. Late Neogene to Quaternary environmental changes in the Antarctic Peninsula region: evidence from drift sediments. Global Planet. Change 45, 165-191.

Hillenbrand, C.-D., Fütterer, D.K., 2002. Neogene to Quaternary deposition of opal on the continental rise west of the Antarctic Peninsula, ODP Leg 178, Sites 1095, 1096, and 1101. In: Barker, P.F., Camerlenghi, A., Acton, G.D., Ramsay, A.T.S. (Eds.), Proc. ODP, Sci. Res. 178. Texas A&M University, College Station, TX, pp. 1-33 [CD-ROM].

Iorio, M., Wolf-Welling, T.C.W., Mörz, T., 2005. Orbital periodicities (~21 to 413 ky) in Plio-Pleistocene glacially-influenced drift sediments from Antarctic Peninsula ODP Sites 1095, 1096, 1101. In: D'Argenio, B., Fischer, A.G., Premoli Silva, I., Weissert, H., Ferreri, V. (Eds.), Cyclostratigraphy: Approaches and case histories. SEPM Special Publication 81. Society for Sedimentary Geology, Tulsa OK.

Iwai, M., Acton, G.D., Lazarus, D., Osterman, L.E., Williams, T., 2002. Magnetobiochronologic synthesis of ODP Leg 178 rise sediments from the Pacific sector of the Southern Ocean: Sites 1095, 1096, and 1101. In: Barker, P.F., Camerlenghi, A., Acton, G.D., Ramsay, A.T.S. (Eds.), Proc. ODP, Sci. Res. 178. Texas A&M University, College Station, TX, pp. 1-40 [CD-ROM].

Jansen, J.H.F., Van der Gaast, S.J., Koster, B., Vaars, A.J., 1998. CORTEX, a shipboard XRF-scanner for element analyses in split sediment cores. Mar. Geol. 151, 143-153.

Kennett, J.P., Hodell, D.A., 1993. Evidence for relative climatic stability of Antarctica during the Early Pliocene: A marine perspective. Geogr. Ann., Ser. A 75, 205-220.

King, T.A., Ellis, W.G., Murray, D.W., Shackleton, N.J., Harris, S., 1997. Miocene evolution of carbonate sedimentation at the Ceara Rise: A multivariate date/proxy approach. In: Shackleton, N.J., Curry, W.B., Richter, C., Bralower, T.J. (Eds.), Proc. ODP, Sci. Res. 154. Texas A&M University, College Station, TX, pp. 349-365.

Larter, R.D., Barker, P.F., 1989. Seismic stratigraphy of the Antarctic Peninsula Pacific margin: A record of Pliocene-Pleistocene ice volume and paleoclimate. Geology 17, 731-734.

Lauer-Leredde, C., Briqueu, L., Williams, T., 2002. A wavelet analysis of physical properties measured downhole and on core from Holes 1095B and 1096C (Antarctic Peninsula). In: Barker, P.F., Camerlenghi, A., Acton, G.D., Ramsay, A.T.S. (Eds.), Proc. ODP, Sci. Res. 178. Texas A&M University, College Station, TX, pp. 1-43 [CD-ROM].

Lawver, L.A., Gahagan, L.M., Coffin, M.F., 1992. The development of paleoseaways around Antarctica. In: Kennett, J.P., Warnke, D.A. (Eds.), The Antarctic paleoenvironment: A perspective on global change, Part 1. Antarctic Research Series 56. American Geophysical Union, Washington, DC, pp. 7-30.

Leventer, A., Domack, E.W., Barkoukis, A., McAndrews, B., Murray, J., 2002. Laminations from the Palmer Deep: A diatom-based interpretation. Paleoceanogr. 17, doi:10.1029/2001PA000624.

Lucchi, R.G., Rebesco, M.A., Busetti, M., Caburlotto, A., Colizza, E., Fontolan, G., 2002a. Sedimentary processes and glacial cycles on the sediment drifts of the Antarctic Peninsula Pacific margin: Preliminary results of SEDANO-II project. New Zealand J Geol. Geophys. 35, 275-280.

Lucchi, R.G., Rebesco, M., Camerlenghi, A., Busetti, M., Tomadin, L., Villa, G., Persico, D., Morigi, C., Bonci, M.C., Giorgetti, G., 2002b. Mid-late Pleistocene glacimarine sedimentary processes of a high-latitude, deep-sea sediment drift (Antarctic Peninsula Pacific margin). Mar. Geol. 189, 343-370.

Martinson, D.G., Pisias, N.G., Hays, J.D., Imbrie, J., Moore, T.C., Shackleton, N.J., 1987. Age dating and the orbital theory of the Ice Ages: Development of a high-resolution 0 to 300,000 year chronostratigraphy. Quaternary Res. 27, 1-29.

Mix, A.C., Harris, S.E., Janecek, T.R., 1995. Estimating lithology from nonintrusive reflectance spectra: Leg 138. In: Pisias, N.G., Mayer, L.A., Janecek, T.R., Palmer-Julson, A., van Andel, T.H. (Eds.), Proc. ODP, Sci. Res. 138: Texas A&M University, College Station, TX, pp. 413-427.

Mörz, T., Wolf-Welling, T.C.W., 2002. Data report: Fine-fraction grain-size distribution data and their statistical treatment and relation to processes, Site 1095 (ODP Leg 178, western Antarctic Peninsula). In: Barker, P.F., Camerlenghi, A., Acton, G.D., Ramsay, A.T.S. (Eds.), Proc. ODP, Sci. Res. 178. Texas A&M University, College Station, TX, pp. 1-27 [CD-ROM].

O'Brien, P.E., Cooper, A.K., Richter, C., Macphail, M.K., Truswell, E.M., Shipboard Scientific Party, 2000. Milestones in Antarctic ice sheet history - preliminary results from Leg 188 drilling in Prydz Bay, Antarctica. JOIDES J 26, 4-10.

Ó Cofaigh, C., Dowdeswell, J.A., Pudsey, C.J., 2001. Late Quaternary iceberg rafting along the Antarctic Peninsula continental rise and in the Weddell and Scotia Seas. Quaternary Res. 56, 308-321.

Potter, P.E., Maynard, J.B., Pryor, W.A., 1980. Sedimentology of shale. Study guide and reference source. Springer, Berlin, pp. 306.

Ragueneau, O., Tréguer, P., Leynaert, A., Anderson, R.F., Brzezinski, M.A., DeMaster, D.J., Dugdale, R.C., Dymond, J., Fischer, G., and Francois, R., 2000. A review of the Si cycle in the modern ocean: recent progress and missing gaps in the application of biogenic opal as a paleoproductivity proxy. Global Planet. Change 26, 317-365.

Pudsey, C.J., Barker, P.F., Larter, R.D., 1994. Ice sheet retreat from the Antarctic Peninsula shelf. Continent. Shelf Res. 14, 1647-1657.

Pudsey, C.J., Camerlenghi, A., 1998. Glacial-interglacial deposition on a sediment drift on the Pacific margin of the Antarctic Peninsula. Antarc. Sci 10, 286-308.

Pudsey, C.J., 2000. Sedimentation on the continental rise west of the Antarctic Peninsula over the last three glacial cycles. Mar. Geol. 167, 313-338.

Pudsey, C.J., 2002. Neogene record of Antarctic Peninsula glaciation in continental rise sediments: ODP Leg 178, Site 1095. In: Barker, P.F., Camerlenghi, A., Acton, G.D., Ramsay, A.T.S. (Eds.), Proc. ODP, Sci. Res. 178. Texas A&M University, College Station, TX, pp. 1-25 [CD-ROM].

Rebesco, M., Larter, R.D., Camerlenghi, A., Barker, P.F., 1996. Giant sediment drifts on the continental rise west of the Antarctic Peninsula. Geo-Mar. Lett. 16, 65-75.

Rebesco, M.A., Larter, R.D., Barker, P.F., Camerlenghi, A., Vanneste, L.E., 1997. The history of sedimentation on the continental rise west of the Antarctic Peninsula. In: Barker, P.F., Cooper, A.K. (Eds.), Geology and seismic stratigraphy of the Antarctic margin, Part 2 71. American Geophysical Union, Washington, DC, pp. 29-49.

Rebesco, M.A., Camerlenghi, A., Zanolla, C., 1998. Bathymetry and morphogenesis of the continental margin west of the Antarctic Peninsula. Terra Antart. 5, 715-728.

Rebesco, M., Pudsey, C., Canals, M., Camerlenghi, A., Barker, P., Estrada, F., Giorgetti, A., 2002. Sediment drifts and deep-sea channel systems, Antarctic Peninsula Pacific Margin. In: Stow, D.A.V., Pudsey, C.J., Howe, J.A., Faugères, J.-C., Viana, A.R. (Eds.), Deep-water contourite systems: Modern drifts and ancient series, seismic and sedimentary characteristics. Geol. Soc. Memoir 22. Geological Society, London, pp. 353-371.

Riedinger, N., Pfeifer, K., Kasten, S., Garming, J.F.L., Vogt., C., and Hensen, C., in press. Diagenetic alteration of magnetic signals by anaerobic oxidation of methane related to a change in sedimentation rate. Geochim. Cosmochim. Acta.

Shipboard Scientific Party, 1999a. Leg 178 summary. In: Barker, P.F., Camerlenghi, A., Acton, G.D. (Eds.), Proc. ODP, Init. Rpts. 178. Texas A&M University, College Station, TX, pp. 1-60 [CD-ROM].

Shipboard Scientific Party, 1999b. Site 1095. In: Barker, P.F., Camerlenghi, A., Acton, G.D. (Eds.), Proc. ODP, Init. Rpts. 178. Texas A&M University, College Station, TX, pp. 1-173 [CD-ROM].

Shipboard Scientific Party, 2001. Leg 188 summary: Prydz Bay-Cooperation Sea, Antarctica. In: O'Brien, P.E., Cooper, A.K., Richter, C. (Eds.), Proc. ODP, Init. Rpts. 188. Texas A&M University, College Station, TX, pp. 1-65 [CD-ROM].

Stammerjohn, S.E., Drinkwater, M.R., Smith, R.C., Liu, X., 2003. Ice-atmosphere interactions during sea-ice advance and retreat in the western Antarctic Peninsula region. J. Gephys. Res. 108, 27.1-27.15.

Thiede, J., Tiedemann, R., 1998. Die Alternative: Natürliche Klimaveränderungen - Umkippen zu einer neuen Kaltzeit? In: Lozán, J.L., Graßl, H., Hupfer, P. (Eds.), Warnsignale Klima - Wissenschaftliche Fakten. GEO, Hamburg, pp. 189-195.

Tomlinson, J.S., Pudsey, C.J., Livermore, R.A., Larter, R.D., Barker, P.F., 1992. GLORIA survey of the Pacific margin of the Antarctic Peninsula: Tectonic fabric and sedimentary processes. In: Yoshida, Y., Kaminuma, K., Shiraishi, K. (Eds.), Recent progress in Antarctic earth science. Terra Scientific Publication, Tokyo, pp. 423-429.

Tucholke, B.E., Hollister, C.D., Weaver, F.M., Vennum, W.R., 1976. Continental rise and abyssal plain sedimentation in the Southeast Pacific Basin: Leg 35 Deep Sea Drilling Project. In: Hollister, C.D., Craddock, C., al., e. (Eds.), Initial Reports of the Deep-Sea Drilling Project 35. U.S. Government Printing Office, Washington, DC, pp. 359-400.

Villa, G., Persico, D., Bonci, M.C., Lucchi, R.G., Morigi, C., Rebesco, M.A., 2003. Biostratigraphic characterization and Quaternary microfossil palaeoecology in sediment drifts west of the Antarctic Peninsula – implications for cyclic glacial-interglacial deposition. Palaeogeogr., Palaeoclimatol., Palaeoecol. 198, 237-263.

Webb, P.N., Harwood, D.M., McKelvey, B.C., Mercer, J.H., Stott, L.D., 1984. Cenozoic marine sedimentation and ice volume variation on the East Antarctic craton. Geology 12, 287-291.

Webb, P.N., Harwood, D.M., 1991. Late Cenozoic glacial history of the Ross Embayment, Antarctica. Quaternary Sci. Rev. 10, 215-223.

Westerhold, T., 2003. The middle Miocene carbonate crash: Relationship to Neogene changes in ocean circulation and global climate [doctoral thesis]. Bremen University, pp. 136.

Wilson, G.S., 1995. The Neogene east Antarctic ice sheet: A dynamic or stable feature? Quaternary Sci. Rev. 14, 101-123.

Wolf-Welling, T.C.W., Cowan, E.A., Daniels, J., Eyles, N., Maldonado, A., Pudsey, C.J., 2002a. Data report: Diffuse spectral reflectance data from rise Sites 1095, 1096, and 1101 and Palmer Deep Sites 1098 and 1099 (Leg 178, western Antarctic Peninsula). In: Barker, P.F., Camerlenghi, A., Acton, G.D., Ramsay, A.T.S. (Eds.), Proc. ODP, Sci. Res. 178. Texas A&M University, College Station, TX, pp. 1-22 [CD-ROM].

Wolf-Welling, T.C.W., Mörz, T., Hillenbrand, C.-D., Pudsey, C.J., Cowan, E.A., 2002b. Data report: Bulk sediment parameters ($CaCO_3$, TOC, and >63 μm) of Sites 1095, 1096, and 1101, and coarse-fraction analysis of Site 1095 (ODP Leg 178, western Antarctic Peninsula). In: Barker, P.F., Camerlenghi, A., Acton, G.D., Ramsay, A.T.S. (Eds.), Proc. ODP, Sci. Res. 178. Texas A&M University, College Station, TX, pp. 1-19 [CD-ROM].

Zachos, J.C., Pagani, M., Sloan, L., Thomas, E., Billups, K., 2001. Trends, rhythms, and aberrations in global climate 65 ma to present. Science 292, 686-693.

Submitted to Marine Geology, under review

2.2 Manuscript 2: A late Miocene-early Pliocene Antarctic deepwater record of cyclic iron reduction events

Daniel A. Hepp[a], Tobias Mörz[a], Christian Hensen[b], Sabine Kasten[a,c], Natascha Riedinger[d] and William W. Hay[e]

[a]MARUM – Center for Marine Environmental Sciences and Faculty of Geosciences, University of Bremen, P.O. Box 330440, 28334 Bremen, Germany
[b]Leibniz Institute of Marine Sciences at the University of Kiel (IFM-GEOMAR), Wischhofstr. 1-3, 24148 Kiel, Germany
[c]Alfred Wegener Institute for Polar and Marine Research (AWI), Am Handelshafen 12, 27570 Bremerhaven, Germany
[d]Max-Planck-Institute for Marine Microbiology, Celsiusstr. 1, 28359 Bremen, Germany
[e]Department of Geological Sciences, University of Colorado, Boulder, Colorado 80309, USA (Emeritus)

Corresponding author: Daniel A. Hepp, E-mail: dhepp@uni-bremen.de, Phone: (+49) 0421-218-65844, Fax: (+49) 0421-218-65810

2.2.1 Abstract

Early diagenetic processes induced pronounced losses of magnetic susceptibility in sixty-four zones of sediment cores from ODP Site 1095, taken on a sediment drift on the Pacific continental rise of the West Antarctic Peninsula in a water depth of 3840 m. We exemplary analyze the sedimentary and geochemical signals across one characteristic magnetic susceptibility minima zone to outline the effects of regional changes in the cryosphere and oceanographic realm on the deep-sea sedimentary record during a period of global enhanced primary productivity in late Miocene-early Pliocene. The loss of the magnetic susceptibility signal is related to the ice sheet collapse at the end of deglaciation phases. Ice sheet collapse and meltwater formation increase the stratification of the water column and weaken the bottom water formation and convection, but foster short lived diatom blooms resulting in high fluxes of organic matter to the seafloor. The high organic fluxes result in temporary suboxic to anoxic near surface sediment conditions causing pronounced diagenetic alteration and demagnetization of magnetic iron. At long time-scales the intensity and loss of magnetic susceptibility reflect global long-term trends as well as the local variability of primary export production. Although early diagenesis may obliterate some primary proxies, here it is indicative of unusual oceanic conditions that otherwise might have been obscured and overlooked in geological records.

Keywords: Ice sheet collapse, magnetic susceptibility minima zone, ODP Site 1095, Pliocene warming, West Antarctic Peninsula

2.2.2 Introduction

The late Miocene-early Pliocene is thought to be a period of global enhanced primary productivity (Dickens and Owen, 1999; Diester-Haass et al., 2005; Farrell et al., 1995). Dramatic

changes in global climate and ocean circulation systems led to an important transition in global nutrient cycling, which left an imprint on opal deposition records in marine sediments. Causes for this late Neogene global change are currently under debate for major tectonic, oceanographic and cryosphere events (Closure of the Isthmus of Panama, establishment of the modern thermohaline circulation, evolution of the Northern Hemisphere ice sheet, development of the West Antarctic ice sheet (Berger and Wefer, 1996; Cortese et al., 2004; Haug et al., 2004; Knorr and Lohmann, 2003), which alters the strength and flow direction of the global overturning circulation, and also affects the meridional partitioning in the ocean of nutrients essential to opal-producing organisms (e.g. diatoms; Cortese et al., 2004). Global sources, sinks and CO_2 feedback mechanisms are currently under debate and glacial-to-interglacial variation in productivity in the Southern Ocean are suggested to play a significant role in the global climate system (Abelmann et al., 2006; François et al., 1997; Frank et al., 2000; Walter et al., 1999). Diatoms are responsible for the ocean primary production and may control the export of carbon to the deep ocean. This confers to the potential to affect changes in atmospheric CO_2 concentrations on a variety of time scales (Abelmann et al., 2006; François et al., 1997). The global evidence for enhanced primary productivity and accumulation of biogenic components in the sediment has been coined the 'biogenic bloom' hypothesis (Cortese et al., 2004; Dickens and Owen, 1999; Diekmann et al., 2003; Diester-Haass et al., 2005; Farrell et al., 1995; Grant and Dickens, 2002; Hermoyian and Owen, 2001).

Today, carbon export productivity south of the polar front is dominated by diatoms, which are light limited and sea ice dependent. Recent global palaeoclimate model simulations emphasize the role of sea ice and related feedback in the Cenozoic evolution of the Antarctic climate and ice sheet (DeConto et al., 2007). Sea ice expansion is highly dynamical during peak warm periods, where it is suggested to be absent in the Southern Hemisphere (Lear et al., 2000; Zachos et al., 2001). In turn sea ice distribution and oceanographic conditions govern the interplay of primary biological and subsequent diagenetic processes all affecting carbon sequestration. This feedback is not well understood for Neogene glacial-to-interglacial variability in the Southern Oceans (Abelmann et al., 2006).

Ice has been present on Antarctica since the Eocene/Oligocene transition and since the late Miocene (~10 Ma) the West Antarctica has been covered by a waxing and vanishing ice sheet that periodically extends to the shelf edge. In our sedimentary and oceanographic study we have compiled a new late Miocene-early Pliocene record of cyclic magnetic susceptibility losses to (1) give an explanation of their origin, (2) outline the mode and the impact of a high dynamic West Antarctic ice sheet with massive ice sheet collapses on primary productivity and bottom water ventilation, and (3) discuss the imprint of global climate signals on our local West Antarctic record.

Here we report on the analysis of three shorter sequences within the MSMZ intervals (171.50-163.50 meter composite depth = mcd, 124.50-115.50 mcd, 107.50-96.50 mcd) in order to determine how the paleoclimatic and palaoceanographic changes and their associated terrigenous and organic fluxes impacted sediment diagenesis. We exemplary show the pattern across core interval 107.50-101.50 mcd (1095B-3H4 to 1095B-4H1) from the upper early Pliocene (Hepp et al., 2006), which is from the diagenetic point of view representative of the entire late Miocene-early Pliocene part of ODP Site 1095.

2.2.3 Regional setting

Along the continental rise of the Pacific margin off the West Antarctic Peninsula a series of twelve sedimentary mounds have been identified (Pudsey and Camerlenghi, 1998; Rebesco et al., 2002; Uenzelmann-Neben, 2006). These sediment mounds are part of a complex glacial sedimentary feeder system composed of lobes and troughs on the outer shelf, a steep slope, and deep-sea channels separating the drifts on the upper rise (Fig. 1). The channel system, separating the drifts from each other and the continental slope, is formed by downslope turbidity currents and alongslope bottom currents (Pudsey and Camerlenghi, 1998; Rebesco et al., 1997). Drift 7 is one of the largest sediment mounds located to the southwest of the Antarctic Peninsula. Its asymmetrical shape, with a short steep side facing southeast and a long gently-sloping side facing northwest, is similar in shape to sediment drifts in this area. The late Miocene-early Pliocene drift build-up occurs by glacially driven turbidity currents and the interglacial pelagic settling (Hepp et al., 2006; Uenzelmann-Neben, 2006). The distal part of Drift 7 was drilled by advanced piston corers (APC) and extended core barrels (XCB) from multiple Holes A and B at Site 1095 during ODP Leg 178 (ODP Leg 178 Shipboard Scientific Party, 1999). Site 1095A was cored from 0 to 87.79 (meter below sea floor, mbsf) with 99.1% recovery, core 1095B was recovered from 83 to 561.78 mbsf with 79.2% recovery. The sediment cores represent a continuous proximal marine sedimentary record of West Antarctic ice sheet dynamics from the late Miocene to the Holocene (~10 Ma; Fig. 2).

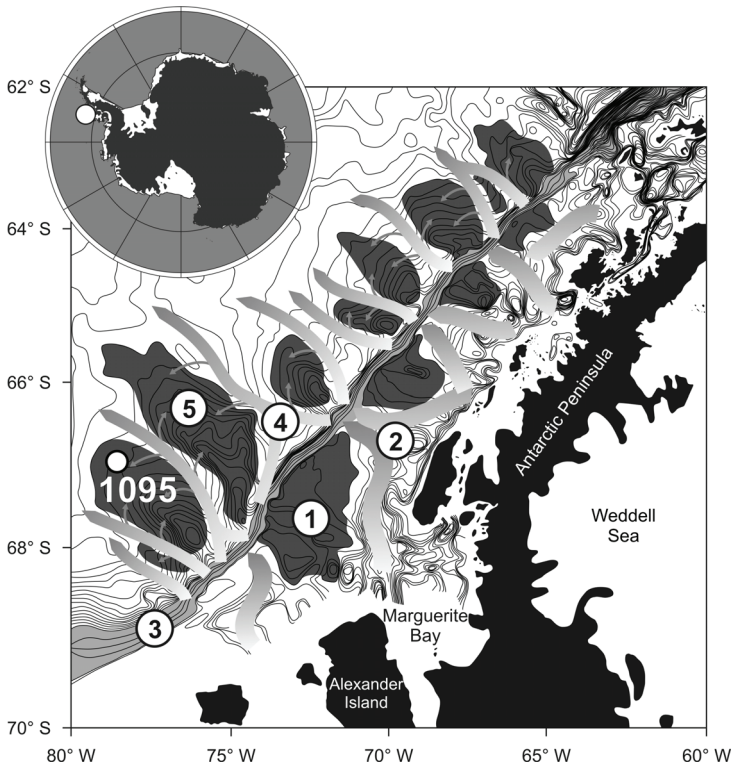

Fig. 1. Bathymetric map of the Pacific continental margin off the Antarctic Peninsula. The map shows a glacial driven sediment feeder system of (1) lobes and (2) troughs on the outer shelf, (3) an oversteepen slope, (4).deep-sea channels and (5) sediment drifts on the continental rise and the location of Site 1095, ODP Leg 178 on the distal part of Drift 7 (modified after Lucchi et al., 2002a; Rebesco et al., 2002).

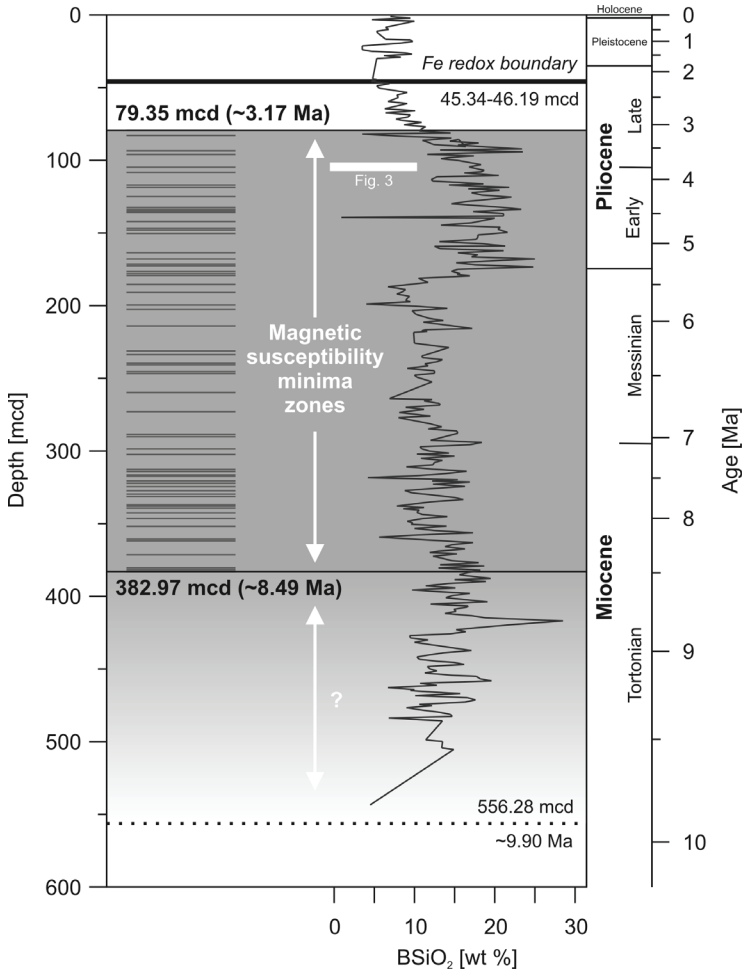

Fig. 2. Schematic representation of core ODP Site 1095 (0-556.28 mcd), the 64 MSMZs (382.97-79.35 mcd; 'bar code') and positions of Fe^{2+}/Fe^{3+}-redox boundary (45.34-46.19 mcd) at present. The biogenic opal ($BSiO_2$) indicates the biological productivity since late Miocene.

2.2.4 Methods

2.2.4.1 Description and sedimentological analyses of glacial and interglacial intervals

The applied methods can be summarized as a combined sedimentological and geochemical approach. We reopened all composite depth cores of ODP Site 1095 for thorough re-description and sedimentological analyses of glacial and interglacial variability and occurrences of diatom oozes, IRD and silt layers. The silt layers and IRD (counts of >1 cm diameter per 10-cm grid; Fig3b) were counted and mapped with the help of X-ray core images. Digital X-ray images were made from selected core sections using a medical 'Fluorospot compact' equipment for radiography.

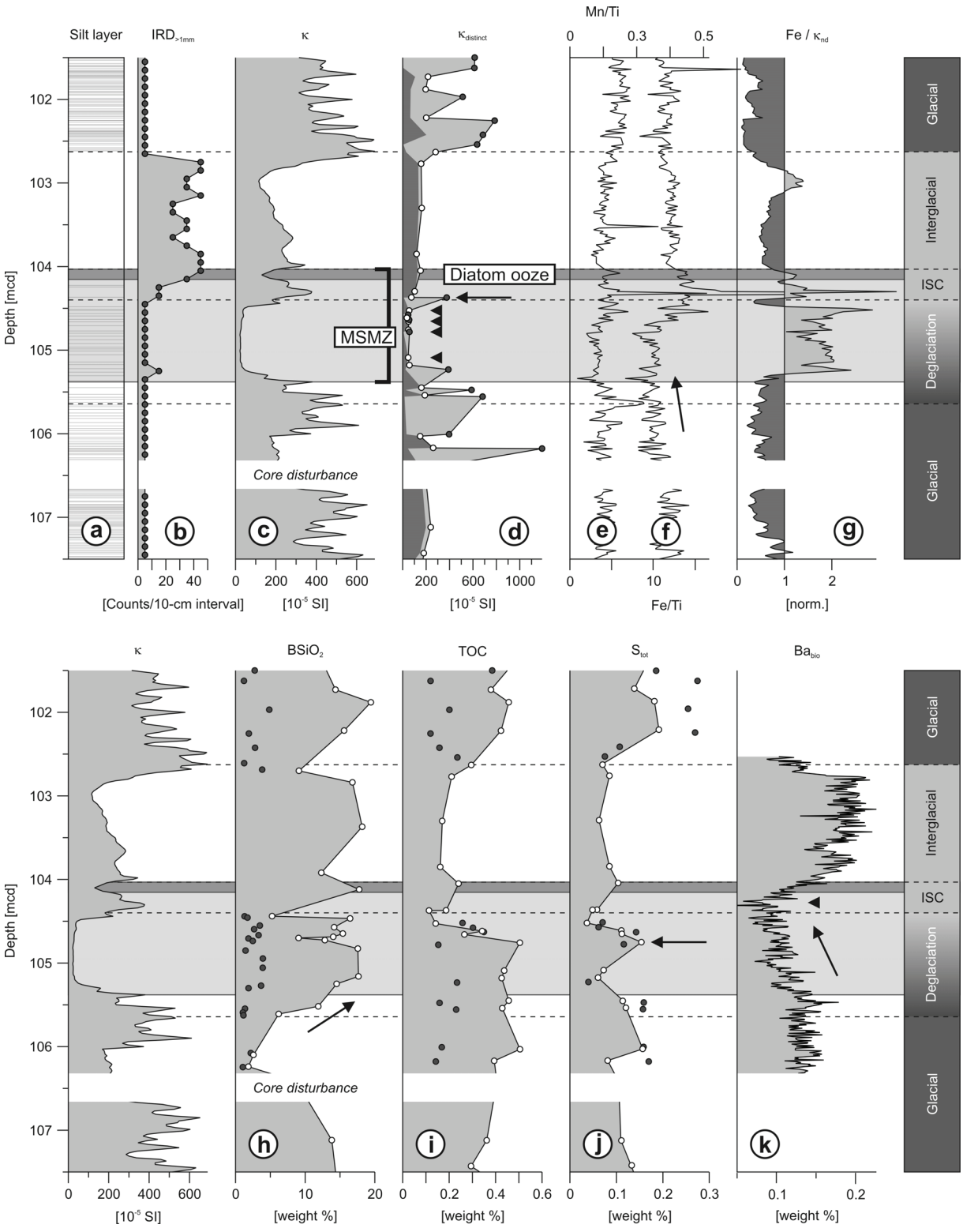

Fig. 3. Example of a MSMZ (105.28 and 104.48 mcd) in the context of a complete glacial-interglacial cycle (107.50 and 101.50 mcd, ODP Leg 178 Site 1095B-3H4 to 4H1): (a) absolute position of silt layers, (b) number of IRD pebbles (>1cm per 10-cm grid), magnetic susceptibility (k) from (c) shipboard logging data and (d) individual measurements (light shading = grain-size coarse fraction >63 µm, dark shading = grain-size fine fraction <63 µm), (e) Mn/Ti ratio and (f) Fe/Ti ratio from X-ray fluorescence spectrometry (XRF) logging, (g) normalized Fe/κ_{nd} ratio, (h) biogenic silica (opal), (i) total organic carbon and (j) total sulfur from individual samples, and (k) biogenic barium from XRF logging (Open circles = samples from hemipelagic sediments, solid circles = samples from silt layers (<63 µm), dark bar = diatom ooze layer, shaded area = MSMZ, dashed lines = boundaries of glacial stages, arrows = as given in text).

2.2.4.2 Identification and mapping of MSMZ

Magnetic susceptibility minima zones (MSMZ) have been reported in studies of the South Atlantic (Funk et al., 2004a; ODP Leg 165 Shipboard Scientific Party, 1997), the western South Atlantic (Garming et al., 2005; Hensen et al., 2003; Riedinger et al., 2005), the North Pacific (Dickens and Owen, 1996; Karlin, 1990; Novosel et al., 2005; Weeks et al., 1995), the Southwest Pacific (ODP Leg 181 Shipboard Scientific Party, 1999) and the East Antarctic continental margin (Florindo et al., 2003a; 2003b). MSMZ occur commonly in the upper centimeters to few meters of the sediment column, but they can also occur at depths of several hundred meters. Commonly their thickness varies from one to several meters; a few MSMZs are only a few centimeters thick.

In a recent study several MSMZs were described in sediments cored in a water depth of 3840 m on Drift 7 (ODP Leg 178, Site 1095) off the continental margin of the West Antarctic Peninsula (Hepp et al., 2006). In this study we map sixty-four MSMZs in a 300 m long core sequence representing a period of ~5 my (Fig. 2; Fig. 5) and suggest sedimentary and diagenetic processes that relate the loss of magnetic susceptibility to short and long term changes in ice sheet dynamics and oceanographic conditions.

Magnetic susceptibility (k; Fig. 3c) is the degree of magnetization of a material in response to a magnetic field and hence a measure of the concentration of magnetic minerals. Magnetic susceptibility was measured with a shipboard whole-core multisensor track logger during ODP Leg 178 (ODP Leg 178 Shipboard Scientific Party, 1999). This fast, high-resolution measuring method allowed a first hand identification and mapping of MSMZ (Hepp et al., 2006). Additional individual measurements of the magnetic susceptibility ($k_{distinct}$; Fig. 3d) on forty samples were carried out with a Kappabridge KL Y-2 at Bremen University to define the upper boundary of the MSMZs in the fine and coarse grain size fraction. In recent studies Funk et al (2004a; 2004b) proposed a new proxy for the identification of diagenetically altered zones using the iron to magnetic susceptibility ratio (Fe/κ, Fig. 3g). This proxy, based on magnetic mineral dissolution, is a sensitive indicator for the intensity of iron reduction independent of biogenic or terrigenous dilution effects. Stable plateau values of Fe/κ, throughout the sediment column are indicative of unaltered mineralogy, while locally elevated values indicate partial demagnetization.

2.2.4.3 X-ray fluorescence spectrometry

The X-ray fluorescence spectrometry (XRF) of the elements manganese (Fig. 3e), iron (Fig. 3f), titanium, aluminum and barium (Fig. 3k) was carried out at the Bremen IODP Core Repository using an AvaaTech XRF scanner. Iron and titanium are interpreted as indicators of terrigenous components. Iron was used to calculate the Fe/κ_{nd} -ratio (Fig. 3c, g). Changes in the Fe/Ti ratio were used to distinguish the effects of Fe dissolution from changes in terrigenous input. Individual XRF measurements on samples were conducted to calibrate the XRF scanner data. The conservative element aluminum was used to estimate the biogenic barium (Ba_{bio}) fraction by subtracting the concentration of terrigenous barium from the total barium concentration (Pfeifer et al., 2001):

(1) $Ba_{bio} = Ba_{tot} - (Al*Ba/Alaluminosilicate)$

with a Ba/Alaluminosilicate ratio of 0.0067 as defined by Nürnberg et al. (1997) for sediments south of 30°S.

2.2.4.4 Geochemical analyses

Biogenic opal (Fig.2; Fig. 5d) content was determined in 320 samples by Hillenbrand and Fütterer (2002). We refined this data by adding fifty $BSiO_2$ analysis from core section 107.5 to 101.5 mcd to differentiate between turbidite and hemipelagic sediments and to document the opal variability at the terminations and during ice sheet collapse phases (Fig. 3h). The homogenized dry bulk samples were analyzed using an automated leaching technique after Müller and Schneider (1993).

Total organic carbon data were provided by Wolf-Welling et al (2002). Forty additional data points for TOC (Fig. 3i) and total sulfur content (Fig. 3j) made by LECO were used for interpretation of short time-scales. Core depth and interval length of MSMZ follows the nomenclature of Ocean Drilling Program (ODP) and is given in meter composite depths (mcd). We used porosity determinations based on shipboard index samples for de-compaction and reconstruction of the original MSMZ interval length (Fig. 5b). To overcome the high glacial and interglacial scatter in Fe/κ_{nd} (Fig. 5c) and total organic carbon (Fig. 5e) data moving average and Hilbert transforms were applied to enhance long term trends.

2.2.5 Results

2.2.5.1 MSMZs on the scale of glacial cycles

The three analyzed magnetic susceptibility minima zones are characterized by an abrupt decrease of about one order of magnitude in magnetic susceptibility (MSMZ average of 38 10-5 SI versus total magnetic susceptibility average of 315 10-5 SI). For our analysis all magnetic susceptibility values less than 100 10-5 SI were classified as MSMZ. These zones occur in a core interval from 79.35 meters composite depth (mcd; ~3.17 Ma) to 382.97 mcd (~8.49 Ma; Fig. 2). The upper termination of the MSMZ interval is very well defined in an early Pliocene core section of excellent quality. Below 382.97 mcd increased sediment compaction and alteration of biogenic opal-A to opal-CT or cryptocrystalline quartz (Volpi et al., 2003) led to a decrease in core quality that prevented the mapping of MSMZs with simple threshold criteria.

The selected sediment section consists of clayey laminated silt-rich and silt-free intervals (Fig. 3a) with high diatom abundance of up to 30% and IRD in the silt-free parts (Fig. 3b; (ODP Leg 178 Shipboard Scientific Party, 1999). These sedimentation patterns are thought to reflect a full glacial-interglacial cycle with characteristic transitions at 104.72 and 102.62 mcd (Hepp et al., 2006). Glacial-to-interglacial transitions are diffuse and characterized by a gradual change in physical and geochemical sediment parameters. Interglacial-to-glacial transitions are distinct and characterized by a sharp boundary and abrupt change in lithology. MSMZs are coupled to the glacial-interglacial cyclicity and consistently occur at glacial terminations (Hepp et al., 2006). Based on detailed previous studies (Camerlenghi et al., 1997; Hepp et al., 2006; Lucchi et al., 2002a; Lucchi et al., 2002b; Pudsey, 2000) and parameters determined for drift site glacial-interglacial intervals (some of them are given in Fig. 3), the following palaeoenvironmental scenario emerges for the warm early Pliocene (see also Hepp et al., 2006):

(1) During glacials grounded ice extended to the shelf edge. Recurring turbidity events transported glacially eroded terrigenous material onto Drift 7 as graded silt layers (mode 30 µm) with an erosive base (Fig. 3a). These turbidites are the carriers of the highest magnetic susceptibility signal (Fig. 3d, solid circles). No IRD was present during fully glacial conditions (Fig. 3b). High terrestrial fluxes increased the overall sedimentation rate and led to an improved total organic carbon burial efficiency (Fig. 3i; Aller et al., 1998). Comparable low biogenic barium records (Fig. 3k) in the glacial sequences reflect a terrigenous dominated sedimentation regime. The elevated sulfur content (Fig. 3j) in glacial sediments is assumed to be linked to the primary lithogenic input of sulfides from the shelf in the terrigenous sediment fraction.

(2) During the deglaciation phase the frequency of ice advances to the shelf edge decreased. This led to a gradual decrease of terrigenous sedimentary silt input (Fig. 3a) and a decrease in sedimentation rate. Concurrently with the shelf ice retreat, open sea conditions expanded leading to an increase in primary bioproduction inferred from an increase in opal accumulation of about 12% (Fig. 3h, arrow). The increasing BSiO2 values correlate with a slight decrease in Fe/Ti ratio of about 3 weight percent (wt. %; Fig. 3f, arrow). The onset of the MSMZ (105.38 mcd, Fig. 3c) during the deglaciation phase is not accompanied by an abrupt lithological change.

(3) The ice sheet collapse (ISC) at the end of the deglaciation phase is characterized by an abrupt cessation of turbidite events (Fig. 3a) and the onset of massive IRD input (Fig. 3b). Coarse lithic fragments of the IRD terminate the MSMZ in the coarse fraction (Fig. 3b). A 2-cm thick diatom ooze layer, seen in core and X-ray images (104.10 mcd), contains well preserved diatom species of *Thalassiosira vulnifica* and *Fragilariopsis interfrigidaria* (For taxonomy of diatom species from ODP Site 1095 see Iwai and Winter, 2002). The massive occurrence and good preservation indicate deposition from the water column without reworking, bottom transport or bioturbation. The top of the diatom ooze layer marks the end of the MSMZ in the fine fraction (Fig. 3, open circles).

(4) The full interglacial phase is marked by high $BSiO_2$ (Fig. 3h) and biogenic barium values (Fig. 3k), common IRD input (Fig. 3b) and the absence of silt layers (Fig. 3a) on the drift, interpreted in terms of a retracted ice sheet that does not reach the shelf edge. Bioturbation and poor organic preservation reflect lower hemipelagic sedimentation rates. The re-advance of grounded shelf ice at interglacial-to-glacial transitions re-initiates frequent turbidites associated with increased sedimentation rates, improved preservation of organic material and an abrupt cessation of IRD supply to the drift.

2.2.5.2 Indications for diagenetic processes

Early diagenetic processes affect the preservation of primary signals and the interpretation of proxies in sediments. After their deposition marine sediments are subject to a variety of geochemical and microbiological processes. The re-mineralization of sediment organic matter plays a key role in many of these processes. Organic degradation at sub-oxic, sulfidic or methanic levels is accompanied by a gradual dissolution of primary ferro-magnetic iron minerals. This gradual, mineral- and grain-size selective process makes rock magnetic parameters, particularly the extent of demagnetization, a sensitive measure for the intensity of diagenetic processes (Funk et al., 2004a; 2004b).

Magnetic susceptibility measurements of individual samples containing hemipelagic sediment, silt or IRD (Fig. 3d) from outside the MSMZ clearly show that the magnetic susceptibility of silt samples (solid circles; average 600 10^{-5} SI) is about three times higher than in hemipelagic samples

(open circles; average 200 10^{-5} SI). High total magnetic susceptibility (between 104.30 and 103.66 mcd, Fig. 3c) is noticed in IRD dominated sections. The loss of magnetic susceptibility in the MSMZ is observed in hemipelagic and silt size samples independent of changes in grain size of the sediment supply (Fig. 3d, small arrows). Within the MSMZ, coarse fraction samples with lithic fragments from IRD are not affected by demagnetization (Fig. 3d, large arrow). Neither the onset of the MSMZ nor the termination coincide with changes in silt or IRD supply: (1) turbidity silt deposition is continuous across the sharp onset of the MSMZ, (2) the recovery of the magnetic signal in the fine fraction marks the end of the MSMZ during an episode of massive IRD supply. We conclude that mineral- and grain-size selective processes, largely independent from changes in the lithogenic flux, modified the magnetic susceptibility signal.

The onset of MSMZ is associated with an increase in diamagnetic $BSiO_2$ (Fig. 3h, arrow) by a factor of 3 and a decrease in Fe/Ti ratio (Fig. 3f) of 10 %. Those changes are, however, insufficient to explain the abrupt drop in magnetic susceptibility by one order of magnitude. Dilution effects by diamagnetic and paramagnetic sediment compounds can be further ruled out since high opal contents continue across the upper termination of the MSMZ. The independence of MSMZ from sedimentary dilution effects is further confirmed by the Fe/κ_{nd} ratio (Fig. 3g) introduced by Funk et al. (2004a; 2004b). This ratio highlights diagenetic magnetic susceptibility loss decoupled from concentration changes of iron bearing mineral. Signs of a diagenetic imprint are seen in strong enrichments of redox sensitive elements like manganese and iron in the upper part of the MSMZ (Fig. 3e,f, large peaks at 104.30 mcd) and the asynchrony of biogenic barium and $BSiO_2$ (Fig. 3k, arrow) within the onset of the MSMZ. Diatom concentrations and biogenic barium are almost synchronous (Pudsey, 2000) in Holocene and Pleistocene sections that lack MSMZs. Hence, we conclude that mineral- and grain-size selective diagenetic processes severely modified the observed magnetic susceptibility signal in the late Miocene to upper early Pliocene core intervals.

2.2.6 Discussion

2.2.6.1 Diagenetic mechanisms

Well resolved combined records of geochemical and rock magnetic data show that the extent of diagenetic overprint is proportional to the magnitude of change encountered in depositional, geochemical and environmental system parameters (Funk et al., 2004b; Garming et al., 2005; Riedinger et al., 2005). This in general makes glacial-interglacial transitions, with their changes in sedimentation rate, palaeoproductivity and the oceanographic-cryospheric setup, most vulnerable to diagenetic processes (Kasten et al., 2003). In a retrospective view the secondary signals may be used as indicators of substantial environmental system changes.

In suboxic conditions the degradation of organic matter leads to a reduction of Fe^{3+} bearing mineral species (Passier et al., 1999) resulting in a loss of sediment magnetic susceptibility (Funk et al., 2004a). The degree of demagnetization is proportional to the amount of mineralized organic material (Funk et al., 2004a). Hence, diagenetic demagnetized zones (Fig. 3c) in general indicate times with enhanced organic carbon flux to the sea floor (Fig. 3i), which is best preserved and seen in the parallel onset of the MSMZ and the rise in opal (Fig. 3h, arrow). Since we can rule out biogenic or terrigenous dilution effects, we believe that iron reduction of magnetic minerals under suboxic conditions is responsible for the onset of the observed MSMZs.

Many examples of organic induced iron reduction events have been discussed in the study of Funk et al. (2004b) as part of their examination of Pleistocene equatorial Atlantic sediment cores. Increased glacial organic carbon fluxes lead to similar periodic reoccurrence of MSMZs. Diagenetic signatures of iron reduction fronts in otherwise well-ventilated open oceanic conditions have also been observed at the tops of organic-rich turbidite deposits in the Madeira abyssal plain (Robinson, 2001; Robinson et al., 2000; Thomson et al., 1998).

The diagenetic process of reductive dissolution of iron occurs likewise in suboxic to anoxic environments (Kasten et al., 2003). Hence, iron reduction alone does not allow differentiating suboxic from sulfidic or methanic conditions or determination of the depth in the sediment column where the reduction process occurred. When looking for signs of sulfate reduction in the Pliocene core sections of ODP Site 1095 we see two indications: (1) a possible enrichment of pyrite indicated by a weak sulfur peak at 104.1 mcd (Fig. 3j, diatom ooze layer) and (2) the asynchronous biogenic barium profile (Fig. 3k, arrow). A sulfur peak located in the middle of the MSMZ (Fig. 3j, arrow) is difficult to interpret since variations in sulfur input may be strongly coupled to the terrigenous flux and diagenetic pyrite may later be re-oxidized during the reestablishment of suboxic conditions. The anomalies in the biogenic barium profile include the already mentioned decoupling from the $BSiO_2$ and the relation of the biogenic barium increase at 104.26 mcd to the diatom ooze layer that coincides with the upper termination of the MSMZ.

In a recent study on the glacial Southern Ocean productivity Abelmann et al. (2006) related changes in the oxygen content of the bottom and pore water to diagenetic remobilization of biogenic barium under reducing conditions (McManus et al., 1999) at the last glacial termination in a sediment core south of the Antarctic Polar Front (APF). Biogenic barium is found to be dissolved under sulfate depleted conditions (Gingele et al., 1999). Microbial sulfate reduction is also shown by Brumsack and Gieskes (1983) to cause barite undersaturation and barium mobilization in anoxic, laminated sediments in the Gulf of California with sulfate-reduction occurring close to the sediment-water interface.

The pronounced dissolution effect on Ba is also the main argument for not implementing the more theoretical findings of Florindo et al (2003b) stating that the demagnetization might be explained by elevated dissolved silica concentrations in the porewater leading to a magnetite smectite transformation.

The diagenetic effects of increased organic carbon accumulation are well-investigated in East Mediterranean sapropels. Near surface sulfate reduction and sulfide formation are the dominating processes addressed in the diagenetic sapropel model of Passier et al. (1999). In a sapropel study of van Os (1991) biogenic barium is shown to be dissolved and mobilized in many sapropel layers under sulfate-reducing conditions in the Bannock basin. However other authors use biogenic barium in sapropels as a palaeoproductivity indicator in time equivalent sapropels (e.g. Weldeab et al., 2003).

In modern high productivity margin settings more than 80% of the total sulfate reduction may occur in the first 30 cm of the sediment column (Fossing et al., 2000). Those values are similar to a 15-25 cm paleo-depth estimate of sulfate depletion, deduced from the relative position of the diatom ooze layer (Fig. 3) and the zone of maximum barium depletion (Fig. 3j, small arrow) in our West Antarctic cores. In modern outer continental margins sulfate reduction is commonly coupled to the process of the anaerobic oxidation of methane rather than to the remobilization of particulate sediment

organic matter (Burdige, 2006). Quasi equilibrium between downward sulfate flux and methane consumption is expressed in linear sulfate profiles (e.g. Riedinger et al., 2005).

However, our cyclic, glacially triggered Pliocene MSMZs are strongly linked to short term changes in organic matter fluxes, which likely prevent the establishment of equilibrium conditions.

The MSMZs commonly terminate at diatom ooze layers (Fig. 3c). Strong excursion of redox sensitive elements species like manganese and iron (Fig. 3e,f) at the depth of the maximal barium depletion zone at 104.31 mcd (Fig. 3k, small arrow) are interpreted as the result of dissolved redox-sensitive element fixation during re-oxidation in post ooze layer deposition. This 'burn-down' effect affects the entire MSMZ leading to an intensive decomposition of organic carbon (Wilson et al., 1986) and possible re-oxidation of sulfides. Following the diatom ooze deposition and MSZM termination barium precipitation and BSiO2 deposition are in phase. Other aspects regarding the MSMZ termination are addressed in the following scenario that attempts to blend the suggested succession of diagenetic processes into a refined and integrated oceanographical-cryospherical and sedimentological conceptual model.

2.2.6.2 Early Pliocene boundary conditions required to produce MSMZ

Diagenesis driven by organic matter re-mineralization is a complex function of organic carbon supply, sedimentation rate, intensity of bioturbation, ocean ventilation and deep water oxygen content. Today, the Southern Ocean biological pump and coupled opal and organic carbon deposition are bound to winds, ocean circulation and sea ice (Anderson et al., 2002). The modern Antarctic opal belt (~520 km north of ODP Site 1095) is located south of the APF (Abelmann et al., 2006; Cortese and Gersonde, 2007; Hillenbrand and Ehrmann, 2005) and north of the winter sea ice edge. It is believed that the position of this opal depocentre was further north during the Last Glacial Maximum but kept its relation to the maximum winter sea ice edge (Abelmann et al., 2006; Anderson et al., 2002; François et al., 1997; Hillenbrand and Cortese, 2006). Late Miocene to early late Pliocene warm climate conditions and a reduction of 22% in sea ice cover at the continental rise, relative to modern conditions, are generally accepted for Antarctica (Anderson et al., 2002; Grützner et al., 2005; Hillenbrand and Fütterer, 2002; Whitehead et al., 2005). Global ice volume records by Lear et al. (2000) indicate a strong reduction in overall ice volume for this time interval.

In a review paper on Southern Ocean palaeoceanography Hillenbrand and Cortese (2006) documented the northward shift of the opal export production depocentre after 2.73 Ma. This suggest a position of ODP Site 1095 within the opal depocentre for the time of MSMZ occurrence, leading to a time of exceptional silica and organic carbon fluxes comparable to fluxes at the modern opal belt (Abelmann et al., 2006). Despite an overall ice volume reduction the late Miocene to early late Pliocene, ice dynamics increased with frequent advances of the inland ice sheet to the shelf edge (Hepp et al., 2006). In this time-frame the frequency of ice advances and sea ice extent is gradually decreased. This coincided with a rise in export $BSiO_2$ leading to suboxic, iron reducing conditions in the rise sediments confirmed by the onset of the MSMZ. At the end of the deglaciation phase there was a rapid break down of the shelf ice sheet (massive IRD supply).

An intense and rapid ISC at the end of the deglaciation phase (Fig. 3b) discharged large amounts of meltwater into the Antarctic surface waters inducing cyclic changes in the regional oceanographic regime (Fig. 4). Following the model of Rohling and Gieskes (1989) an increased freshwater discharge shoaled the pycno- and nutricline into the photic zone, promoting high export

productivity in the lower photic zone. At this time, high export productivity was also enhanced by fertilization of the ocean by terrigenous and dust-bound iron (Cortese and Gersonde, 2007; Kumar et al., 1995). Today the release of nutrients from the spring melt of sea ice is well documented (Stickley et al., 2005). As long as stratification is maintained, this can stimulate phytoplancton production in the melt zone. Water column stratification along the Antarctic shelf break weakened the bottom water formation. The diminished the oxygen supply and reduced bottom water current strength resulting in a strong decrease of ventilation at the continental rise. Nearly stagnant deep water conditions were required to preserve the current sensitive and easy to relocate diatom ooze on top of an elevated topographic feature like Drift 7.

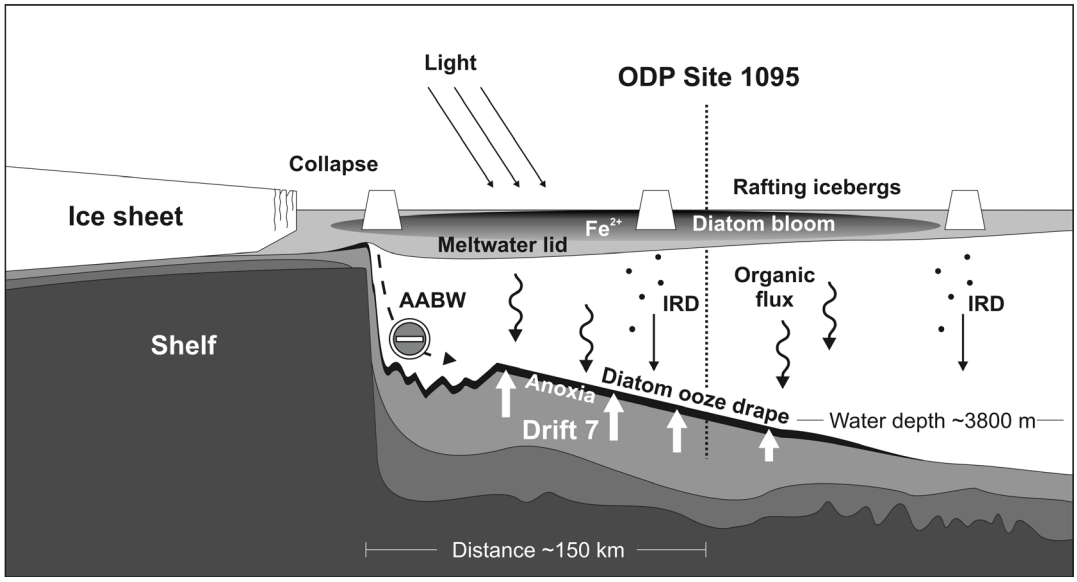

Fig. 4. During intense ice sheet collapse, the retreating ice sheet and a large meltwater lid leads to increased iron fertilization, a short-term diatom bloom and the stratification water column. Weakening of AABW formation and high export productivity foster the preservation a thick diatom ooze drape on the drift resulting in periodic anoxic conditions in surface sediments.

High organic export rates and reduced bottom water ventilation in this marginal setting during the ISC provided the framework for reducing conditions in the sediment and for sulfate reduction close to the sediment water interface (Fig. 4). This is supported by the absence of bioturbation. Comparable hydrographic scenarios have been proposed to explain the Mediterranean sapropel formation (Weldeab 2003).

For the last deglaciation, Abelmann et al. (2006) suggest that meltwater causes substantial changes diatom floral assemblages resulting in short-term (maximum duration 3000 years) increases in silica and organic carbon export to the seafloor. Similar mechanisms may have acted during the late Miocene to early late Pliocene ISC. However, the meltwater induced productivity peaks of the West Antarctic did not occur in an open ocean setting but along the continental margin. We propose that cyclic freshwater pulses from partial collapse of the West Antarctic ice sheet initiated massive short-term diatom blooms above the continental rise leading to thick diatom ooze layers on the sea floor. The diatom ooze drape sealed off the underlying sediments (Fig. 4) resulting in initiation of diagenetic reduction of sulfate, a mobilization of biogenic barium, and its loss to the water column in the near surface sediments, which were already in a suboxic state.

Following the meltwater pulse the exhaustion of the supply of ice-bound nutrients led to a rapid decline of export productivity. The break-up of stratification of the water allowed the re-establishment of bottom water formation, circulation and re-ventilation of the upper sediment column. The diminishing supply of organic carbon led to an organic 'burn down' (Frank et al., 2000; Thomson et al., 1998) with manganese and iron precipitation at the oxic/suboxic boundary.

2.2.6.3 Long-time record of redox events

On long time scales anoxic sediment conditions coupled to high productivity and meltwater events are well documented for the period from 8.49 to 3.17 Ma during which there were sixty-four MSMZs (Fig. 2, Fig. 5a).

Iron reduced deep-sea sediment facies as a product of elevated export productivity during late Miocene-early Pliocene has been globally documented and is not restricted to high southern latitudes (Dickens and Owen, 1996).Cortese et al. (2004) showed that the opal depocentres are subject to large scale shifts. Between 4.5 Ma and 2.7 Ma peaks in opal accumulation occur at locations proximal to the Antarctic Peninsula. In addition to this global link to enhanced productivity the cyclic occurrence of iron reduction events at ODP Site 1095 is closely coupled to the regional waxing and vanishing of the West Antarctic Peninsula ice sheet.

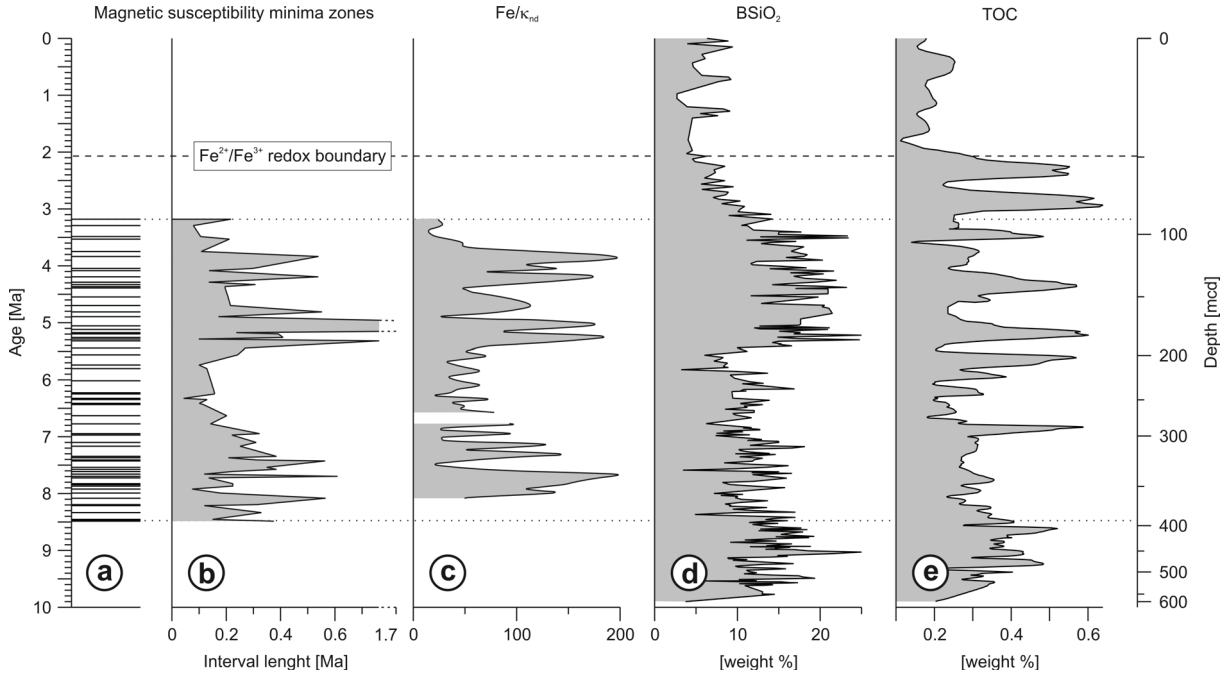

Fig. 5. MSMZs from ODP Site 1095A and B. The 'bar code' and the dotted lines represent the occurrence and range of (a) MSMZs. The dashed lines represent the modern positions of Fe^{2+}/Fe^{3+}-redox boundary. Curves represent (b) the de-compacted interval length of MSMZs as a parameter related to the relative duration or extent of penetration of the diagenetic event, (c) the Fe/κ_{nd} ratio as an indicator for the intensity of diagenesis, (d) biogenic silica (opal) as proxy for palaeoproductivity, and (e) total organic carbon as proxy for organic preservation. Core lengths were de-compacted on primary length using factor of porosity. Curves of Fe/κ_{nd} ratio and total organic carbon were smoothed using moving average and Hilbert transformations.

The periodicity of the melting events shows a close linkage to the short eccentricity cycles in the time interval from 7 to 2.7 Ma as proposed by Iorio et al. (2004). The de-compacted interval length of MSMZs (Fig. 5b) is plotted as a parameter indirectly related to the relative duration or extent of penetration of the diagenetic event. The Fe/κ_{nd} ratio (Fig. 5c) indicates the intensity of diagenesis. Both parameters show a close correlation to the export productivity proxy BSiO2 (Fig. 5d) and the relic preservation of total organic carbon (TOC; Fig. 5e). In brief, our records show that on long time-scales the organic input controls the intensity and duration of diagenesis. Trends in the long-term records reflect paleoceanographical and paleoclimatological changes. The general Subantarctic South Atlantic oceanographic conditions were relatively warm and stable between ~11 and 6.6 Ma (Müller et al., 1991; Warnke, 1992).

However, for the late Miocene major cooling episodes with increasing global ice volume have been reported (see review by Hodell and Kennett, 1986). This may explain the decrease in diagenetic intensity between 8.5 and 5.6 Ma linked to the decline in export productivity (Fig. 5d; (Hillenbrand and Fütterer, 2002). The low in diagenetic indicators between 7.1 and 5.6 Ma correlates with an inferred decrease in Northern Component Water production as a consequence of a cessation of Mediterranean Overflow Water during the Messinian stage (Hillenbrand and Fütterer, 2002; Müller et al., 1991). The concomitant reduction of heat injection into the Circumpolar Deep Water may have triggered enhanced sea-ice coverage with a northward shift of the opal productivity zone (Müller et al., 1991) and lower export production at the rise (Hillenbrand and Fütterer, 2002). Interestingly during this time interval laminated oozes at ODP Site 701 (latitude 52°S) and DSDP Site 520 (latitude 26°S) have been interpreted as evidence of suboxic bottom conditions (Müller et al., 1991). During the Pliocene warming phase the indicators for intensity and duration of diagenesis, for biogenic input ($BSiO_2$) and for preservation of organic matter in the sediment (TOC) increased to maximum values (between 190.0 mcd and 46.0 mcd; 5.6-2.7 Ma). This can be explained by a southward shift of the opal depocentre that reached to ODP Site 1095 (for details see the Pliocene scenario described above). Following this 3 Ma period of exceptionally high productivity, the late Pliocene saw a gradual decrease of biogenic silica deposition south of the APF. This is observed in a multitude of sediment records in the Atlantic and Pacific sector of Southern Ocean and has been used to document the northward shift of the APF between 3.3 and 2.3 Ma (Hillenbrand and Cortese, 2006). Synchronous with the decrease of biogenic silica deposition the MSMZs cease at 79.35 mcd (~3.17 Ma). This reflects the global cooling trend coupled to the Northern hemisphere glaciation and the stabilization of the Antarctic ice sheets. The global cooling resulted in a reduction of Antarctic ice sheet dynamics, decreased terrigenous sediment input, a seaward spread of sea ice and less pronounced ISC phases during Antarctic deglaciations. At 3.17 Ma, organic export productivity and sedimentation rates fell below a threshold level, preventing sulfate reduction to occur at significant rates in surface sediments (see modern position of sulfate penetration depth, Fig. 2, Fig. 5). The modern Fe^{2+}/Fe^{3+}-redox boundary at ~46 mcd coincides with the termination of the late Pliocene decrease in export productivity (Fig. 5). This shows that the relic organic reservoir of the early Pliocene productivity high (Fig. 5e) still controls Fe reduction today (Funk et al., 2004b).

Deglacial vigorous Antarctic Bottom Water (AABW) formation after 3.17 Ma resulted in deep water ventilation and oxygenation preventing the development of lasting diatom ooze drapes. The secession of near surface anoxic conditions coupled to short-term water stratification contradicts the idea of long-term increased vertical Southern Ocean stratification after the late Pliocene cooling (Sigman et al., 2004).

2.2.7 Conclusion

On the basis of a new late Miocene-early Pliocene record of cyclic magnetic susceptibility losses (MSMZ) we have demonstrated how global climatic and oceanographic scenarios interact with regional ice sheet dynamics and ocean circulation in West Antarctic regions to form a unique diagenetic record at a period of global enhanced primary productivity.

Similar to organic carbon-rich layers (sapropels) of the Mediterranean, the reoccurring MSMZ layers off the Antarctic Peninsula are indicative of very special oceanographic conditions and times of unusual short-term cyclic inputs of organic matter.

Late Miocene to early late Pliocene warm climate conditions are characterized by an enhanced global bioproductivity ('biogenic bloom'), an overall reduced ice volume, and a reduced sea ice cover around Antarctica. At that time ODP Site 1095 was within a southward-shifted opal depocentre. It experienced exceptional opal and organic carbon fluxes comparable to those at the modern opal belt. Late Miocene to early late Pliocene ice sheet dynamics involved frequent advances and retreats of the inland ice sheet leading to more pronounced ISCs and meltwater pulses during deglaciations. The discharge of large amounts of meltwater to the Antarctic surface waters caused stratification and shoaling of the pycno- and nutricline into the photic zone, promoting high export productivity from the lower photic zone. Water column stratification weakened the AABW formation and reduced deep ocean water ventilation. Export productivity pulses in nearly stagnant deep water conditions led to reducing conditions in the sediment and sulfate reduction close to the sediment water interface (MSMZs). Following the meltwater pulses the reduction of the supply of nutrients that had been bound in the ice led to a rapid decline of export productivity. The break-up of water stratification allowed the re-establishment of bottom water formation, circulation and ventilation, affecting of the upper sediment column.

On long time-scales the intensity and duration of diagenesis reflect major trends in global paleoceanographic and climatic change and the consequent variability in primary export production. After Antarctic ice sheet stabilization, between 3.3 to 2.3 Ma, the flux of organic matter and sedimentation rates fell below a threshold level preventing development of reducing conditions in the surface sediments.

The mapping and documentation of 64 MSMZ provide the first long term record of cyclic meltwater pulses and high export productivity events resulting in reducing conditions in the near surface sediments in the high latitudinal Southern Ocean. Meltwater events originating in the Antarctic (Licht, 2004; Weaver et al., 2003) may have had a major impact on the global thermohaline overturning strength (Ganopolski and Rahmstorf, 2001; Knorr and Lohmann, 2003; McManus et al., 2004; Stocker, 2003). Further, increased carbon burial in the high latitudes during extensive green-house conditions may have been a negative feed-back to atmospheric CO_2 concentrations.

We showed that meltwater events are common regional features of the retreating Antarctic ice sheets during the early Pliocene and that diagenesis may obliterate primary proxies but may also serve as evidence of unusual oceanic conditions that might have otherwise be obscured and overlooked in geological records.

2.2.8 Acknowledgement

Samples were provided by Ocean Drilling Program (ODP). We thank the Bremen Core Repository (BCR) team for their kind support. Thanks to Jens Grützner and Ursula Röhl at Bremen University who provided XRF data. Some BSiO2 data from individual samples were part of a bachelor thesis by Sophie Fath prepared in our working group. In this regard the help of Gerhard Kuhn and Rita Froehlking (Alfred Wegener Institute for Polar and Marine Research, AWI, Bremerhaven) during the measurements is greatly acknowledged. We thank Ismene Seeberg-Elverfeldt at Bremen University for her expertise on diatoms. Fruitful discussions with Syee Weldeab (Leibniz Institute of Marine Sciences, IFM-GEOMAR, Kiel) improved our understanding of water mass stratification. We are grateful to Gerald Dickens (Rice University, Houston TX) for his constructive comments on an earlier version of the manuscript. This research was funded by the Deutsche Forschungsgemeinschaft (DFG project MO1059/1) and by the DFG-Research Center MARUM – Center for Marine Environmental Sciences of University of Bremen.

2.2.9 Reference list

Abelmann, A., Gersonde, R.E., Cortese, G., Kuhn, G. and Smetacek, V., 2006. Extensive phytoplankton blooms in the Atlantic sector of the glacial Southern Ocean. Paleoceanography, 21(PA1013).

Aller, R.C., Hall, P.O.J., Rude, P.D. and Aller, J.Y., 1998. Biogeochemical heterogeneity and suboxic diagenesis in hemipelagic sediments of the Panama Basin. Deep-Sea Research Part I, 45(1): 133-165.

Anderson, R.F., Chase, Z., Fleisher, M.Q. and Sachs, J., 2002. The Southern Ocean's biological pump during the Last Glacial Maximum. Deep-Sea Research Part II, 49(9-10): 1909-1938.

Berger, W.H. and Wefer, G., 1996. Central themes of South Atlantic circulation. In: G. Wefer, W.H. Berger, G. Siedler and D.J. Webb (Editors), The South Atlantic: Present and past circulation. Springer, Berlin, Heidelberg, New York, pp. 1-11.

Brumsack, H.-J. and Gieskes, J.M., 1983. Interstitial water trace-metal chemistry of laminated sediments from the Gulf of California, Mexico. Marine Chemistry, 14(1): 89-106.

Burdige, D.J., 2006. Geochemistry of marine sediments. Princeton University Press, Princeton, Oxford, 609 pp.

Camerlenghi, A., Rebesco, M.A. and Pudsey, C.J., 1997. High resolution terrigenous sedimentary record of a sediment drift on the continental rise of the Antarctic Peninsula pacific margin (inital results of the 'SEDANO' Program). In: C.A. Ricci (Editor), The Antarctic region: Geological evolution and processes. Terra Antarctica Publication, Siena, pp. 705-710.

Cortese, G. and Gersonde, R., 2007. Morphometric variability in the diatom Fragilariopsis kerguelensis: Implications for Southern Ocean paleoceanography. Earth and Planetary Science Letters, 257(3-4): 526-544.

Cortese, G., Gersonde, R., Hillenbrand, C.-D. and Kuhn, G., 2004. Opal sedimentation shifts in the World Ocean over the last 15 Myr. Earth and Planetary Science Letters, 224(3-4): 509-527.

DeConto, R.M., Pollard, D. and Harwood, D.M., 2007. Sea ice feedback and Cenozoic evolution of Antarctic climate and ice sheets. Paleoceanography, 22: doi:10.1029/2006PA001350.

Dickens, G.R. and Owen, R.M., 1996. Sediment geochemical evidence for an early-middle Gilbert (Early Pliocene) productivity peak in the North Pacific Red Clay Province. Marine Micropaleontology, 27(1-4): 107-120.

Dickens, G.R. and Owen, R.M., 1999. The Latest Miocene-Early Pliocene biogenic bloom: a revised Indian Ocean perspective. Marine Geology, 161(1): 75-91.

Diekmann, B., Fälker, M. and Kuhn, G., 2003. Environmental history of the south-eastern South Atlantic since the Middle Miocene: Evidence from the sedimentological records of ODP Sites 1088 and 1092. Sedimentology, 50(3): 511-529.

Diester-Haass, L., Billups, K. and Emeis, K.-C., 2005. In search of the late Miocene-early Pliocene “biogenic bloom” in the Atlantic Ocean (Ocean Drilling Program Sites 982, 925, and 1088). Paleoceanography, 20: doi:10.1029/2005PA001139.

Farrell, J.W. et al., 1995. Late Neogene sedimentation patterns in the eastern equatorial Pacific ocean In: N.G. Pisias, L.A. Mayer, T.R. Janecek, A. Palmer-Julson and T.H. van Andel (Editors), Proceedings of the Ocean Drilling Program, Scientific Results. Texas A&M University, College Station, TX, pp. 717-756.

Florindo, F. et al., 2003a. Magnetobiostratigraphic chronology and palaeoenvironmental history of Cenozoic sequences from ODP Sites 1165 and 1166, Prydz Bay, Antarctica. Palaeogeography, Palaeoclimatology, Palaeoecology, 198(1-2): 69-100.

Florindo, F., Roberts, A.P. and Palmer, M.R., 2003b. Magnetite dissolution in siliceous sediments. Geochemistry, Geophysics, Geosystems, 4(7): 1053, doi:10.1029/2003GC000516.

Fossing, H., Ferdelman, T.G. and Berg, P., 2000. Sulfate reduction and methane oxidation in continental margin sediments influenced by irrigation (South-East Atlantic off Namibia). Geochimica et Cosmochimica Acta, 64(5): 897-910.

François, R. et al., 1997. Contribution of Southern Ocean surface-water stratification to low atmospheric CO_2 concentrations during the last glacial period. Nature, 389: 929-935.

Frank, M. et al., 2000. Similar glacial and interglacial export bioproductivity in the Atlantic sector of the Southern Ocean: Multiproxy evidence and implications for glacial atmospheric CO_2. Paleoceanography, 15(6): 642-658.

Funk, J.A., von Dobeneck, T. and Reitz, A., 2004a. Integrated rock magnetic and geochemical quantification of redoxomorphic iron mineral diagenesis in Late Quaternary sediments from the equatorial Atlantic. In: G. Wefer, S. Mulitza and V. Ratmeyer (Editors), The South Atlantic in the Late Quaternary: Reconstruction of material budgets and current systems. Springer, Berlin, Heidelberg, New York, pp. 237-260.

Funk, J.A., von Dobeneck, T., Wagner, T. and Kasten, S., 2004b. Late Quaternary sedimentation and early diagenesis in the equatorial Atlantic ocean: Patterns, trends and processes deduced from rock magnetic and geochemical records. In: G. Wefer, S. Mulitza and V. Ratmeyer (Editors), The South Atlantic in the Late Quaternary: Reconstruction of material budgets and current systems. Springer, Berlin, Heidelberg, New York, pp. 461-497.

Ganopolski, A. and Rahmstorf, S., 2001. Rapid changes of glacial climate simulated in a coupled climate model. Nature, 409: 153-158.

Garming, J.F.L., Bleil, U. and Riedinger, N., 2005. Alteration of magnetic mineralogy at the sulfate-methane transition: Analysis of sediments from the Argentine continental slope. Physics of the Earth and Planetary Interiors, 151(3-4): 290-308.

Gingele, F.X., Zabel, M., Kasten, S., Bonn, W.J. and Nürnberg, C.C., 1999. Biogenic barium as a proxy for paleoproductivity: Methods and limitations of application. In: G. Fischer and G. Wefer (Editors), Use of proxies in paleoceanography: Examples from the South Atlantic. Springer, Berlin, Heidelberg, New York, pp. 345-364.

Grant, K.M. and Dickens, G.R., 2002. Coupled productivity and carbon isotope records in the southwest Pacific Ocean during the late Miocene-early Pliocene biogenic bloom. Palaeogeography, Palaeoclimatology, Palaeoecology, 187(1-2): 61-82.

Grützner, J., Hillenbrand, C.-D. and Rebesco, M.A., 2005. Terrigenous flux and biogenic silica deposition at the Antarctic continental rise during the late Miocene to early Pliocene: Implications for ice sheet stability and sea ice coverage. Global and Planetary Change, 45: 131-149.

Haug, G.H., Tiedemann, R. and Keigwin, L.D., 2004. How the Isthmus of Panama put ice in the Arctic: Drifting continents open and close gateways between oceans and shift Earth's climate. Oceanus Magazin, 42(2): 1-4.

Hensen, C. et al., 2003. Control of sulfate pore-water profiles by sedimentary events and the significance of anaerobic oxidation of methane for the burial of sulfur in marine sediments. Geochimica et Cosmochimica Acta, 67(14): 2631-2647.

Hepp, D.A., Mörz, T. and Grützner, J., 2006. Pliocene glacial cyclicity in a deep-sea sediment drift (Antarctic Peninsula Pacific Margin). Palaeogeography, Palaeoclimatology, Palaeoecology, 231(1-2): 181-198.

Hermoyian, C.S. and Owen, R.M., 2001. Late Miocene-early Pliocene biogenic bloom: Evidence from low-productivity regions of the Indian and Atlantic Oceans. Paleoceanography, 16(1): 95-100.

Hillenbrand, C.-D. and Cortese, G., 2006. Polar stratification: A critical view from the Southern Ocean. Palaeogeography, Palaeoclimatology, Palaeoecology, 242(3-4): 240-252.

Hillenbrand, C.-D. and Ehrmann, W.U., 2005. Late Neogene to Quaternary environmental changes in the Antarctic Peninsula region: Evidence from drift sediments. Global and Planetary Change, 45(1-3): 165-191.

Hillenbrand, C.-D. and Fütterer, D.K., 2002. Neogene to Quaternary deposition of opal on the continental rise west of the Antarctic Peninsula, ODP Leg 178, Sites 1095, 1096, and 1101. In: P.F. Barker, A. Camerlenghi, G.D. Acton and A.T.S. Ramsay (Editors), Proceedings of the Ocean Drilling Program, Scientific Results. Texas A&M University, College Station, TX, pp. 1-33 [CD-ROM].

Hodell, D.A. and Kennett, J.P., 1986. Late Miocene-early Pliocene stratigraphy and paleoceanography of the South Atlantic and Southwest Pacific Ocean: A synthesis. Paleoceanography, 1(3): 285-311.

Iorio, M., Wolf-Welling, T.C.W. and Mörz, T., 2004. Antarctic sediment drift and Plio-Pleistocene orbital periodicities (ODP Sites 1095, 1096, and 1101). In: B. D'Argenio, A.G. Fischer, I. Premoli Silva, H. Weissert and V. Ferreri (Editors),

Cyclostratigraphy: Approaches and case histories. SEPM Special Publication. Society for Sedimentary Geology, Tulsa, pp. 231-244.

Iwai, M. and Winter, D., 2002. Taxonomic notes of Neogene diatoms from the Western Antarctic Peninsula: Ocean Drilling Program Leg 178. In: P.F. Barker, A. Camerlenghi, G.D. Acton and A.T.S. Ramsay (Editors), Proceedings of the Ocean Drilling Program, Scientific Results. Texas A&M University, College Station, TX, pp. 1-57 [CD-ROM].

Karlin, R., 1990. Magnetite diagenesis in marine sediments from the Oregon continental margin. Journal of Geophysical Research, 95: 4405-4419.

Kasten, S., Zabel, M., Heuer, V. and Hensen, C., 2003. Processes and signals of nonsteady-state diagenesis in deep-sea sediments and their pore waters. In: G. Wefer, S. Mulitza and V. Ratmeyer (Editors), The South Atlantic in the Late Quaternary: Reconstruction of material budgets and current systems. Springer, Berlin, Heidelberg, New York, pp. 431-459.

Knorr, G. and Lohmann, G., 2003. Southern Ocean origin for the resumption of Atlantic thermohaline circulation during deglaciation. Nature, 424(6948): 532-536.

Kumar, N. et al., 1995. Increased biological productivity and export production in the glacial Southern Ocean. Nature, 378: 675-680.

Lear, C.H., Elderfield, H. and Wilson, P.A., 2000. Cenozoic deep-sea temperatures and global ice volumes from Mg/Ca in benthic Foraminiferal calcite. Science, 287: 269-272.

Licht, K.J., 2004. The Ross Sea's contribution to eustatic sea level during meltwater pulse 1A. Sedimentary Geology, 165(3-4): 343-353.

Lucchi, R.G. et al., 2002a. Sedimentary processes and glacial cycles on the sediment drifts of the Antarctic Peninsula Pacific margin: Preliminary results of SEDANO-II project. New Zealand Journal of Geology and Geophysics, 35: 275-280.

Lucchi, R.G. et al., 2002b. Mid-late Pleistocene glacimarine sedimentary processes of a high-latitude, deep-sea sediment drift (Antarctic Peninsula Pacific margin). Marine Geology, 189(3-4): 343-370.

McManus, J., Berelson, W.M., Hammond, D.E. and Klinkhammer, G.P., 1999. Barium cycling in the north Pacific: Implications for the utility of Ba as a paleoproductivity and paleoalkalinity proxy. Paleoceanography, 14(1): 53-61.

McManus, J.F., François, R., Gherardi, J.-M., Keigwin, L.D. and Brown-Leger, S., 2004. Collapse and rapid resumption of Atlantic meridional circulation linked to deglacial climate changes. Nature, 428: 834-837.

Müller, D.W., Hodell, D.A. and Ciesielski, P.F., 1991. Late Miocene to earliest Pliocene (9.8–4.5 Ma) Paleoceanography of the subantarctic Southeast Atlantic: Stable isotopic, sedimentologic, and microfossil evidence. In: P.F. Ciesielski and Y. Kristoffersen (Editors), Proceedings of the Ocean Drilling Program, Scientific Results. Texas A&M University, College Station, TX, pp. 459-474.

Müller, P.J. and Schneider, R.R., 1993. An automated leaching method for the determination of opal in sediments and particulate matter. Deep-Sea Research Part I, 40(3): 425-444.

Novosel, I., Spence, G.D. and Hyndman, R.D., 2005. Reduced magnetization produced by increased methane flux at a gas hydrate vent. Marine Geology, 216(4): 265-274.

Nürnberg, C.C., Bohrmann, G., Schlüter, M. and Frank, M., 1997. Barium accumulation in the Atlantic sector of the Southern Ocean: Results from 190,000-year records. Paleoceanography, 12(4): 594-603.

ODP Leg 165 Shipboard Scientific Party, 1997. Site 998. In: H. Sigurdsson, R.M. Leckie and G.D. Acton (Editors), Proceedings of the Ocean Drilling Program, Initial Reports. Texas A&M University, College Station, TX, pp. 49-130.

ODP Leg 178 Shipboard Scientific Party, 1999. Site 1095. In: P.F. Barker, A. Camerlenghi and G.D. Acton (Editors), Proceedings of the Ocean Drilling Program, Initial Reports. Texas A&M University, College Station, TX, pp. 1-173 [CD-ROM].

ODP Leg 181 Shipboard Scientific Party, 1999. Site 1124: Rekohu Drift - from the K/T boundary to the deep western boundary current. In: R.M. Carter, I.N. McCave, C. Richter and L. Carter (Editors), Proceedings of the Ocean Drilling Program, Initial Reports. Texas A&M University, College Station, TX, pp. 1-137 [CD-ROM].

Passier, H.F., Middelburg, J.J., de Lange, G.J. and Bottcher, M.E., 1999. Modes of sapropel formation in the eastern Mediterranean: some constraints based on pyrite properties. Marine Geology, 153(1-4): 199-219.

Pfeifer, K., Kasten, S., Hensen, C. and Schulz, H.D., 2001. Reconstruction of primary productivity from the barium contents in surface sediments of the South Atlantic Ocean. Marine Geology, 177(1-2): 13-24.

Pudsey, C.J., 2000. Sedimentation on the continental rise west of the Antarctic Peninsula over the last three glacial cycles. Marine Geology, 167(3-4): 313-338.

Pudsey, C.J. and Camerlenghi, A., 1998. Glacial-interglacial deposition on a sediment drift on the Pacific margin of the Antarctic Peninsula. Antarctic Science, 10(3): 286-308.

Rebesco, M.A., Larter, R.D., Barker, P.F., Camerlenghi, A. and Vanneste, L.E., 1997. The history of sedimentation on the continental rise west of the Antarctic Peninsula. In: P.F. Barker and A.K. Cooper (Editors), Geology and seismic stratigraphy of the Antarctic margin, Part 2. American Geophysical Union, Washington, DC, pp. 29-49.

Rebesco, M.A. et al., 2002. Sediment drifts and deep-sea channel systems, Antarctic Peninsula Pacific Margin. In: D.A.V. Stow, C.J. Pudsey, J.A. Howe, J.-C. Faugères and A.R. Viana (Editors), Deep-water contourite systems: Modern drifts and ancient series, seismic and sedimentary characteristics. Geological Society Memoir. Geological Society, London, pp. 353-371.

Riedinger, N. et al., 2005. Diagenetic alteration of magnetic signals by anaerobic oxidation of methane related to a change in sedimentation rate. Geochimica et Cosmochimica Acta, 69(16): 4117-4126.

Robinson, S.G., 2001. Early diagenesis in an organic-rich turbidite and pelagic clay sequence from the Cape Verde Abyssal Plain, NE Atlantic: magnetic and geochemical signals. Sedimentary Geology, 143(1): 91-123.

Robinson, S.G., Sahota, J.T.S. and Oldfield, F., 2000. Early diagenesis in North Atlantic abyssal plain sediments characterized by rock-magnetic and geochemical indices. Marine Geology, 163(1-4): 77-107.

Rohling, E.J. and Gieskes, W.W.C., 1989. Late Quaternary changes in Mediterranean intermediate water density and formation rate. Paleoceanography, 4: 531-545.

Sigman, D.M., Jaccard, S.L. and Haug, G.H., 2004. Polar ocean stratification in a cold climate. Nature, 428: 59-63.

Stickley, C.E. et al., 2005. Deglacial ocean and climate seasonality in laminated diatom sediments, Mac.Robertson Shelf, Antarctica. Palaeogeography, Palaeoclimatology, Palaeoecology, 227(4): 290-310.

Stocker, T.F., 2003. South dials north. Nature, 424: 496-499.

Thomson, J., Jarvis, I., Green, D.R.H. and Green, D., 1998. Oxidation fronts in Madeira abyssal plain turbidites: Persistence of early diagenetic trace-element enrichments during burial, Site 950. In: H.-U. Schmincke, P.P.E. Weaver, J.V. Firth and W. Duffield (Editors), Proceedings of the Ocean Drilling Program, Scientific Results. Texas A&M University, College Station, TX, pp. 559-572.

Uenzelmann-Neben, G., 2006. Depositional patterns at Drift 7, Antarctic Peninsula: Along-slope versus down-slope sediment transport as indicators for oceanic currents and climatic conditions. Marine Geology, 233(1-4): 49-62.

van Os, B.J.H., Middelburg, J.J. and de Lange, G.J., 1991. Possible diagenetic mobilization of barium in sapropelic sediment from the eastern Mediterranean. Marine Geology, 100(1-4): 125-136.

Volpi, V., Camerlenghi, A., Hillenbrand, C.-D., Rebesco, M.A. and Ivaldi, R., 2003. Effects of biogenic silica on sediment compaction and slope stability on the Pacific margin of the Antarctic Peninsula. Basin Research, 15(3): 339-363.

Walter, H.-J., Rutgers van der Loeff, M.M. and François, R., 1999. Reliability of the 231Pa/230Th activity ratio as a tracer for bioproductivity of the ocean. In: G. Fischer and G. Wefer (Editors), Use of proxies in paleoceanography: Examples from the South Atlantic. Springer, Berlin, Heidelberg, New York, pp. 393-408.

Warnke, D.A., 1992. Miocene-Pliocene Antarctic glacial evolution: A synthesis of ice-rafted debris, stable-isotope and planktonic foraminiferal indicators, ODP Leg 114. In: J.P. Kennett and D.A. Warnke (Editors), The Antarctic paleoenvironment: A perspective on global change, Part 1. Antarctic Research Series. American Geophysical Union, Washington, DC, pp. 311-325.

Weaver, A.J., Saenko, O.A., Clark, P.U. and Mitrovica, J.X., 2003. Meltwater Pulse 1A from Antarctica as a Trigger of the Bolling-Allerod Warm Interval. Science, 299: 1709-1713.

Weeks, R.J., Roberts, A.P., Verosub, K.L., Okada, M. and Dubuisson, G.J., 1995. Magnetostratigraphy of upper Cenozoic sediments from Leg 145, North Pacific Ocean. In: D.K. Rea, I.A. Basov, D.W. Scholl and J.F. Allan (Editors), Proceedings of the Ocean Drilling Program, Scientific Results. Texas A&M University, College Station, TX, pp. 491-521.

Weldeab, S., Emeis, K.-C., Hemleben, C., Schmiedl, G. and Schulz, H., 2003. Spatial productivity variations during formation of sapropels S5 and S6 in the Mediterranean Sea: evidence from Ba contents. Palaeogeography, Palaeoclimatology, Palaeoecology, 191(2): 169-190.

Whitehead, J.M., Wotherspoon, S. and Bohaty, S.M., 2005. Minimal Antarctic sea ice during the Pliocene. Geology, 33(2): 137-140.

Wilson, T.R.S. et al., 1986. Oxidation fronts in pelagic sediments: Diagenetic formation of metal-rich layers. Science, 232: 972-975.

Wolf-Welling, T.C.W., Mörz, T., Hillenbrand, C.-D., Pudsey, C.J. and Cowan, E.A., 2002. Bulk sediment parameters (CaCO3, TOC, and >63 μm) of Sites 1095, 1096, and 1101, and coarse-fraction analysis of Site 1095 (ODP Leg 178, western Antarctic Peninsula). In: P.F. Barker, A. Camerlenghi, G.D. Acton and A.T.S. Ramsay (Editors), Proceedings of the Ocean Drilling Program, Scientific Results. Texas A&M University, College Station, TX, pp. 1-19 [CD-ROM].

Zachos, J.C., Pagani, M., Sloan, L., Thomas, E. and Billups, K., 2001. Trends, rhythms, and aberrations in global climate 65 ma to present. Science, 292: 686-693.

Submitted to Antarctic Science, under review

2.3 Manuscript 3: An approach to quantify the Pliocene ice sheet dynamics via slope failure frequencies recorded in Antarctic Peninsula rise sediments

Daniel A. Hepp and Tobias Mörz

MARUM – Center for Marine Environmental Sciences and Faculty of Geosciences, University of Bremen, P.O. Box 330440, 28334 Bremen, Germany

Corresponding author: Daniel A. Hepp, E-mail: dhepp@uni-bremen.de

2.3.1 Abstract

The understanding of the glacial driven sedimentary transport system across the shelf to the slope and subsequently to deep-sea sediment bodies along the Pacific Continental Margin of West Antarctic Peninsula is a crucial feature for interpreting ice sheet dynamics. The main focus of this paper lies on the quantification of slope failure frequencies recorded in Pliocene core intervals of ODP Site 1095. We used the long term sedimentation rate dependency of the marine carbon burial efficiency in the drift sediment to calculate a ratio of glacial to interglacial sedimentation rates. Using the decompacted average length of glacial-interglacial cycles it was possible to solve a set of linear equations to derive average half periods of 61.59 and 59.77 kyr respectively for the time interval 5.8-3 .2 Ma. The resulting frequency distribution of slope failures reflects short and rapid but cyclic ice advances every ~375 yrs. Short retention times between slope loading and slope failure are supported by biogenic silica dissolution analyses. This study demonstrates the potential of the rise record to improve models of orbital controlled size variations of the West Antarctic ice sheet and confirms the hypothesis of a highly dynamic ice sheet during the early Pliocene warm period.

Keywords: Ice sheet dynamic, ODP Site 1095, Pliocene, sedimentation rate, turbidite frequency, West Antarctic Peninsula

2.3.2 Introduction

2.3.2.1 Slope failure mechanisms along the Antarctic Peninsula Continental Margin

Slope instabilities along ocean margins are the result of various geological processes such as plate tectonics, eustatic sea level variations or erosion associated with slope loading. Sedimentary slope failures are the most important trigger mechanism for sediment gravity flows (e.g. turbidites; Løseth 1999).

Turbidites are common deep-water deposits (Stow & Mayall 2000). Turbidity currents can be initiated on slopes by the transformation of slides and slumps into turbulent debris flows as they incorporate more water (Stow 1986, Løseth 1999). In numerical experiments with a multi-process sedimentation model, O'Grady and Syvitski (2001) showed that the type of mass movement depends on the failed sediment type. Sandy or silty material results in turbidite down-slope transport, whereas clayey materials lead to debris flows. The frequency with which turbidity currents are generated depends on source area, delivery system, slope angel and seismic activity.

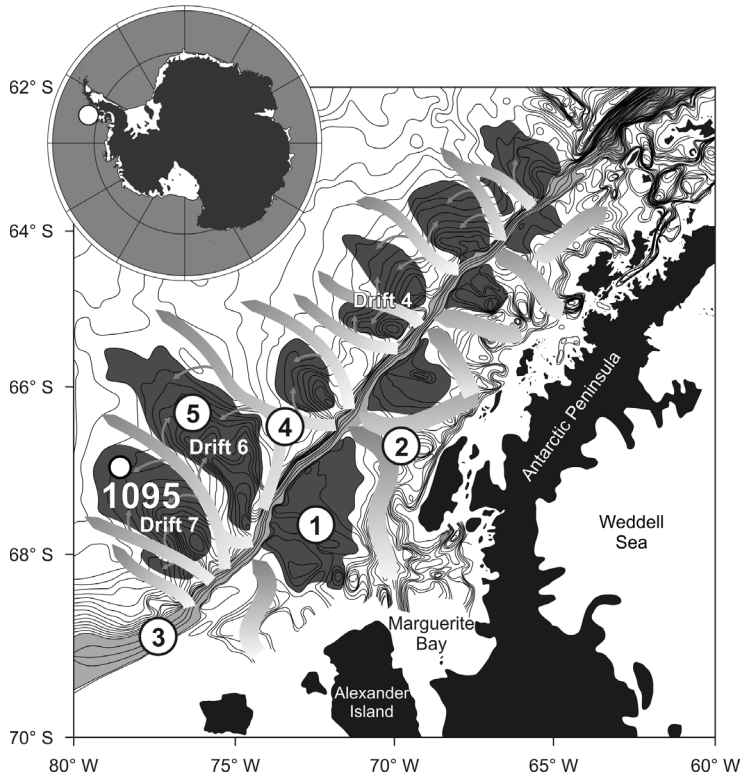

Fig. 1. Bathymetric map of the Pacific Continental Margin off the Antarctic Peninsula. The map shows a glacial driven sediment feeder system of (1) lobes and (2) troughs on the outer shelf, (3) an oversteepen slope, (4).deep-sea channels and (5) sediment drifts on the continental rise and the location of Site 1095, ODP Leg 178 on the distal part of Drift 7 (modified after Lucchi et al. 2002, Rebesco et al. 2002).

Along the Pacific Continental Margin of the West Antarctic Peninsula, the driving mechanisms for slope loading and failure are erosion of the shelf or hinterland by advancing ice sheets during glacials (Raymond 2002, Dowdeswell et al. 2004, Bart et al. 2007). The most rapid flow of the West Antarctic ice sheet occurs in areas of ice streams. They occupy glacial troughs, which were observed on the West Antarctic Peninsula shelf (Fig. 1.1; Pudsey & Camerlenghi 1998, Faugères et al. 1999, Rebesco et al. 2002) and around West Antarctica (Anderson et al. 2001). Ice stream flow velocities are typically a few hundred meters per year (Anderson et al. 2001). Elverhøi et al. (1998) compared sediment fluxes of ice streams with the efficacy of large fluvial systems and demonstrated that glaciers are far more effective in terms of erosion than rivers. They compiled glacial erosion data from sediment budget and sediment yield studies from the Svalbard-Barents Sea region. According to this study, fast flowing ice streams have the potential to erode terrigenous material at rates more than 1 mm yr^{-1}.

Along the Pacific Continental Margin of the West Antarctic Peninsula, the grounded ice streams (Fig. 1.2) transport eroded terrigenous material over the shelf edge to the over steepened slope (Fig. 1.3; Rebesco et al. 1996). Frequent slope failures trigger turbidity currents, which run in channels (Fig. 1.4) between large elongated sediment bodies (Fig. 1.5) to the abyssal plain. The passage of large turbidity currents through channels (Diviacco et al. 2006) results in spillover silt lamina deposits on twelve sediment bodies along the Antarctic Continental Rise. These sediment drifts were developed by a complex interplay of down-slope and along-slope processes. The origin of these so called 'drift bodies' is still a matter of controversy and depends on the relative importance given to both processes (McGinnis & Hayes 1995, Rebesco et al. 1996, Rebesco et al. 2002, Uenzelmann-Neben 2006).

An exception from the otherwise frequent, small scale glacially controlled turbidite events along the West Antarctic Continental Margin are two documented, large debris flow deposits between Drift 6 and 7 and within sediment Drift 4 (Fig. 1). This Mega flow events are associated with catastrophic continental margin collapse in the late Pliocene (Diviacco et al. 2006, Rebesco & Camerlenghi 2008, Volpi et al. in press).

The interaction of ice volume evolution, slope loading and turbidity depositional processes plays a major role in drift build up during glacials and the subsequent deglaciation phase. On the passive and tectonic stable Pacific margin of the West Antarctic Peninsula (Barker 1982), the time interval between slope loading and slope failure mainly depends on slope angle and sediment type. The slope of the outer continental shelf is very steep with an average angle of 16°, making simple slope loading by the 'ice sheet feeder system' sufficient to trigger slope failure. This means that local slope instabilities along the Pacific margin of the Antarctic Peninsula are directly linked to regional ice events resulting in turbidity depositions on the drift. Mörz (2002) showed that the drift bodies represent the most proximal continuous sedimentary recorders for West Antarctic ice events and glacial-interglacial cyclicity.

2.3.2.2 Organic matter burial and preservation

Organic carbon and biogenic silica are important components in the marine record. They are used as proxies for West Antarctic paleoproductivity but are also prone to diagenetic recycling.

The burial efficiency of organic carbon in marine sediments is linked to the marine carbon cycle and plays a major role controlling atmospheric CO_2 and O_2 (Burdige 2006a, b). Several factors control the preservation of organic matter in marine sediments, e.g. organic matter-mineral interactions, organic matter composition and reactivity, and the time of sediment oxygen 'exposure' (Burdige 2006b). Typical recent open-ocean deep-sea sediment have organic carbon content as low as 0.3 weight percent (wt.%; Stein 1990, Burdige 2006b). Higher amounts of organic matter preservation require special environmental conditions, e.g. fast burial of organic matter by turbidites (Stein 1990). Burdige (2006b) suggests that the organic carbon burial efficiency with respect to the original carbon rain rate to the sediment surface is on average ~10-20%.

The abundance of $BSiO_2$ in deep-sea sediments is often interpreted in terms of productivity pattern of e.g. diatoms (Koning et al. 1997). Biogenic silica or opal is a major component of the skeletal structure of diatoms, radiolaria, silicoflagellates and sponges (Koning et al. 2002). Among them, diatoms are the main producers of opal and strongly influence the cycling of silicon and carbon in the oceanic ecosystem (Cortese et al. 2004). Smear slides from ODP Site 1095 core sediments show that diatoms assemblages dominate (10-30%) and radiolarians and foraminifers are underrepresented

(Hillenbrand & Fütterer 2002). The accumulation of biogenic opal on the seafloor is controlled by bioproductivity, dissolution in the water column and diagenetic dissolution within the sediments. The opal preservation in sediments after burial is very poor. Schlüter (1990) assumes that in the Weddell Sea, more than 90% of buried opal is dissolved in surficial sediments and released to the sediment-water interface. In general, higher sediment flux leads to faster burial and to better opal preservation (Ragueneau et al. 2000, Rickert 2000).

This study assume that diatoms are the main carrier of the opal signal (Treguer et al. 1995), slope loading is dominated by terrigenous material from the shelf and hinterland during glacials, the quantity of diatom fossils settling down from water column is continuous between two consecutive slope failures, and the laboratory determined leaching rate of biogenic silica ($BSiO_2$) from the skeletal structure of diatoms is a function of their diagenetic and transport history.

2.3.2.3 Regional settings

This study is focussed on the early Pliocene sedimentary record from Drift 7, which is one of the largest sediment mounds located southwest of the Antarctic Peninsula (Fig. 1). Its asymmetrical shape, with a short steep side facing southeast and a long, gently-sloping side facing northwest, is similar in shape to the other sediment drifts in this area.

The distal part of Drift 7 was drilled by advanced piston corers and extended core barrels from multiple Holes A and B at Site 1095 during ODP Leg 178 (ODP Leg 178 Shipboard Scientific Party 1999). The 561.78 m long composite record covers the late Miocene to the Holocene (~10 Ma).

2.3.2.4 Aims of this study

Our study is aimed to quantify the early Pliocene ice sheet dynamics via slope failure frequencies recorded in Antarctic Peninsula rise sediments. Crucial questions are (a) how to determine the average time period between two consecutive turbidite events (turbidite frequency), and (b) what other indicators can be used to support the derived model for paleo ice sheet dynamics. The presented quantification approach of paleo ice sheet dynamics is a contribution to the following issues: (c) Is the postulated switch of an early Pliocene warm, highly dynamic Antarctic ice sheet regime (Barrett et al. 1992, Wilson 1995, Bart 2001), to Pleistocene cold-based, stable conditions at about 3 Ma (Rebesco & Camerlenghi 2008) expressed in the tubidite frequency record?, and (d) is the Pliocene Antarctic Peninsula ice shield dynamics forced by Milankovich eccentricity (Grützner et al. 2003, Iorio et al. 2004, Grützner et al. 2005, Hepp et al. 2006) or does it behave rather autocyclic (Pudsey 2002)?

2.3.3 Methods

X-ray images, sedimentary and geochemical analyzes from three core intervals of ODP Site 1095 (1095B-3H6, 104.5-105.5 meter composite depth = mcd, uppermost early Pliocene; 1095B-5H5, 121.5-122.5 mcd, middle early Pliocene; 1095B-10H2, 165.0-166.0 mcd, lowermost early Pliocene) were used to reconstruct turbidite recurrence frequencies in order to obtain a measure of the regional paleo ice sheet dynamics.

2.3.3.1 Measurements

Digital X-ray images (Fig. 2) were made from selected core sections at the Rotes Kreuz Krankenhaus Bremen using 'Fluorospot compact' radiography equipment. The dimension of the detector (measuring 40 to 80 cm) determines the size of the single X-ray image. Four overlapping images were produced to cover a 1.5 m core section. Ray penetration of 66 kV and an exposure time of 7.1 mA/s was used. The high-resolution images were used to detect and map single silt layers, some of them with distinguishable Bouma-sequences. Many of the mapped laminae with a total thickness less than <1 mm have not been detected before from core images or visual descriptions. The exact definition of glacial-interglacial boundaries was outlined by Hepp et al. (2006).

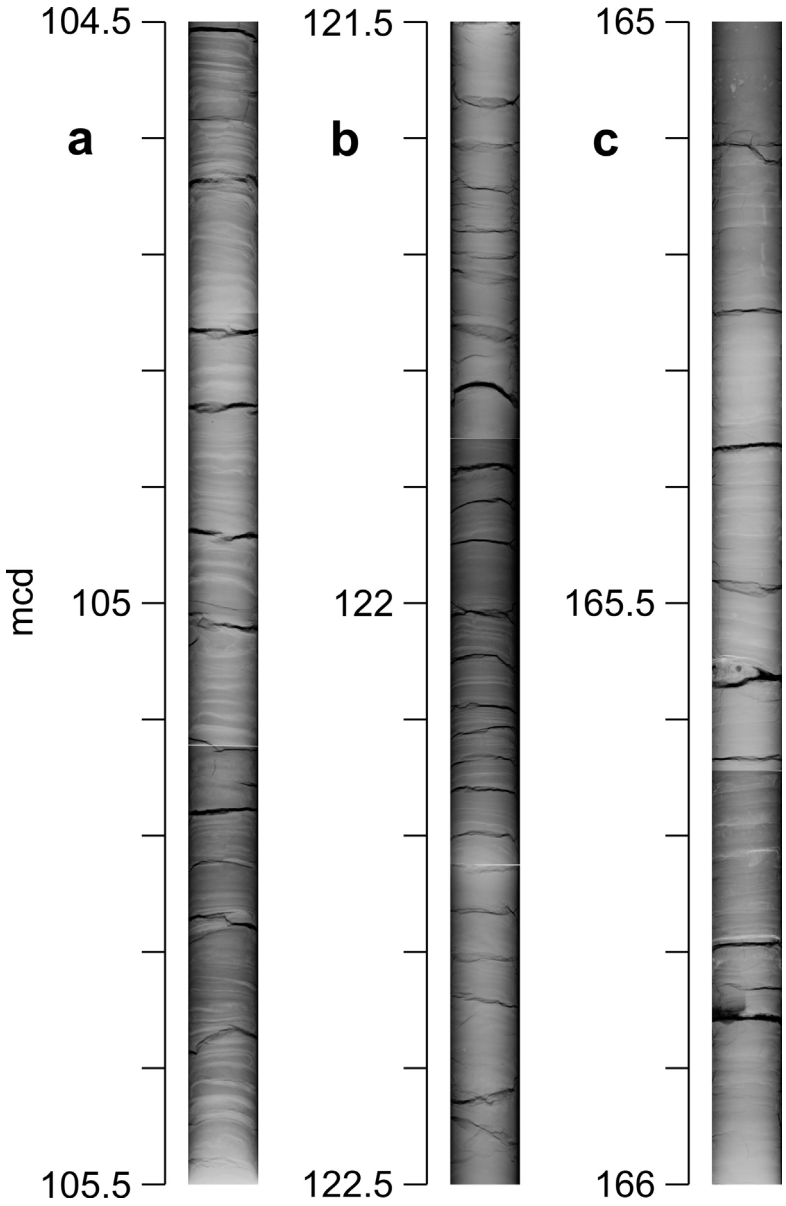

Fig. 2. Digital X-ray images from early Pliocene glacial intervals of ODP Site show the typical fine lamination of silt layer sequences. (a) shows core section 1095B-3H6, 104.5-105.5 mcd from uppermost early Pliocene, (b) 1095B-5H5, 121.5-122.5 mcd from middle early Pliocene, and (c) 1095B-10H2, 165.0-166.0 mcd from lowermost early Pliocene (see Fig. 3).

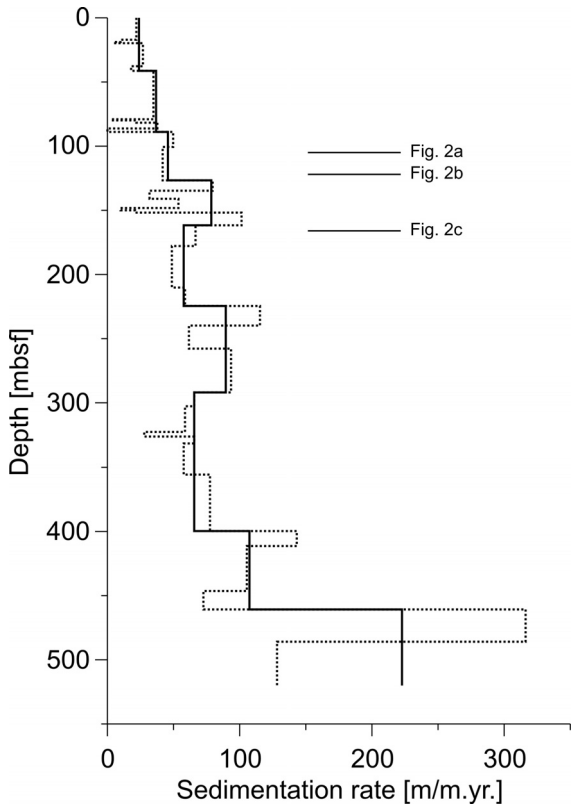

Fig. 3. Sedimentation rates (cm/kyr) for Site 1095 plotted vs. depth. The dotted line shows the sedimentation rate based on a linear model from magnetostratigraphic-biochronologic tie-points given in Acton (2002) and Iwai (2002). The black line shows the simplified linear sedimentation rate model with intervals A to I. For depth (meter below seafloor = mbsf) and age (Ma) tie-points see Tab. 1. The black barks show the depth position of the investigated core intervals (see Fig. 2).

The sedimentation rate (Fig. 3) is based on an magnetostratigraphic-biochronologic age model given in Acton et al. (2002) and Iwai et al. (2002; dotted line). The black line shows a simplified linear sedimentation rate model.

Fig. 4 shows parameter of magnetic susceptibility (κ), total organic carbon content (TOC), biogenic silica content ($BSiO_2$) and the reaction rate constant of leached biogenic silica (K_m) from two core intervals, 171.5-166.0 and 108.0-101.0 mcd, of ODP Site 1095 in relation to glacial and interglacial stages proposed by (Hepp et al. 2006). Fig. 5 shows the parameters κ, $BSiO_2$ and K_m of the Pleistocene-Holocene section (0-4.5 mcd). Magnetic susceptibility (κ) data were obtained during ODP Leg 178 using the shipboard whole-core multisensor track logger (ODP Leg 178 Shipboard Scientific Party 1999). This fast, high-resolution measuring method is used here to distinguish glacial from deglaciation, ice sheet break down and interglacial intervals (MSMZ, see Hepp et al. 2006). The total organic carbon content (TOC) was measured by LECO on 55 samples. Left over material from the same samples was used to determine the biogenic silica content ($BSiO_2$). The homogenized dry bulk samples were analyzed using an automated leaching technique after Müller and Schneider (1993) and the reaction rate constant (K_m) was calculated using a leaching model after Koning et al. (2002, Model 4). The TOC, $BSiO_2$ and K_m measurements were distinguished in sediment samples from pure silt layers (Fig. 4, dark circles) and silt layer free sediments with a fine fraction <63 μm (Fig. 4, light circles).

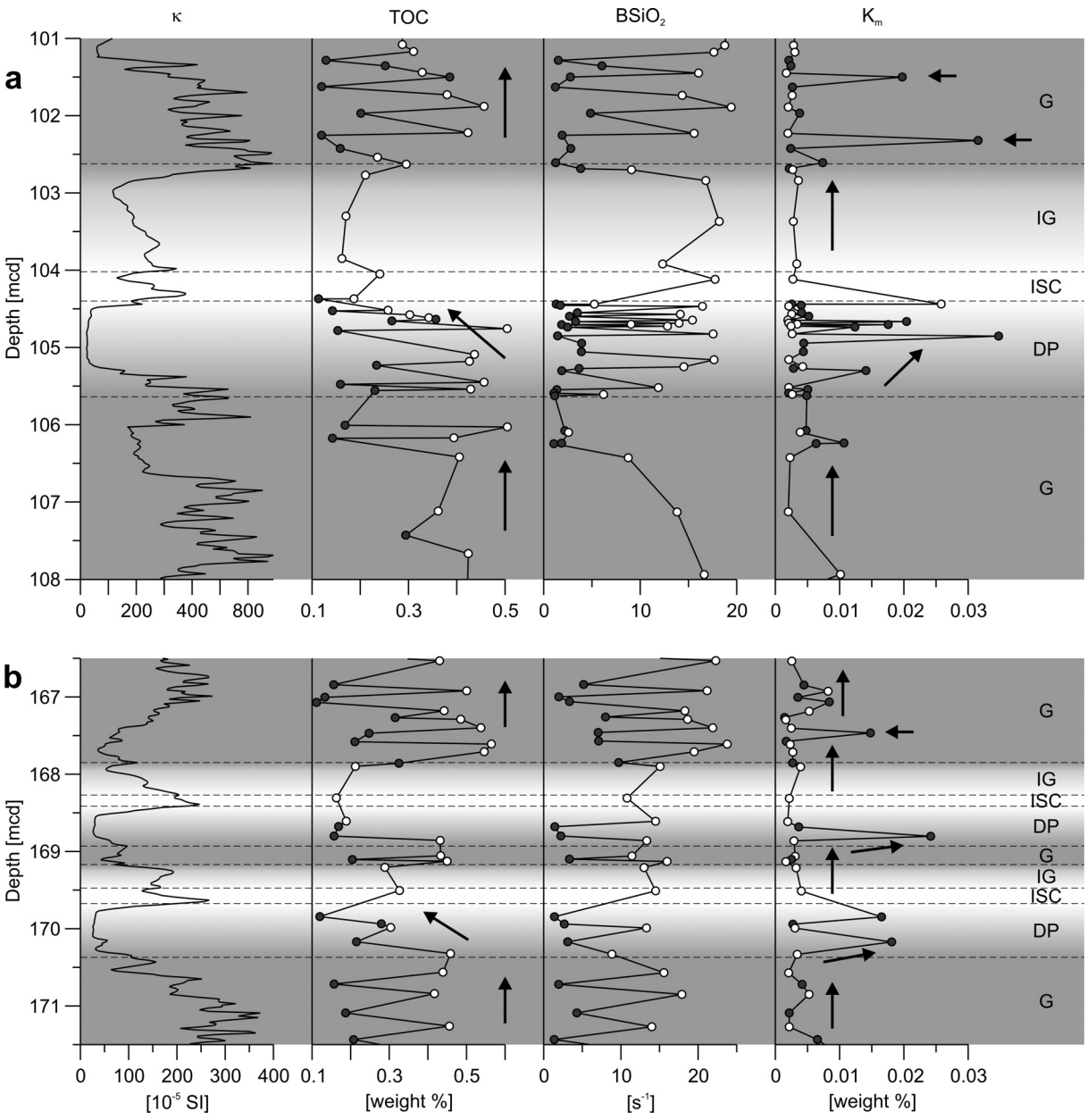

Fig. 4. The diagram shows magnetic susceptibility (κ), total organic carbon (TOC), biogenic silica content ($BSiO_2$) and the reaction rate constant of leached biogenic silica (K_m) in relation to glacial (G) and true interglacial (IG) stages, as well as deglaciation phases (DP) including the ice sheet collapse (ISC). The sediment samples were distinguished in samples from pure silt layers (dark circles) and silt layer free sediments with a fine fraction <63 µm (light circles). Characteristic gradients of TOC and BSiO2 in relation to glacial stages are marked by arrows.

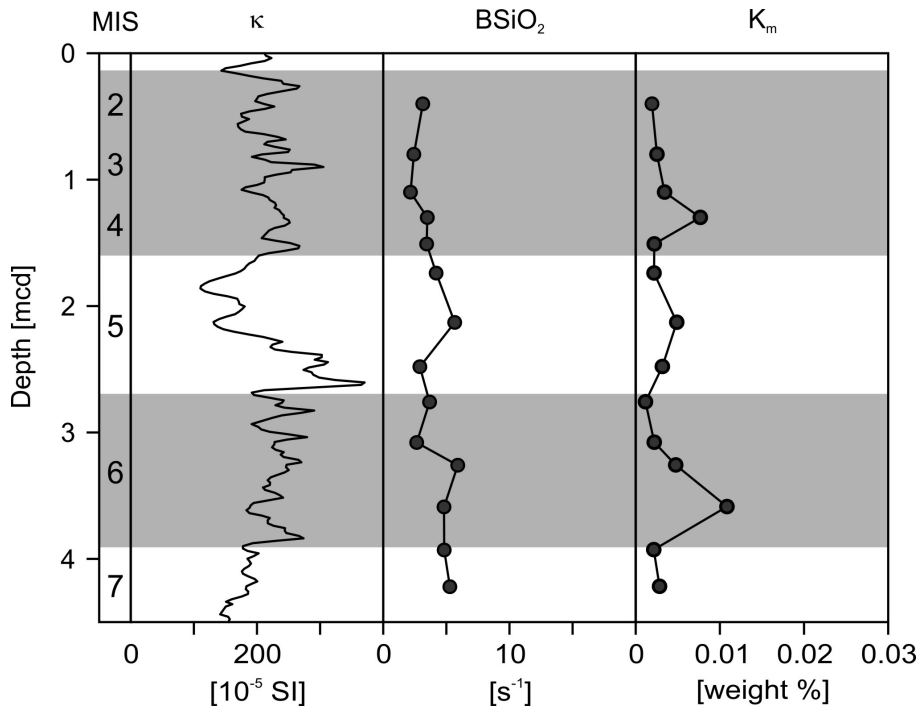

Fig. 5. Magnetic susceptibility (κ), biogenic silica content ($BSiO_2$) and the reaction rate constant of leached biogenic silica (K_m) in relation to marine isotope stages (MIS). In comparison to early Pliocene sections (Fig. 4) the average leaching rate is much lower (~0.003 s^{-1}).

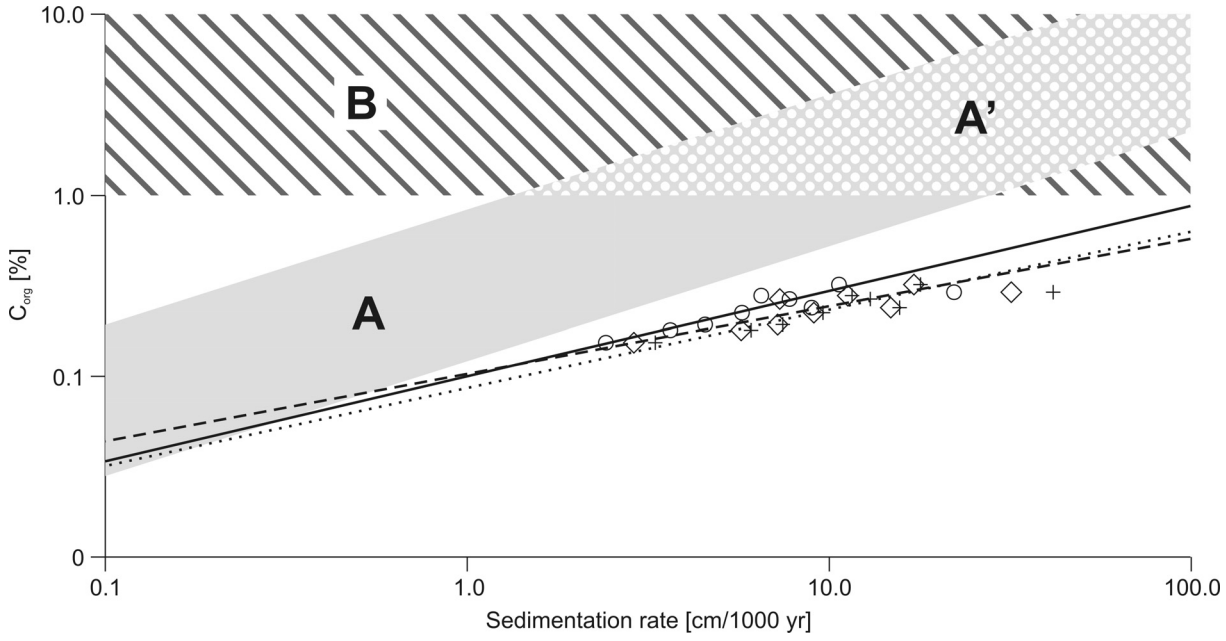

Fig. 6. Correlation between marine organic carbon and sedimentation rate (modified and simplified after Stein 1986, Stein 1990). The model is based on data derived from Miocene to Pleistocene/Holocene sediment deposits in open-marine (A) oxic, (A') upwelling high-productivity and (B) anoxic environments. The symbols and power fit graphs show ODP Site 1095 data of compacted sediments (open circles, black line) and decompacted sediments after Stein (1990) (Eq. 3; crosses, dotted line) or after Terzaghi (Eq. 4; open rhombs, dashed line) respectively.

2.3.3.2 Relationship of organic carbon and sedimentation rate

In order to determine the average period between two consecutive turbidite events preserved in the silt layer record, glacial-interglacial sedimentation rates were derived from a positive long-term correlation of sedimentation rate and marine organic carbon content.

Stein (1990) showed that a positive correlation between organic carbon content and sedimentation rate exists (Fig. 6A and A'), since high sedimentation rates favor the preservation of organic matter by reducing the retention time in the shallow subsurface zone of bioturbation and oxic decomposition. Under anoxic deep bottom-water conditions (Fig. 6B) he recognized no positive correlation between organic carbon and sedimentation rate. According to Stein (1990), the relationship between marine organic carbon (C_{org}) and sedimentation rate (ω, cm/kyr) in recent sediments can be expressed as a log-linear function:

(1) $$C_{org} = a\omega^{b}$$

or

(2) $$\omega = \left(\frac{C_{org}}{a} \right)^{\frac{1}{b}}$$

where the factor a is 0.36 and the slope b is 0.64 of Stein's (1990) data set.

To apply these functions to the relationship between preserved marine organic carbon and sedimentation rate of Miocene to Pleistocene sediments it is necessary to correct the apparent sedimentation rate by a decompaction factor (DF). Stein (1990) proposed the following relationship for the decompacted sedimentation rate (ω_0, cm/kyr):

(3) $$\omega_0 = \omega \cdot DF = \omega \cdot \frac{100 - \phi}{100 - \phi_0}$$

where Φ is the mean porosity of the Miocene to Pleistocene samples in percent and Φ_0 is the porosity of the freshly deposited sediment in the same depositional environment. In this study, the porosity of near surface sediments of ODP Site 1095 was Φ_0 = 75%. For comparison, the average porosity for the late Miocene-Pliocene section is 57%.

A second approach to calculate decompacted sedimentation rates is based on Terzaghi's one dimensional consolidation theory (Azizi 2000) and restores the original sedimentation rates based on the volume independent pore numbers:

(4) $$\omega_0 = \frac{\Delta z_{\text{int}} + dh}{\Delta t_{\text{int}}} = \frac{\Delta z_{\text{int}} + \frac{\Delta z_{\text{int}} \cdot (e_0 - e)}{1 + e_0 - (e_0 - e)}}{\Delta t_{\text{int}}} = \frac{\Delta z_{\text{int}} + \Delta z_{\text{int}} \cdot e_0}{\Delta t_{\text{int}} + \Delta t_{\text{int}} \cdot e}$$

where *dh* is the height loss by compaction, Δz_{int} is the compacted interval length and Δt_{int} is the time of deposition of each interval; e_0-e is the difference between the initial and the measured pore number of the compacted sediment as retrieved from the cores.

2.3.3.3 Mean duration of glacials and interglacial in relation to the deglaciation phase

On the basis of the mean average organic carbon content of each core interval from a composite splice of ODP Site 1095, the long term correlation (9.8 Ma) between organic carbon and the compacted and decompacted sedimentation rate was calculated using Eq. 3 and 4, respectively. The data is plotted to a log-log scale and fitted by a power function (Fig. 6). The decompacted sedimentation rate is based on a simplified model (Fig. 3, black line) of the linear sedimentation rate from magnetostratigraphic-biochronologic age tie-points given in Acton (2002) and Iwai (2002; Fig. 3, dotted line). The data are given in Tab. 1.

Interval	Depth [mbsf]		Age [Ma]		C_{org} [wt. %]	Sedimentation rate [cm/kyr]		
(Fig. 3)	Top	Bottom	Top	Bottom	Mean average	Compacted	Decompacted (Eq. 3)	Decompacted (Eq. 4)
A	0.00	41.29	0	1.95	0.15	2.43	3.32	2.90
B	41.29	88.68	1.95	3.33	0.18	3.66	6.11	5.74
C	88.68	126.20	3.33	4.18	0.19	4.56	7.48	7.24
D	126.20	161.31	4.18	4.98	0.27	7.81	13.05	7.33
E	161.31	224.30	4.98	6.137	0.22	5.77	9.66	9.11
F	224.30	292.04	6.137	6.935	0.24	8.98	15.73	14.87
G	292.04	399.86	6.935	8.635	0.28	6.52	11.62	11.30
H	399.86	460.87	8.635	9.23	0.32	10.69	17.96	17.22
I	460.87	520.50	9.23	9.58	0.29	22.24	41.77	32.00
			Mean average		0.24	8.07	14.08	11.97

Tab. 1. Simplified sedimentation rate model (see Fig. 3) computed for compacted and decompacted (Eq. 3and Eq. 4) sediments.

The compacted and decompacted linear sedimentation rates were used to calculate the mean duration of glacials (Δt_{avG}) between neighboring magnetostratigraphic-biochronologic age tie-points in the time interval from 5.98 to 3.22 Ma:

$$\Delta t_{avG} = \frac{\Delta z_{avG} \cdot \Delta t_{avGIG}}{\Delta z_{avG} + \Delta z_{avIG} \cdot \omega_{av\ ratio}} \quad (5)$$

where Δz_{avG} and Δz_{avIG} are the mean average length of glacials and interglacials respectively, Δt_{avGIG} is the mean average period defined by the age tie-points 5.98 Ma and 3.22 Ma (= 2.67 Ma) divided by the number of identified glacial-interglacial cycles (= 22). The linear sedimentation rate ratio ($\omega_{av\ ratio}$) between glacials and interglacials is calculated from the compacted mean average linear sedimentation rate and decompacted linear sedimentation rates using Eq. 3 and Eq. 4.

To further refine the mean duration of glacials and interglacials, a model of three main sedimentary stages within a glacial-interglacial cycle was used (Hepp et al. 2006): (a) Full glacial (G), (b) deglaciation phase (DP) including the ice sheet collapse (ISC), and (c) ice sheet growth phase, here referred as true interglacial (IG). An example for this model is shown in Fig. 4.

The refinement is necessary since the deglaciation phase was previously unconsidered. This could lead to an inaccurate estimate of the initial, mean average glacial-interglacial interval length and period respectively, because the boundaries of the deglaciation phase are only definable with a complex multi-parameter approach (Hepp et al. 2006). Deglaciation phases are influenced by a decline in glacial silt deposition and increase in interglacial organic input.

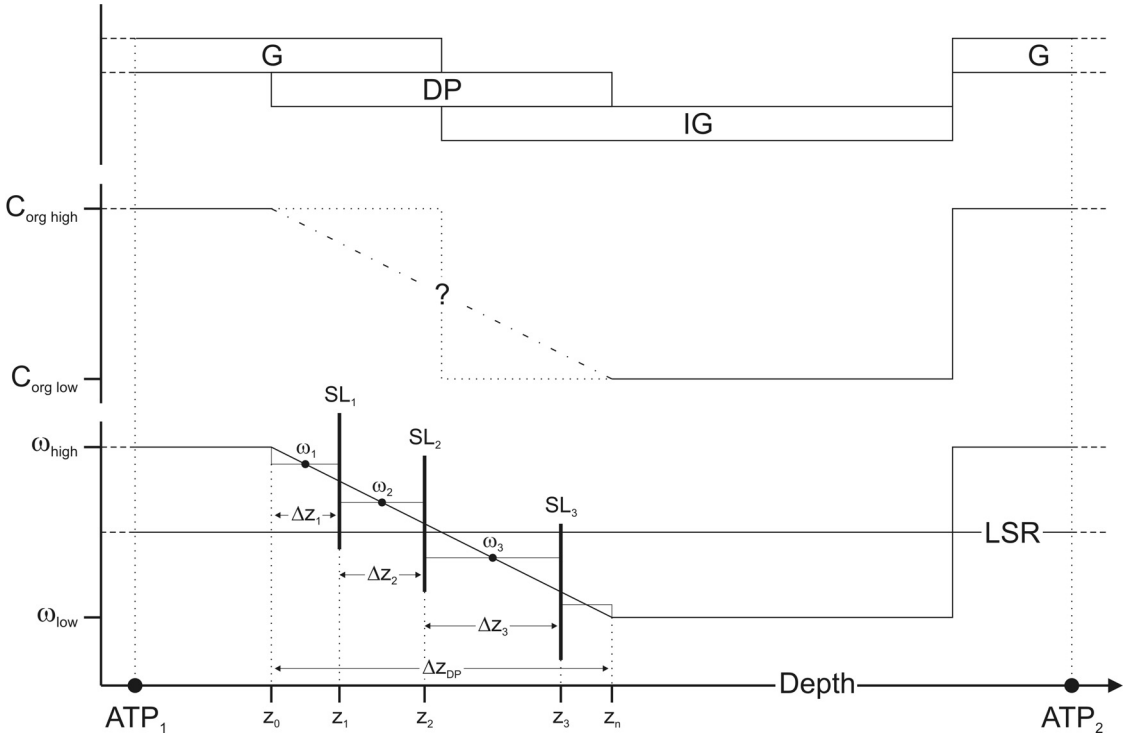

Fig. 7. Combined model of glacial-interglacial cycles, organic carbon content and sedimentation rate. The proportion of glacial (G) and interglacial (IG) intervals according to the time period is similar. The deglaciation phase (DP) spans equally both intervals. The linear sedimentation rate (LSR) was computed using the tie-points TP_1 and TP_2. The mean sedimentation rate (ω) correlates positive with mean marine organic carbon content (C_{org}). Both are high in glacials, decrease during deglaciation phase (glacial-to-interglacial transition), then achieve a lower level in the upper part of the interglacial and jumps again to a high at the interglacial-glacial transition. For deglaciation phase we calculated the duration and the relative timing ($t_{(z)}$) of each silt layer (SL) depositions z on the basis of the length of the deglaciation phase (z_{DP}) and glacial and interglacial sedimentation rates (ω_G, ω_{IG}) using the function given in Eq. 6.

Another problem using the positive correlation of sedimentation rate and marine organic carbon content arise from the significant diagenetic influence on the organic carbon preservation during the deglaciation phase reported by Hepp et al. (2006). The model of the organic carbon-sedimentation rate correlation is unfeasible to calculate the duration of the deglaciation phase. To limit the uncertainties introduced by the 'deglaciation phase problem' a linear decrease of the sedimentation rate from a higher glacial to a lower interglacial level was assumed. A simple glacial-interglacial model with a deglaciation phase spanning equal parts of both depths intervals was used. The duration of the deglaciation phase and the relative timing *t(z)* of each silt layer (SL) depositions (*z*) was

calculated on the basis of the length in decompacted core meters of the deglaciation phase z_{DP} and glacial and interglacial sedimentation rates ω_G, ω_{IG} using the function:

$$(6)\quad t(z) = \frac{1}{2} \cdot \frac{\omega_{IG} - \omega_G}{z_{DP}} \cdot z^2 + \omega_G \cdot z$$

The model is sketched in Fig. 7 and the results are given in Tab. 2.

Model	$\Delta z_{avG+DP/2}$ [cm]	$\Delta z_{avIG+DP/2}$ [cm]	ΔTOC_{avG} [wt%]	ΔTOC_{avIG} [wt%]	ω_{avG} [cm/kyr]	ω_{avIG} [cm/kyr]	$\omega_{avG/IG}$ ratio	Δt_{avG} [kyr]	Δt_{avIG} [kyr]
1	252.700	155.167	0.324	0.296	12.383	10.636	1.164	71.068	50.295
2	417.323	257.014	0.324	0.296	21.801	17.644	1.236	65.264	56.100
3	400.202	245.561	0.324	0.296	21.614	16.930	1.277	63.983	57.381

Tab. 2. Computation of the mean average period of glacials ($\Delta t_{zavG+DP/2}$) and interglacials ($\Delta t_{zavIG+DP/2}$), each include a half deglaciation phase, between the magnetostratigraphic-biochronologic age tie-points 5.98 and 3.22 Ma. The table shows the results from different models on basis of linear sedimentation rates (see Tab. 1) from (a) compacted sediments and decompaction models after (b) Stein ((1990); see Eq. 3) and (3) Terzaghi (see Eq. 4). The values were used for Eq. 5.

2.3.3.4 *Leaching rate of biogenic silica (opal-A)*

In order to support the derived turbidite frequency data we also looked at opal dissolution parameters as an additional approach to quantify the retention time between two consecutive slope failures. The reaction rate constant from automated leaching methods of biogenic silica, in the following called leaching rate, were used as an indicator for the preservation state of diatom frustules due to transport and depositional processes on continental shelf, slope and rise.

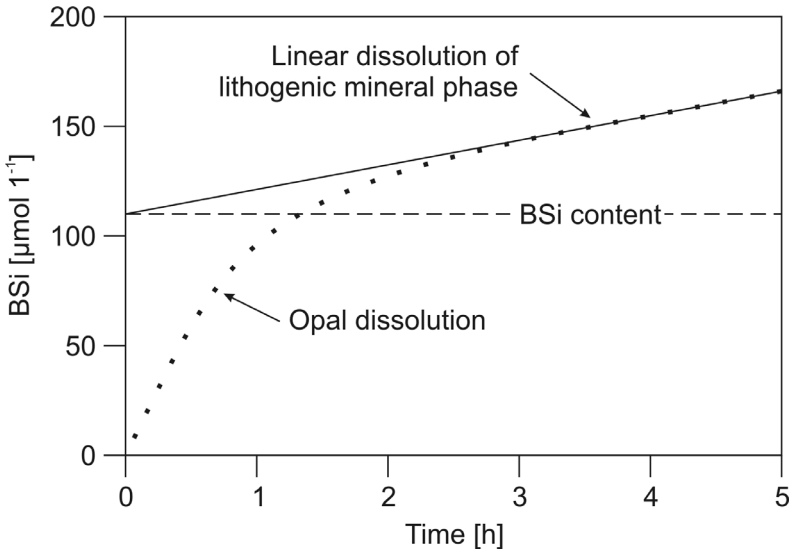

Fig. 8. Schematic sketch of a biogenic silica (BSi) dissolution curve (dotted line). The SiO_2 contribution of the lithogenic mineral phase can be extracted by a backward extrapolation of the linear fit of the dissolution curve. The corrected BSi content is retrieved from the fit curve at time zero (modified from Koning et al. 2002).

Most of the reactive silica in marine sediments has a biogenic origin (Koning et al. 2002). Since the Si-dissolution of $BSiO_2$ occurs independently from dissolution of the lithogenic phase from clay minerals (DeMaster 1981, 2002) it is necessary to distinguish between dissolving biogenic silica and silica from clay minerals. Si-dissolution from clay minerals has a linear and much slower reaction rate than of $BSiO_2$. Corrections for $BSiO_2$ from the lithogenic mineral phase can be achieved by extrapolation of the linear dissolution trend and subtraction from the measured total dissolved $BSiO_2$ (Fig. 8).

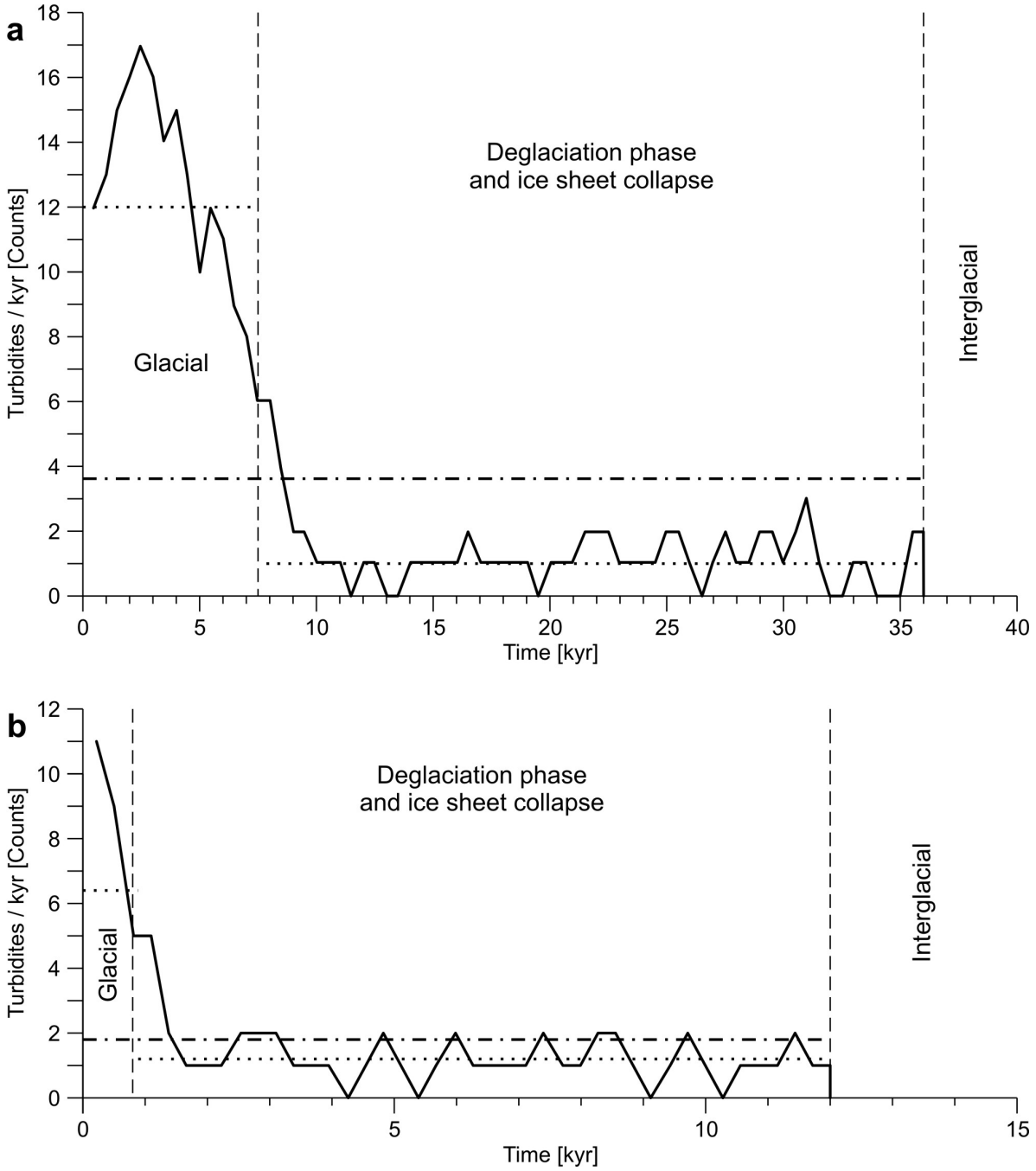

Fig. 9. Turbidite frequency for ODP 1095 core section between (a) 110.97 and 105.66 mcd and (b) 169.29 and 168.95 mcd. The diagram shows a decrease in turbidite frequency during the deglaciation and the ice sheet collapse phase. The number of turbidites per 1 kyr were plotted on the ordinate. The dotted line shows the mean average turbidite ratio for the glacial interval and the deglaciation phase respectively. The chain line shows the mean average of the total turbidite interval.

Müller and Schneider (1993) proposed an automated alkaline leaching method to determine the biogenic silica content in surface sediments and to discriminate between leached silica from the biogenic fraction and the lithogenic fraction. The digital data of the leaching curves were run through a fitting procedure after Koning et al. (2002, Model 4) to obtain a measure of the biogenic silica reactivity via the reaction rate constant (K_m):

$$(7)\quad K_m \frac{\nu}{\alpha([Si_{extr}])^{1/\nu}}$$

where Si_{extr} is the initial extractable Si (µm 1^{-1}), α measures the average lifetime of the extractable components in the mixture and ν is a non-dimensional parameter.

2.3.4 Results

The early Pliocene turbidite frequency for Drift 7 was determined via the calculation of the glacial-interglacial duration, which is based on the organic carbon correlated sedimentation rate model (Fig. 9, Tab. 1, Tab. 2). The results from leaching rate measurements of biogenic silica show the interaction of retention time, transport mechanisms and burial rate during glacial-interglacial cycles (Tab. 3).

TIME SCALE / STADIAL		SHELF AND SLOPE		DOWN SLOPE PROCESSES	DRIFT	LABORATORY MEASUREMENT
		Retention time	Opal dissolution	Mechanical fragmentation	Burial rate	Leaching rate
Pliocene	Full glacial	short	low	high	high	low
	Deglaciation phase	increase	increase	high	decrease	high
	Interglacial	long	high	none	low	low
	Onset of glacial	long	high	high	high	high
Pleistocene-Holocene		long	high	high?	low	low

Tab. 3. Conceptual model for the interplay of retention time of diatom skeletons on the shelf and slope, transport by downslope mass wasting processes, burial rate on the drift and their effects on laboratory opal leaching rate under different glacial-interglacial conditions in the Pliocene. A combination of prolonged retention times, fragmentation and relatively fast burial leads to increased laboratory leaching rates. The last row summarizes the Pleistocene conditions with less frequent and more irregular occurring down slope transport and low burial rates leading to low laboratory leaching rates.

2.3.4.1 Positive correlation of organic carbon and sedimentation rate

The mean organic carbon content (0.24 wt.%; see Tab. 1) from ODP Site 1095 samples is typical for open-ocean deep-sea sediments. The compacted and decompacted sediment data (Fig. 6) show that a positive correlation exists between organic carbon content and sedimentation rate. The power fit of the data in a log-log distribution can be described with the function given in Eq. 1 and 2, where for compacted sediments the constant *a* is 0.9 and *b* is 0.47, and for decompaction using Eq. 3 or 4, *a* is ~0.1 and *b* is 0.43 or 0.37 respectively.

2.3.4.2 Compaction-decompaction models

The calculated glacial-interglacial duration (Tab. 2, Δt_{avG} and Δt_{avIG}) show differences of up to 7 kyr between the compaction-decompaction models. The glacial-interglacial sedimentation rate ratio of the two models using decompacted sedimentation rates (Eq. 3 and 4; Tab. 2) is very similar. In the following calculation, Model 3 was used since the pore number (conservation of mass) based decompaction method (Terzaghi) is more physical stringent and therefore best accounts for glacial-to-interglacial material property changes. The found sedimentation rate ratio of 1.28 (Tab. 2, Model 3) matches the mean average glacial-interglacial thickness ratio of 1.27 suggested in an earlier paper of Hepp et al. (2006). The application of model 3 (Tab. 2), leads to reasonable mean average glacial periods of 63.98 kyr and mean average interglacial periods of 57.38 kyr, given the ice proximity of the core location.

2.3.4.3 Turbidite frequency

To estimate the frequency distribution of silt layers from ODP Site 1095 cores, the results from Model 3 were integrated with the X-ray derived turbidite counts. The resulting turbidite frequency model (Fig. 7) is based on the following axioms:

1. The glacial-interglacial periodicity is strongly controlled by Milankovitch cycles (Grützner et al. 2003, Iorio et al. 2004) and the average proportion of glacial to interglacial time periods follow Model 3.
2. The ice sheet evolution on the shelf is closely coupled to the sedimentary depositional patterns on the drift and changes in the sedimentary supply reflect regional ice sheet advances, retreats and collapses (Hepp et al. 2006, Bart et al. 2007).
3. The sediments of glacials are strongly dominated by terrigenous supply (turbidites) with high sedimentation rates. The sediments of interglacials are dominated by pelagic settling of biogenic material and terrigenous material derived from ice rafted debris and wind transport with lower sedimentation rates (Hepp et al. 2006).
4. The linear sedimentation rate computed from magnetostratigraphic-biochronologic tie-points given in Acton (2002) and Iwai (2002) corresponds to the mean average sedimentation rate from all glacials and interglacials of the studied Pliocene core section.
5. Excellent preservation of turbidite derived silt layers on the distal part of the drift at ODP site 1095.

On the basis of this conceptual model, the frequency distribution of silt layers for two early Pliocene glacial-to-interglacial transitions (169.29 to 168.95 and 110.97 to 105.66 mcd) from core sections of ODP Site 1095 was calculated. For these two sections, the average turbidite re-occurrence is ~375 yrs. A moving average with a 1-kyr window for the section between 110.97 and 105.66 mcd (Fig. 9a) and a 0.5-kyr window for the section between 169.29 and 168.95 mcd (Fig. 9b) was used to determine frequencies from silt layer reoccurrences.

The resulting graphs (Fig. 9) show a decrease in turbidite frequency during the deglaciation phase and the ice sheet collapse phase which correlates to a time interval of reduced terrigenous sedimentation supply as proposed by (Hepp et al. 2006). Fig. 9 shows the mean average number of turbidites per 1 kyr is ~6.6 turbidites/kyr for glacial intervals and ~2.8 turbidites/kyr for the

deglaciation phase. The early Pliocene turbidite frequency is considerably different in depositional pattern from Pleistocene glacial sections of the same site. Pleistocene turbidite depositional patterns are less continuos and characterized by irregular occurring silt layer packages.

2.3.4.4 Retention time between two consecutive slope failures

In Fig. 4, the total organic carbon (TOC), biogenic opal ($BSiO_2$) content, and the opal leaching rate (K_m) of two early Pliocene core sections (171.5-166.5 and 108-101 mcd) are shown. The bulk magnetic susceptibility (κ) aids in differentiating glacial and stages. All opal data are measured on the fine fraction (<63 μm) and distinguishes data from silt layers (dark circles) and silt layer free sediment samples (light circles).

The $BSiO_2$ data show that the opal content of the silt layer samples (1.06-3.93 wt.%) is generally significantly lower than the content of the silt layer free hemipelagic sediments (2.57-18.19 wt.%). In general the opal content in interglacials (mean average of silt layer free sediments is 15.90 wt.%) is slightly higher than in glacials (mean average of silt layers is 2.16 and of silt layer free sediments is 11.35 wt.%).

The leaching rate of opal (K_m) is independent of the total concentration in the sample and shows no significant variances between glacial to interglacial stages. Focused on deglaciation phases (Fig. 4, DP) and the lower part of glacials (Fig. 4, G) the leaching rate from silt layer samples (mean average 0.0089 s^{-1}) diverges from the overall low rates in background and glacial controlled sediment (mean average 0.0027 s^{-1}). In Fig. 4a, a gradual increase in leaching rate during the deglaciation phase was determined with the exception of the last three samples with low values, which correlates negatively with the gradual decrease in silt layer frequency (Fig. 9a). The beginning of glacials is characterized by distinct peaks in leaching rate. A comparison of the investigated Pliocene with the Pleistocene-Holocene section of ODP Site 1095 (15 K_m values from 4.2 mbsf to 0.1 mbsf, marine isotope stage 7-2; Fig. 5) shows a much lower, average leaching rate (~0.003 s^{-1}) and no significant glacial-to-interglacial variation. Thus, increases in leaching rates during the deglaciation phases were not determined.

2.3.5 Discussion

2.3.5.1 Close relationship of ice sheet advances, slope loading and frequent slope failure

In the absence of major fluvial systems the ice sheet is the main driving force behind erosion, transport and deposition of terrigenous material from the continental shelf to the drift. Ice thickness, flow velocity and frequency of advances to the shelf edge determine the amount of the material transport to the continental slope. The slope angle is another important component determining fast or more retarded transportation rate to the rise. The slope angle is determined by the type of transported material (e.g.coarse material from an erosive glacial advance leads to a steep slope; (Rebesco et al. 1996).

The current West Antarctic ice sheet is assumed to have the capability of rapidly shrinking, because the grounding line between the continental ice shield and the floating ice shelves is mostly far

below sea level and thus unstable (Bentley 1998, Raymond 2002). In a recent study of ice sheet dynamics controlled by sedimentary processes along the West Antarctic Peninsula Continental Margin Hepp et al. (2006) proposed a highly dynamic early Pliocene ice sheet with abrupt changes in lithology at interglacial-to-glacial transitions. A conspicuous feature is the abrupt cessation of ice rafted debris (IRD) input and the synchronous onset of frequent silt layer depositions. The factors controlling the rapid interglacial-to-glacial transition are not completely understood, but rapid ice re-advances to the shelf edge may point towards an ice sheet which does not fully retreat to the shore during interglacials.

In view of the glacial-interglacial cyclicity in the Pliocene, the turbidite depositional regime on ODP Site 1095 shows a consistent pattern in silt layer distribution and frequency (Hepp et al. 2006). The silt layer distribution is narrow and the frequency continuously high in glacials. The frequency distribution of silt layers reflects short and rapid but continuing ice advances every ~375 yrs. This full glacial depositional pattern is followed by a gradual decrease in silt layer frequency during the deglaciation phase. The ice sheet collapse and the ice sheet growth phases within the interglacial intervals are silt layer free.

The reaction rate constant (K_m), determined from the $BSiO_2$ leaching measurements, was used as an indicator of the diagenetic and transport history of the diatom frustules. The rate constant describes the dissolving rate of opal and depends on texture and preservation stage of diatom frustules and the deposition mode. Large diatom frustules with complex constitution have a more dissolvable surface than smaller and simpler frustule structures (McManus et al. 1995, Rabouille et al. 1997). A larger surface of fragmented or dissoluted diatom frustules dissolves faster then intact skeletons. Van der Wejden and van der Weijden (2002) demonstrated the dependency of opal dissolution rate on the reactivity of the opal, and showed that both linked processes decrease with increasing burial depth of the biogenic silica matter. Rapid burial under high sedimentation rate (e.g. turbidite events) reduces the reaction time and increases the preservation of reactive opal in the sedimentary record, whereas, under low sedimentation rates, long exposures at the sediment-water interface foster the consumption of reactive opal. This leads to diatom remnants in the sediment record and show a slow reaction rate constant in laboratory leaching tests. Thus, the reaction rate constant (K_m) is an indicator for the exposure time and subsequent transport process of biogenic opal from the continental self or slope to the drift recorder.

The results from this study suggest that the combined effects of retention time, transport mechanisms and burial rate are sufficient to explain the observed glacial-interglacial patterns in the opal leaching rate constant. High leaching rates result from a combination of long retention times on the shelf or slope, subsequent mechanical size reduction during reworking of the already weakened frustules during turbiditiy transport, and rapid burial. Low leaching rates indicate either short retention times in combination with rapid burial or long retention times in combination with slow burial. An overview of the transport and deposition effects on laboratory opal leaching rate under different glacial-interglacial conditions is given in Tab. 3.

Characteristic gradients of TOC and $BSiO_2$ in relation to glacial stages are marked by arrows in Fig. 4 and will be discussed in the following: Low opal leaching rates during glacials point to a dynamic ice sheet during warm Pliocene ice sheet conditions. Periodically advancing and retreating ice streams discharge large amounts of terrigenous material to the continental slope triggering frequent slope failures (7-12 events per kyr; Fig. 9). Contained in every mass wasting are diatom skeletons deposited on the slope and shelf between two consecutive turbidite events. Short retention times on the

shelf or slope prevent a dissolution induced weakening of the frustules. The dissolution in turn reduces the mechanical downsizing of the frustules during turbiditic reworking and leads to less reactive opal on the drift. During deglaciations a decrease in turbidite frequency and prolonged exposition times lead to weak frustules that experience more mechanical downsizing during turbiditic reworking. Together with the fast deposition and burial, reactive opal gets preserved on the drift. The last three turbidites of the deglaciation phase, however, show lower leaching rate constants. These low leachin rates indicate a subsequent burial below a critical threshold rate that would be necessary to preserve the reactive opal fraction. In contrast, the interglacials show that long retention times, no turbiditic reworking and low hemipelagic burial rates allow an effective removal of reactive silica. A few peaks in the leaching rate from silt layer samples during the onset of glacials supports our conceptual model.

The observed differences in glacial-to-interglacial leaching rates between the investigated Pliocene and the Pleistocene-Holocene sections of ODP Site 1095 can be explained in terms of ice sheet dynamics. Less frequent mass wasting events, with more irregular slope loading and failures (Pudsey 2000, Hepp et al. 2006) results in prolonged exposition times on the continental rise that in turn lead to an intensified degradation of reactive opal near the sediment water interface. Our data supports the hypothesis of less dynamic, cold based Pleistocene ice sheet (Rebesco & Camerlenghi 2008).

2.3.5.2 Highly dynamic early Pliocene Antarctic ice sheet regime during warm early Pliocene vs. cold Pleistocene

The described close relationship between silt layer frequency and dissolution constant K_m shows that shelf and slope retention times (slope failure frequencies) are controlled by ice sheet advances. Retention times on the slope, however, are also a function of the slope angle (Tab. 3). In a seismostratigraphic shelf model Camerlengi et al. (2002) show a strong increase in slope angle following the late Pliocene. An increase in slope angle implies that the retention times in the Pleistocene are probably shorter than in Pliocene times. This is supported by our Pleistocene K_m data with values three times lower than observed in the early Pliocene (Fig. 5, Tab. 3). Despite uncertainties in the slope buffer size, the presented silt layer record from ODP Site 1095 cores is a useful tool for reconstructing the Antarctic Peninsula ice sheet dynamics. Given the limited number of grounding lines on the continental shelf (Bart et al. 2007) the rise with its high preservation potential is the only proximal long time recorder.

On the basis of shipboard ODP core images (ODP Leg 178 Shipboard Scientific Party 1999) and newly prepared X-ray images and the silt layer frequency data, a comparison with core sections from the early Pliocene with core sections from the uppermost late Pliocene and Pleistocene show distinct differences in silt layer characteristics. The early Pliocene sediments contain thin commonly parallel laminated silt and mud couplets. The silt layers can be divided into two laminated facies showing thin laminated silty clays, with slightly erosional bases or less common sharp-based parallel laminated silts and laminated silty clays. The frequency of the silt layers is consistent throughout the glacial intervals. In contrast, the late Pliocene and Pleistocene sediments contain rare thin irregular and variable packets of beds with sharp-based parallel laminated silts. This is interpreted in terms of a less dynamic ice sheet suggesting longer retention periods of the grounded ice sheet at the shelf edge with lower ice flow velocities resulting in a less periodic slope loading and failure. The change in the sedimentary record seen in terms of silt layer frequency and opal leaching rates, supports the theory of a switch from an warm, highly dynamic Antarctic ice sheet regime during early Pliocene to the current

cold-based, stable conditions since the late Pliocene climate transition at about 3 Ma (Rebesco & Camerlenghi 2008).

2.3.5.3 Orbital periodicity in the early Pliocene

The invested area is very sensitive to changes in ice sheet volume in West Antarctica and can only give regional insights. Barker and Camerlenghi (2002) showed that the release of glacial sediments was cyclic and orbitally controlled. From early to late Pliocene intervals of Site 1095 cores Iorio et al. (2004) compiled strong short eccentricity periodicities (~95-125 kyr). This findings correspond to our results with periodicities at ~120 kyr. For Pliocene time sections of ODP Site 1095 cores, a forcing by obliquity periodicities at about 50-60 kyr were reported in different studies: Wavelet analyses of petrophysical measurements show periodicities at 56 kyr and 87 kyr (Lauer-Leredde et al. 2002), and power spectra analyses show periodicities at 63 kyr (Pudsey 2002) and at 50 kyr and 64 kyr (Iorio et al. 2004) in magnetic susceptibility and chromaticity parameter a*. This study demonstrated that these periodicities are most likely to respond to the glacial or interglacial half-cycles at 61.59 kyr and 59.77 kyr. Thus, for regional ice sheet behavior we suggest that these periodicities do not reflect the combined effect of precession and obliquity periodicities as predicted by (Berger 1977, Iorio et al. 2004, Grützner et al. 2005).

2.3.6 Conclusion

This study improves the understanding of the interaction of ice sheet dynamics, slope loading slope failure as reflected in turbidity sediment depositions along the Pacific Continental Margin of the West Antarctic Peninsula during the Pliocene. The turbidite frequency and the average time period between two consecutive turbidite events, were linked to reaction rate constant measurements on reworked biogenic opal to derive an indirect measure of the slope retention times for three core intervals of ODP Site 1095.

By using the long term sedimentation rate dependency of the marine carbon burial efficiency in Antarctic drift sediments, it was possible to calculate a ratio of glacial to interglacial sedimentation rates for the Pliocene. Pliocene glacial-interglacial periodicities were determined by using sparse magneto and bio-stratigraphic tie points and counts of glacial and interglacial intervals. Together with the decompacted average length of glacial and interglacials, a set of linear equations for the glacial and interglacials half periods and thus absolute half cycle sedimentation rates were calculated. Decompaction following Terzaghi's one dimensional consolidation theory and a glacial-interglacial ratio of 1:1 for the deglaciation phase worked best in minimizing uncertainties in our calculation. The deglaciation phase required a special adjustment because a diagenetic imprint on the organic carbon preservation prevents the organic carbon-sedimentation rate correlation approach for the calculation of the duration of the deglaciation phase. Even for this shelf proximal site the glacial and interglacial half periods have on average equal durations of 63.98 kyr and 57.38 kyr, respectively. Derived average glacial turbidite recurrences of ~375 yr are interpreted as short and rapid ice sheet advances at relatively regular intervals resulting in continuous and periodic slope failures in the late Miocene/early Pliocene warm phase.

Frequent turbidite recurrences imply short retention times between slope loading and slope failure. This finding is supported by low reaction rate constants of opal leaching experiments during

early Pliocene glacials. A significant increase of the leaching rate from silt layer samples, which is associated with a decrease of the turbidite frequency during the deglaciation phase is explained with a conceptual model of opal exposure, transport and burial. The findings from silt layer frequency distribution and biogenic silica leaching rates imply a close interaction between ice sheet dynamics, sediment discharge, slope loading and slope failure. A highly dynamic early Pliocene ice sheet with regular advances to the shelf edge is in clear contrast to longer retention periods of the grounded ice sheet at the shelf edge, lower flow velocities and more irregular slope loading during the uppermost late Pliocene and Pleistocene period.

The ~120 kyr Pliocene glacial-interglacial periodicities correspond to data from wavelet and power spectra analyses from ODP Site 1095 on the Pacific continental rise of the West Antarctic Peninsula. The previously predicted combined effect of precession and obliquity periodicity of ~60 kyr from magnetic susceptibility data could be identified as glacial or interglacial half-cycles respectively.

2.3.7 Acknowledgement

Samples were provided by the Ocean Drilling Program (ODP). We thank the Bremen Core Repository (BCR) team for their kind support. The $BSiO_2$ measurements were carried out at the Alfred-Wegener-Institut für Polar- und Meeresforschung (AWI) in Bremerhaven. The help of Dr. Gerhard Kuhn und Rita Fröhlking during these measurements is greatly appreciated. We thank Jens Seeberg-Elverfeldt for his useful advice for the linear fitting of opal dissolution curves. Some $BSiO_2$ data from individual samples were part of a bachelor thesis by Sophie Fath prepared in our working group. Special acknowledgment goes to Stefan Kreiter (MARUM) for his help with the calculation of the turbidite frequencies. We thank Rüdiger Stein (AWI) for careful reading of our manuscript. This research was funded by the Deutsche Forschungsgemeinschaft (DFG project MO1059-1 and HE5377-1) and by the DFG-Research Center MARUM – Center for Marine Environmental Sciences of University of Bremen.

2.3.8 References

Acton, G.D., Guyodo, Y., & Brachfeld, S.A. 2002. Magnetostratigraphy of sediment drifts on the continental rise of West Antarctica (ODP Leg 178, Sites 1095, 1096, and 1101). *In* Barker, P.F., et al. *eds. Proceedings of the Ocean Drilling Program, Scientific Results.* College Station, TX: Texas A&M University, 1-61 [CD-ROM].

Anderson, J.B., Wellner, J.S., Lowe, A.L., Mosola, A.B., & Shipp, S.S. 2001. Footprint of the expanded West Antarctic ice sheet: Ice stream history and behavior. *GSA Today,* 11(10), 4-9.

Azizi, F. 2000. *Applied analyses in Geotechnics.* London, New York: E & FN Spon. 254 pp.

Barker, P.F. 1982. The Cenozoic subduction history of the Pacific margin of the Antarctic Peninsula: Ridge crest–trench interactions. *Journal of the Geological Society,* 139(6), 787-801.

Barker, P.F., & Camerlenghi, A. 2002. Glacial history of the Antarctic Peninsula from Pacific margin sediments. *In* Barker, P.F., et al. *eds. Proceedings of the Ocean Drilling Program, Scientific Results.* College Station, TX: Texas A&M University, 1-40 [CD-ROM].

Barrett, P.J., Adams, C.J., McIntosh, W.C., Swisher, C.C., & Wilson, G.S. 1992. Geochronological evidence supporting Antarctic deglaciation three million years ago. *Nature,* 359, 816-818.

Bart, P.J. 2001. Did the Antarctic ice sheets expand during the early Pliocene? *Geology,* 29(1), 67-70.

Bart, P.J., Hillenbrand, C.-D., Ehrmann, W.U., Iwai, M., Winter, D., & Warny, S.A. 2007. Are Antarctic Peninsula Ice Sheet grounding events manifest in sedimentary cycles on the adjacent continental rise? *Marine Geology,* 236(1-2), 1-13.

Bentley, C.R. 1998. Ice on the fast track. *Nature,* 394, 21-22.

Berger, A.L. 1977. Support for the astronomical theory of climatic change. 269(5623), 44-45.

Burdige, D.J. 2006a. The controls on organic carbon preservation in marine sediments. *In* Burdige, D.J. *ed. Geochemistry of marine sediments.* Princeton, Oxford: Princeton University Press, 408-441.

Burdige, D.J. 2006b. *Geochemistry of marine sediments*. Princeton, Oxford: Princeton University Press. 609 pp.

Camerlenghi, A., Rebesco, M.A., De Santis, L., Volpi, V., & De Rossi, A. 2002. The Antarctic Peninsula Pacific margin: Modelling flexure and decompaction with constraints from ODP Leg 178 initial results. *In* Gamble, J.A., et al. *eds. Antarctica at the close of a millennium: Proceedings of the 8th international symposium on Antarctic earth sciences.* Wellington: The Royal Society of New Zealand, 261-267.

Cortese, G., Gersonde, R., Hillenbrand, C.-D., & Kuhn, G. 2004. Opal sedimentation shifts in the World Ocean over the last 15 Myr. *Earth and Planetary Science Letters,* 224(3-4), 509-527.

DeMaster, D.J. 1981. The supply and accumulation of silica in the marine environment. *Geochimica et Cosmochimica Acta,* 45(10), 1715-1732.

DeMaster, D.J. 2002. The accumulation and cycling of biogenic silica in the Southern Ocean: Revisiting the marine silica budget. *Deep-Sea Research Part II,* 49(16), 3155-3167.

Diviacco, P., Rebesco, M.A., & Camerlenghi, A. 2006. Late Pliocene mega debris flow deposit and related fluid escapes identified on the Antarctic Peninsula continental margin by seismic reflection data analysis. *Marine Geophysical Researches,* 27(2), 109-128.

Dowdeswell, J.A., Ó Cofaigh, C., & Pudsey, C.J. 2004. Continental slope morphology and sedimentary processes at the mouth of an Antarctic palaeo-ice stream. *Marine Geology,* 204(1-2), 203-214.

Elverhøi, A., Hooke, R.L., & Solheim, A. 1998. Late Cenozoic erosion and sediment yield from the Svalbard-Barents Sea region: implications for understanding erosion of glacierized basins. *Quaternary Science Reviews,* 17(1-3), 209-241.

Faugères, J.-C., Stow, D.A.V., Imbert, P., & Viana, A.R. 1999. Seismic features diagnostic of contourite drifts. *Marine Geology,* 162(1), 1-38.

Grützner, J., Hillenbrand, C.-D., & Rebesco, M.A. 2005. Terrigenous flux and biogenic silica deposition at the Antarctic continental rise during the late Miocene to early Pliocene: Implications for ice sheet stability and sea ice coverage. *Global and Planetary Change,* 45, 131-149.

Grützner, J., Rebesco, M.A., Cooper, A.K., Forsberg, C.F., Kryc, K.A., & Wefer, G. 2003. Evidence for orbitally controlled size variations of the East Antarctic ice sheet during the late Miocene. *Geology,* 31(9), 777-780.

Hepp, D.A., Mörz, T., & Grützner, J. 2006. Pliocene glacial cyclicity in a deep-sea sediment drift (Antarctic Peninsula Pacific Margin). *Palaeogeography, Palaeoclimatology, Palaeoecology,* 231(1-2), 181-198.

Hillenbrand, C.-D., & Fütterer, D.K. 2002. Neogene to Quaternary deposition of opal on the continental rise west of the Antarctic Peninsula, ODP Leg 178, Sites 1095, 1096, and 1101. *In* Barker, P.F., et al. *eds. Proceedings of the Ocean Drilling Program, Scientific Results.* College Station, TX: Texas A&M University, 1-33 [CD-ROM].

Iorio, M., Wolf-Welling, T.C.W., & Mörz, T. 2004. Antarctic sediment drift and Plio-Pleistocene orbital periodicities (ODP Sites 1095, 1096, and 1101). *In* D'Argenio, B., et al. *eds. Cyclostratigraphy: Approaches and case histories.* Tulsa: Society for Sedimentary Geology, 231-244.

Iwai, M., Acton, G.D., Lazarus, D.B., Osterman, L.E., & Williams, T. 2002. Magnetobiochronologic synthesis of ODP Leg 178 rise sediments from the Pacific sector of the Southern Ocean: Sites 1095, 1096, and 1101. *In* Barker, P.F., et al. *eds. Proceedings of the Ocean Drilling Program, Scientific Results.* College Station, TX: Texas A&M University, 1-40 [CD-ROM].

Koning, E., Brummer, G.-J., van Raaphorst, W., van Bennekom, J., Helder, W., & van Iperen, J. 1997. Settling, dissolution and burial of biogenic silica in the sediments off Somalia (northwestern Indian Ocean). *Deep-Sea Research Part II,* 44(6-7), 1341-1360.

Koning, E., Epping , E., & van Raaphorst, W. 2002. Determining biogenic silica in marine samples by tracking silicate and aluminium concentrations in alkaline leaching solutions. *Aquatic Geochemistry,* 8(1), 37-67.

Lauer-Leredde, C., Briqueu, L., & Williams, T. 2002. A wavelet analysis of physical properties measured downhole and on core from Holes 1095B and 1096C (Antarctic Peninsula). *In* Barker, P.F., et al. *eds. Proceedings of the Ocean Drilling Program, Scientific Results.* College Station, TX: Texas A&M University, 1-43 [CD-ROM].

Løseth, T.M. 1999. *Submarine massflow sedimentation: Computer modelling and basin-fill stratigraphy*. Berlin, Heidelberg, New York: Springer. 156 pp.

Lucchi, R.G., Rebesco, M.A., Busetti, M., Caburlotto, A., Colizza, E., & Fontolan, G. 2002. Sedimentary processes and glacial cycles on the sediment drifts of the Antarctic Peninsula Pacific margin: Preliminary results of SEDANO-II project. *New Zealand Journal of Geology and Geophysics,* 35, 275-280.

McGinnis, J.P., & Hayes, D.E. 1995. The roles of downslope and along-slope depositional processes: Southern Antarctic Peninsula continental rise. *In* Cooper, A.K., et al. *eds. Geology and seismic stratigraphy of the Antarctic margin.* Washington, DC: American Geophysical Union, 141-156.

McManus, J., Hammond, D.E., Berelson, W.M., Kilgore, T.E., Demaster, D.J., Ragueneau, O.G., & Collier, R.W. 1995. Early diagenesis of biogenic opal: Dissolution rates, kinetics, and paleoceanographic implications. *Deep Sea Research Part II: Topical Studies in Oceanography,* 42(2-3), 871-903.

Mörz, T. 2002. *From the inner shelf to the deep sea: Depositional environments on the West Antarctic Peninsula margin: A sedimentological and seismostratigraphic study (ODP Leg 178)*. Bremerhaven: Alfred-Wegener-Institut für Polar- und Meeresforschung. 236 pp.

Müller, P.J., & Schneider, R.R. 1993. An automated leaching method for the determination of opal in sediments and particulate matter. *Deep-Sea Research Part I,* 40(3), 425-444.

O'Grady, D.B., & Syvitski, J.P.M. 2001. Predicting profile geometry of continental slopes with a multi-process sedimentation model. *In* Merriam, D.F., & Davis, J.C. *eds. Geologic modeling and simulation: Sedimentary systems.* New York: Kluwer/ Plenum, 99-117.

ODP Leg 178 Shipboard Scientific Party. 1999. Site 1095. *In* Barker, P.F., et al. *eds. Proceedings of the Ocean Drilling Program, Initial Reports.* College Station, TX: Texas A&M University, 1-173 [CD-ROM].

Pudsey, C.J. 2000. Sedimentation on the continental rise west of the Antarctic Peninsula over the last three glacial cycles. *Marine Geology,* 167(3-4), 313-338.

Pudsey, C.J. 2002. Neogene record of Antarctic Peninsula glaciation in continental rise sediments: ODP Leg 178, Site 1095. *In* Barker, P.F., et al. *eds. Proceedings of the Ocean Drilling Program, Scientific Results.* College Station, TX: Texas A&M University, 1-25 [CD-ROM].

Pudsey, C.J., & Camerlenghi, A. 1998. Glacial-interglacial deposition on a sediment drift on the Pacific margin of the Antarctic Peninsula. *Antarctic Science,* 10(3), 286-308.

Rabouille, C., Gaillard, J.-F., Treguer, P., & Vincendeau, M.-A. 1997. Biogenic silica recycling in surficial sediments across the Polar Front of the Southern Ocean (Indian Sector). *Deep-Sea Research Part II,* 44(5), 1151-1176.

Ragueneau, O., Tréguer, P., Leynaert, A., Anderson, R.F., Brzezinski, M.A., DeMaster, D.J., Dugdale, R.C., Dymond, J., Fischer, G., & François, R. 2000. A review of the Si cycle in the modern ocean: Recent progress and missing gaps in the application of biogenic opal as a paleoproductivity proxy. *Global and Planetary Change,* 26(4), 317-365.

Raymond, C.F. 2002. Ice sheets on the move. *Science,* 298, 2147-2148.

Rebesco, M., & Camerlenghi, A. 2008. Late Pliocene margin development and mega debris flow deposits on the Antarctic continental margins: Evidence of the onset of the modern Antarctic Ice Sheet? *Palaeogeography, Palaeoclimatology, Palaeoecology,* 260(1-2), 149-167.

Rebesco, M.A., Larter, R.D., Camerlenghi, A., & Barker, P.F. 1996. Giant sediment drifts on the continental rise west of the Antarctic Peninsula. *Geo-Marine Letters,* 16, 65-75.

Rebesco, M.A., Pudsey, C.J., Canals, M., Camerlenghi, A., Barker, P.F., Estrada, F., & Giorgetti, A. 2002. Sediment drifts and deep-sea channel systems, Antarctic Peninsula Pacific Margin. *In* Stow, D.A.V., et al. *eds. Deep-water contourite systems: Modern drifts and ancient series, seismic and sedimentary characteristics.* London: Geological Society, 353-371.

Rickert, D. 2000. *Dissolution kinetics of biogenic silica in marine environments*. Bremerhaven: Alfred-Wegener-Institut für Polar- und Meeresforschung. 211 pp.

Schlüter, M. 1990. *Early diagenesis of organic carbon and opal in sediments of the southern and eastern Weddell Sea: Geochemical analysis and modelling*. Bremerhaven: Alfred-Wegener-Institut für Polar- und Meeresforschung. 156 pp.

Stein, R. 1986. Organic carbon and sedimentation rate -- Further evidence for anoxic deep-water conditions in the Cenomanian/Turonian Atlantic Ocean. *Marine Geology,* 72(3-4), 199-209.

Stein, R. 1990. Organic carbon content/sedimentation rate relationship and its paleoenvironmental significance for marine sediments. *Geo-Marine Letters,* 10(1), 37-44.

Stow, D.A.V. 1986. Deep clastic seas. *In* Reading, H.G. *ed. Sedimentary environments and facies.* Oxford: Blackwell, 399-444.

Stow, D.A.V., & Mayall, M. 2000. Deep-water sedimentary systems: New models for the 21st century. *Marine and Petroleum Geology,* 17(2), 125-135.

Treguer, P., Nelson, D.M., Van Bennekom, A.J., DeMaster, D.J., Leynaert, A., & Queguiner, B. 1995. The silica balance in the world ocean: A reestimate. *Science,* 268, 375-379.

Uenzelmann-Neben, G. 2006. Depositional patterns at Drift 7, Antarctic Peninsula: Along-slope versus down-slope sediment transport as indicators for oceanic currents and climatic conditions. *Marine Geology,* 233(1-4), 49-62.

van der Weijden, A.J., & van der Weijden, C.H. 2002. Silica fluxes and opal dissolution rates in the northern Arabian Sea. *Deep-Sea Research Part I,* 49(1), 157-173.

Volpi, V., Amblas, D., Camerlenghi, A., Canals, M., Rebesco, M., & Urgeles, R. in press. Late Neogene to recent seafloor instability on the deep pacific margin of the Antarctic Peninsula. *In* Shipp, C., et al. *eds. Mass-transport deposits in deepwater settings.* Tulsa: Society for Sedimentary Geology.

Wilson, G.S. 1995. The neogene East Antarctic ice sheet: A dynamic or stable feature? *Quaternary Science Reviews,* 14(2), 101-123.

3 Selected Abstracts

1st General EGU Assembly Nice, France, 25-30 April 2004
Published in Geophysical Research Abstracts 6, 2004, No. 06413

3.1 Reconstruction of Antarctic ice-sheet history from drift sediments

D.A. Hepp[a,b], T. Moerz[b], J. Thiede[c], W.-C. Dullo[d]

[a]Faculty of Geosciences, University Bremen
[b]Research Center Ocean Margins, University Bremen
[c]Alfred Wegener Institute for Polar and Marine Research, Bremerhaven
[d]Leibniz-Institute of Marine Science, Kiel
dhepp@uni-bremen.de

The West Antarctic Peninsula rise is made up of a series of giant, up to 700 m high, deep-sea sedimentary drift bodies separated by turbidity canyons. Palaeomagnetic and biostratigraphic investigations on cores from Ocean Drilling Program Leg 178 (Site 1095 and 1101) show that the drift bodies hold a clay- to silt-size, quasi-continuous sedimentary record with prominent glacial-interglacial cyclicity. Similar drift bodies are also known from Prydz Bay, East Antarctica (ODP Leg 188, Site 1165, Wild Drift). Initial studies demonstrate that most of the mass accumulation occurs during glacial periods when more frequent continental ice advances to the shelf edge provide primarily terrigene sediment to the upper continental slope. Sediment transport from the upper slope to the drifts is conducted by frequent small-scale failures of the oversteepened slope. Each advance of grounded ice to the shelf break therefore leaves a distinct sedimentary fingerprint in the drift record. The sedimentary deep-sea drift bodies along the Antarctic continental rise are therefore unique continuous recorders of ice advances due to their proximity and relative long-term stability.

Our recently started project aims to characterize ice controlled depositional events and quantify their frequency for the last 10 Ma. Samples with mixed depositional influence will be detected and assigned to a dominant process using statistical methods. Past ice volume calculations are possible since ice extent and ice advancing frequencies are closely linked to changes in the total continental ice volume. Recent long-term ice models show a near constant ice-cover to ice-volume ratio.

The sediment supply to the Antarctic deep-sea drift bodies has four main sources: turbiditic relocation of slope material during glacial and interglacial times, hemipelagic supply, IRD input and contour current derived and removed sediment. Here we present initial grain-size characteristics for all four depositional processes during exemplary glacial-interglacial changes.

XXVIII SCAR Science and XVI COMNAP Meeting, Bremen, Germany, 25-31 July 2004
Published in Terra Nostra 4, 2004, p. 266

3.2 Comparison of glacial-interglacial turbidite deposits in West Antarctic Peninsula deep-sea drifts

D.A. Hepp[a,b], T. Moerz[b], J. Thiede[c], W.-C. Dullo[d]

[a]Faculty of Geosciences, University Bremen
[b]Research Center Ocean Margins, University Bremen
[c]Alfred Wegener Institute for Polar and Marine Research, Bremerhaven
[d]Leibniz-Institute of Marine Science, Kiel
dhepp@uni-bremen.de

A series of giant deep-sea sedimentary drift bodies (up to 700 m high), separated by turbidity canyons, are known from the West Antarctic Peninsula continental rise. The drift bodies possess a clay- to silt-size, quasi-continuous sedimentary record with prominent glacial-interglacial cyclicity confirmed by palaeomagnetic and biostratigraphic investigations on cores from Ocean Drilling Program Leg 178, Site 1095 (Drift 7) and 1101 (Drift 4). A comparable East Antarctic drift body is also investigated in Prydz Bay during Ocean Drilling Program Leg 188, Site 1165 (Wild Drift).

Most of the mass accumulation occurs during glacial periods when more frequent continental ice advances to the shelf edge provide primarily terrigene sediment to the upper continental slope. Sediment transport from the upper slope to the drifts is conducted by frequent small-scale failures of unstable sediments at the oversteepened slope. Each advance of grounded ice to the shelf break therefore leaves a distinct sedimentary fingerprint in the drift record. The sedimentary deep-sea drift bodies along the Antarctic continental rise are therefore unique continuous recorders of ice advances because of their proximity and relative long-term stability. Recent long-term ice models linked ice-extent and ice-advancing frequencies closely to changes in the total continental ice volume and show a near constant ice-cover to ice-volume ratio. Thereby, past ice volume calculations are possible now.

The project aims primarily to characterize ice controlled depositional events and quantify their frequencies for the last 10 Ma. Samples with mixed depositional influence were identified and assigned to a dominant process using statistical methods. The sediment supply to the Antarctic deep-sea drift bodies has four main sources: turbiditic relocation of terrigene slope material during glacial and interglacial times, hemipelagic supply, IRD input and contour current derived and removed sediment. A comparative micro-scale analysis of selected glacial and interglacial turbidite sequences shows principal differences and similarities in depositional style. This knowledge is critical to understand glacial-interglacial sediment supply and transport mechanism which act for long timescales and govern sediment built-up in most other West Antarctic Peninsula drifts.

AGU fall meeting, San Francisco CA, USA, 5-9 December 2005
Published in American Geophysical Union (ed.), AGU fall meeting. San Francisco, American Geophysical Union, 2005, p. 341 (No. PP41B-0651)

3.3 Pliocene glacial cyclicity and diagenetic effects in a deep-sea sediment drift on the Pacific margin of the Antarctic Peninsula (ODP Leg 178, Site 1095)

D.A. Hepp[a,b], T. Moerz[b], J. Thiede[c], W.-C. Dullo[d]

[a]Faculty of Geosciences, University Bremen, P.O. Box 330440, Bremen, 28334, dhepp@uni-bremen.de
[b]Research Center Ocean Margins (RCOM), University Bremen, P.O. Box 330440, Bremen, 28334, tmoerz@uni-bremen.de
[c]Alfred Wegener Institute for Polar and Marine Research (AWI), Bremerhaven, Am Handelshafen 12, Bremerhaven, 27570 Germany, jthiede@awi-bremerhaven.de
[d] Leibniz-Institute of Marine Science (IFM-GEOMAR), Wischhofstr. 1-3, Kiel, 24148 Germany, cdullo@ifm-geomar.de

Giant deep-sea sediment drifts are widespread features along the continental rise of the West Antarctic Peninsula, representing the most proximal continuous sedimentary recorders for West Antarctic ice events and glacial-interglacial cyclicity. Sediment physical, geochemical records and X-ray images derived from ODP Leg 178 Site 1095 (Sediment Drift 7) show characteristics in glacial-interglacial cyclicity and associated sedimentary processes during Pliocene. Two boundary types dividing half-cycles have been recognized: (1) interglacial-to-glacial transitions that are distinct and characterized by a sharp boundary and abrupt change in lithology, (2) glacial-to-interglacial transitions that are diffuse and characterized by a gradual decline of sediment physical and geochemical values with a marked reduction in sedimentation rates. The last-mentioned transition is accompanied by a minima zone in magnetic susceptibility, which comprises the upper portion of glacials and lower portions of interglacials. This minima zone is linked to diagenetic processes that transform magnetic iron minerals to paramagnetic minerals. We assume anaerobic oxidation of methane at the sulfate/methane transition with a release of hydrogen sulfide that in turn reduces ferrimagnetic magnetite to paramagnetic sulfides. This process gets especially prominent in sections with low sedimentation rates and high organic fluxes. The glacial/interglacial boundaries defined in conjunction with magneto- and biostratigraphic tie-points form the framework for the calculation of relative sedimentation and accumulation rates used for reconstructing early Pliocene paleoproductivity and terrigenous flux to the drift. Warm early Pliocene climate conditions for West Antarctic Peninsula region are indicated by open ocean conditions in glacials, short residence times of the grounded ice sheet at the shelf edge with sporadic fluctuations as well as periodic collapses of the ice-sheet front. We propose a 5-phase drift sedimentation model for the early Pliocene and postulate a highly dynamic ice sheet, sensitive to Milankovich eccentricity forcing and regional climate conditions. The ice sheet lay closer to the shelf edge than it was the case during the late Quaternary.

EGU General Assembly Vienna, Austria, 2-7 April 2006
Published in Geophysical Research Abstracts 8, 2006, No. 05720

3.4 Cyclic diagenetic alterations in drift sediments (Antarctic Peninsula pacific margin)

D.A. Hepp[a,b], T. Moerz[b], J. Thiede[c], W.-C. Dullo[d]

aDepartment of Geosciences, Bremen University, Germany
bResearch Center Ocean Margins (RCOM), Bremen University, Germany
cAlfred Wegener Institute for Polar and Marine Research (AWI), Germany
dLeibniz-Institute of Marine Science (IFM-GEOMAR), Germany
Contact: dhepp@uni-bremen.de

The Antarctic ice sheet is the largest on earth today. It acts as key component in the global climate regime since the late Eocene. Ice volume variations influence the ocean thermohaline circulation and control the eustatic sea level. The compilation of benthic oxygen isotope data describes a general cooling trend for the global climate during the Neogene. Within this general cooling trend, a number of global warming and cooling episodes can be identified. The Pacific margin off the Antarctic Peninsula is very sensitive to climate and ice-sheet volume changes. Climatic variations on the Antarctic Peninsula continental shelf control regional sedimentary depositional processes and affect the build-up of giant deep-sea sediment drifts. These drifts are widespread features along the continental rise of the Antarctic Peninsula Pacific margin. They contain a nearly continuous sedimentary record for West Antarctic ice events and glacial-interglacial cyclicity. We used sediment physical, geochemical records and X-ray images derived from ODP Leg 178 Site 1095 (Sediment Drift 7) to show characteristics in glacial-interglacial cyclicity and associated sedimentary processes during Pliocene. The data display two boundary types dividing half-cycles: (1) interglacial-to-glacial transitions that are distinct and characterized by a sharp boundary and abrupt change in lithology and (2) glacial-to-interglacial transitions that are diffuse and characterized by a gradual decline of sediment physical and geochemical values with a marked reduction in sedimentation rates. The second boundary type is accompanied by a minima zone in magnetic susceptibility. This minima zone comprises the upper portion of glacials and lower portions of interglacials and is linked to diagenetic alterations that transform magnetic iron minerals to paramagnetic minerals. The nearly complete loss of magnetic susceptibility is coupled with glacial controlled cyclic decreases in sedimentation rate. We assume that this loss is caused by the anaerobic oxidation of methane. This process leads to a depletion f sulfate at the sulfate/methane transition and the alteration of iron oxides to iron sulfides. The minima zones are especially prominent in sections with a drastic decrease in sedimentation rate, which causes a stagnation of the sulfate/methane transition. This stagnation affects an enhanced diagenetic dissolution of ferrimagnetic iron minerals within the sulfidic zone.

4 Conclusion

The presented study improves the understanding of the influence of the West Antarctic Ice Sheet evolution and coupled changes in oceanographic conditions on sedimentary processes and the preservation of sedimentary records during late Miocene and Pliocene times. Different sediment physical and geochemical records and X-ray images indicate that sedimentary and diagenetic processes are closely linked to the regional ice sheet evolution and oceanographic changes.

The giant deep-sea sediment Drift 7 on the Pacific continental margin of the West Antarctic Peninsula represents the most proximal continuous sedimentary recorder for West Antarctic Ice Sheet evolution and glacial-interglacial cyclicity. The gradients of magnetic susceptibility and other parameters have been used to define two characteristic boundaries of glacial and interglacial cycles:

1. The interglacial-to-glacial transitions are well definable and characterized by a sharp boundary and abrupt change in lithology from a full glacial to a full interglacial. The factors controlling the rapid interglacial-to-glacial transition are not completely understood, but rapid ice re-advances may point towards an ice sheet which does not fully retreat to the shore during interglacials.
2. The glacial-to-interglacial transitions are diffuse and can be described as a gradual change from a full glacial to a full interglacial stage. The transitions are characterized by a gradual decline of sediment physical and geochemical values with a marked reduction in coarse terrigenous input and sedimentation rates.

The interglacial-to-glacial transition is a substitute for the deglaciation phase and ice sheet collapse. The ice sheet collapse marks the end of the deglaciation phase. In the sedimentary record, almost each glacial-to-interglacial transition is accompanied by a significant loss of the magnetic susceptibility signal and a pronounced diatom ooze layer. In a more detailed investigation we demonstrated that processes of diagenetic alteration and demagnetization of magnetic iron minerals caused the loss of the magnetic susceptibility signal. The discovery of the cyclic loss of the magnetic susceptibility signal with well preserved ooze layers and their formation hints toward repeated suboxic or anoxic conditions in the surface sediments. Comparable suboxic and anoxic processes were observed in sediments of the Madeira abyssal plain turbidite system and in Mediterranean sapropels.

Late Miocene to early late Pliocene warm climate conditions are characterized by an enhanced global bioproductivity (‘biogenic bloom’), an overall reduced ice volume, and a reduced sea ice cover around Antarctica. At that time, ODP Site 1095 was within a southward-shifted opal depocentre, with exceptional biogenic silica and organic carbon fluxes comparable to those at the modern opal belt. An enhanced ice sheet dynamic involved frequent advances and retreats of the inland ice sheet. This enhancement led to more pronounced ice sheet collapses and meltwater pulses at the end of deglaciation phases. The ice sheet melting events fostered diatom blooms with a strong flux of organic matter to the sediment and a simultaneous weakening of bottom water circulation, which leads to the assumed suboxic or anoxic conditions in the surface sediments.

The presented phenomenon of dagenesis is not yet documented for the deep and open Circum-Antarctic Ocean and may have important global climatic implications. The findings are an important step in understanding the interplay of ice sheet evolution and changes in oceanographic conditions. It will be of interest to find additional proxies that may be used as indicators for decreased bottom water

current dynamics and Antarctic bottom water formation in the critical intervals where sea ice is reduced, the ice sheet collapses, and meltwater production is high.

On long time-scales the intensity and duration of diagenesis reflect major trends in global paleoceanographic and climatic change and the consequent variability in primary export production. After Antarctic ice sheet stabilization, between 3.3 and 2.3 Ma, the flux of organic matter and the sedimentation rate fell below a threshold level preventing the development of reducing conditions in the surface sediments. The mapping and documentation of 64 magnetic suszeptibility minima zones provide the first long term record of cyclic meltwater pulses and high export productivity events resulting in reducing conditions in the near surface sediments in the high latitudinal Southern Ocean.

On the basis of the defined glacial-interglacial transitions we computed the average turbidite frequency for Pliocene glacials and interglacials. The turbidite frequency and the average time period between two consecutive turbidite events were linked to reaction rate constant measurements on reworked biogenic opal to derive an indirect measure of the slope retention times. Even for the shelf proximal ODP Site 1095 the glacial and interglacial half periods have on average equal durations of 63.98 kyr and 57.38 kyr, respectively. The ~120 kyr Pliocene glacial-interglacial periodicities correspond to data from wavelet and power spectra analyses from ODP Site 1095 on the Pacific continental rise of the West Antarctic Peninsula. The previously predicted combined effect of precession and obliquity periodicity of ~60 kyr from magnetic susceptibility data could be identified as glacial and interglacial half-cycles. The initial glacial-interglacial cyclicity from sedimentary parameters of OPD Site 1095 shows strong evidence of 100 kyr eccentricity in late Miocene/Pliocene time periods without an evidence of the 41 kyr obliquity, as reported in the literature. This suggests that the sedimentary parameters are orbitally controlled.

Derived average glacial turbidite recurrences of ~375 yr are interpreted as short and rapid ice sheet advances at relatively regular intervals resulting in continuous and periodic slope failures in the late Miocene/early Pliocene warm phase. Frequent turbidite recurrences imply short retention times between slope loading and slope failure. This finding is supported by low reaction rate constants of opal leaching experiments during early Pliocene glacials. A significant increase of the leaching rate from silt layer samples, which is associated with a decrease of the turbidite frequency during the deglaciation phase, is explained with a conceptual model of opal exposure, transport and burial. The findings from silt layer frequency distribution and biogenic silica leaching rates imply a close interaction between ice sheet dynamics, sediment discharge, slope loading and slope failure. A highly dynamic early Pliocene ice sheet with regular advances to the shelf edge is in clear contrast to longer retention periods of the grounded ice sheet at the shelf edge, lower flow velocities and more irregular slope loading during the uppermost late Pliocene and Pleistocene period.

As a contribute to the controversial discussion on the East and West Antarctic Ice Sheet response to warmer oceanographic conditions ('Warm stable ice-sheet hypothesis' versus 'Early Pliocene deglaciation hypothesis') the results from our studies indicate warm early Pliocene climate conditions for West Antarctic Peninsula region. We postulate a fast moving and highly dynamic early Pliocene ice sheet, highly sensitive to Milankovich eccentricity forcing and regional climate conditions. The temporal evolution of suboxic or anoxic conditions in surface sediments along the continental margin of the West Antarctic Peninsula as documented by prominent losses in the magnetic susceptibility signal can be used as an indicator for changes in the sedimentary regimes and the water column.

5 Acknowledgement (Danksagung)

Für die Vergabe und die Betreuung des Themas bedanke ich mich bei Herrn Prof. Dr. Tobias Mörz. Seinem unermüdlichen Einsatz verdanke ich den fachlichen Wechsel aus der Ur- und Frühgeschichte in die spannende Wissenschaft der Marinen Geologie. Herrn Prof. Dr. Rüdiger Stein danke ich für die Übernahme des Zweitgutachtens.

Mein besonderer Dank gilt Dr. Jens Grützner für die Bereitstellung seiner Röntgendiffraktionsmessdaten und seine wissenschaftliche Unterstützung. Ebenso danke ich Dr. Christian Hensen, PD Dr. Sabine Kasten, Dr. Natascha Riedinger und Prof. Dr. Katrin Huhn, von deren Fachkenntnis ich viel lernen konnte, für ihre unermüdliche Diskussionsbereitschaft und hilfreichen Anregungen im Verlauf der Arbeit.

Ein herzlicher Dank geht an Prof. Dr. William W. Hay, Fabio Florindo, Alan Cooper sowie Jayne und Thomas Wolf-Welling, die durch Diskussionen und Anregungen zur inhaltlichen und stilistischen Verbesserung meiner Manuskripte beigetragen haben. Weiter danke ich Herrn Prof. Dr. Rüdiger Henrich, Herrn Prof. Dr. Tilo von Dobeneck, Dr. Ismene und Dr. Jens Seeberg-Elverfeldt, Dr. Christine Franke, Dr. Till Hanebuth und Dr. Stefan Mulitza für die zahlreichen anregenden Diskussionen.

Für die Tatkräftige Hilfe bei den Messungen und Laborarbeiten am Alfred-Wegener-Institut für Polar- und Meeresforschung in Bremerhaven (AWI) möchte ich mich bei Dr. Gerhard Kuhn und Rita Fröhlking bedanken. Für die Bereitstellung des Korngrößenlasermessgerätes „analysette 22“ zur Korngrößenmessung und des Kappabridge KL Y-2 zur Messung der magnetischen Suszeptibilität an Einzelproben danke ich der Arbeitsgruppe Marine Geophysik von Tilo von Dobeneck.

Ich danke den studentischen Hilfskräften Sünje Dallmeier-Tiessen, Viola Stratmann, Sophie Fath und Katharina Behrens für ihre Unterstützung bei der Probenaufbereitung und Messung. Sophie danke ich für die Überlassung der Messdaten aus ihrer Bachelorarbeit, welche ich mit betreuen durfte.

Desweiteren möchte ich mich bei meinen Kolleginnen und Kollegen aus den Arbeitsgruppen Marine Ingenieurgeologie von Prof. Dr. Tobias Mörz und Marine Geotechnik von Prof. Dr. Achim Kopf für das gute Arbeitsklima und die unzähligen gemeinsamen Mensagänge bedanken. Dieser Dank gilt auch allen Mitgliedern des Fachbereichs Geowissenschaften und des MARUM, die hier im Einzelnen nicht genannt wurden.

Ich danke dem Ocean Drilling Program/Integrated Ocean Drilling Program (ODP/IODP) für die großzügige Bereitstellung der Proben von ODP Leg 178, Site 1095. Ich bedanke ich mich auch bei den Mitarbeitern des IDOP Bremen Core Repository, insbesondere bei Walter Hale und Alexius Wülbers, für ihre tatkräftige Unterstützung bei der Probennahme und ihr Vertrauen bei der Überlassung einiger Kernabschnitte zur Anfertigung von Röntgenaufnahmen am Roten Kreuz Krankenhaus Bremen. In diesem Zusammenhang danke ich den Mitarbeitern des Instituts für klinische Radiologie, die mir die Röntgenaufnahmen ermöglicht haben.

Die Arbeit wurde als Teil des Projektantrags „Quantitative reconstruction of the Neogene East and West Antarctic Ice Sheet history from drift sediments (ODP Leg 178 and Leg 188): A synthesis“ (MO1059/1-1) im Rahmen des DFG Schwerpunktprogramms IODP/ODP (SPP 527) angefertigt. Ich

danke hiermit der Deutschen Forschungsgemeinschaft für ihre bereitwillige finanzielle Unterstützung, durch die diese Arbeit überhaupt erst ermöglicht worden ist.

Mein persönlicher Dank gilt Dr. Warner Brückmann. Er war der erste, der mein Interesse an der Marinen Geologie geweckt hat.

Bei meiner Familie und meinen Freunden möchte ich mich für die Unterstützung in den letzten Jahren bedanken. Bei meinen Eltern, die mir mein Studium ermöglicht haben und mir bei schwierigen Entscheidungen zur Seite standen.

Die wichtigste Stütze war mir meine liebe Ehefrau Nele, die nicht nur einen Umzug von Kiel nach Bremen auf sich genommen sondern auch in schwierigen Phasen meine Launen ertragen hat und viele Abende und Wochenenden ohne mich verbringen musste. Während der Zeit, in der diese Arbeit angefertigt wurde, wurde mein Sohn Emil geboren, der nun gerade die Sprache entdeckt und seine eigene Wissenschaft darin findet.